VOL 9
ISSUE 3
MAY 2024

eMetN
METEOR JOURNAL

eJournal for meteor observers www.emetn.net

At 9h04m pm on the evening of March 13th 2024, a meteorite-dropping fireball shot across the South Island of New Zealand. This photo was captured by NZ0015 at Arthurs Point, Queenstown, New Zealand. (credit: Dennis Behan).

- New Zealand's meteorite
- Beta-Tucanids (BTU, #108)
- New shower in Hercules
- GCR #1047 outburst
- CAMS reports
- Radio meteor work

ISSN 3041 - 4261

Contents

New Zealand's meteor camera network leads to recovery of the Tekapo/Takapō meteorite

James M. Scott[1], Denis Vida[2], Dennis Behan[3], Mia R. Boothroyd[1], Daniel L. Burgin[4], David Grieg[5], Peter McKellar[6], Marshall C. Palmer[1], Terry Richardson[7], Jim Rowe[8], Damir Šegon[9], Jesse Stayte[10], Thomas Stevenson[1], Tingting Wang[1], Jack Weterings[11], Steve Wyn-Harris[12]

[1] **University of Otago, Department of Geology, 360 Leith Street, Dunedin 9016, New Zealand**
James.scott@otago.ac.nz

[2] **Department of Physics and Astronomy, University of Western Ontario, London, Ontario, N6A 3K7, Canada**
dvida@uwo.ca

[3] **Queenstown, New Zealand**

[4] **Wellington, New Zealand**

[5] **Tauranga Astronomical Society, New Zealand**

[6] **Rotorua, New Zealand**

[7] **West Melton, New Zealand**

[8] **Brighton, United Kingdom**

[9] **Astronomical Society Istra Pula, Park Monte Zaro 2, HR-52100 Pula, Croatia**

Višnjan Science and Education Center, Istarska 5, HR-51463 Višnjan, Croatia

[10] **Auckland University, New Zealand**

[11] **Wellington, New Zealand**

[12] **Waipukurau, New Zealand**

At 9^h04^m pm on the evening of March 13th 2024, a fireball shot across the South Island of New Zealand. The combined fireball path was calculated from 96 to 23 km elevation by four camera stations, which showed that it decelerated from 18 km/s to 5 km/s. The dark flight model and Monte Carlo simulation for the main mass resulted in a strewn field in the Tekapo/Takapō region of the central South Island, and an 810 gm fusion-encrusted stoney meteorite was recovered within 30 minutes of initiation of the public search.

1 Introduction

New Zealand's meteor camera network, known as Fireballs Aotearoa[1], comprises over 120 Raspberry Pi Meteor Station (RMS) cameras and one Allsky7 camera (*Figure 1*). The cameras are mounted in schools, observatories and with the public. The goals of this non-commercial and citizen science network are to aid the discovery of New Zealand's next meteorite, feed into global meteor shower observations, and engage the public in night-sky observations. Recovered meteorites will be characterized and then donated to a national museum.

The network has been active for just over two years and has achieved near total coverage of the night-sky above the country down to 25 km elevation, which is critical for observing endpoint of meteorite-dropping fireballs. The Southern Hemisphere position makes it an important global component in detecting meteor showers (e.g., Šegon et al., 2022; Roggemans et al., 2024; Jenniskens, 2024), which are not well studied as Northern Hemisphere showers. On December 12th 2023, for example, the New Zealand network led the detection of a new meteor shower called lambda-Sculptorids, which was produced by comet 46P/Wirtanen (Roggemans et al., 2024; Vida et al., 2024). However, despite several fireballs possibly dropping small meteorites and a one multi-day coordinated search for a 10 kg possible iron meteorite in 2022, no meteorites had been recovered using camera data until now.

2 March 13th fireball

At 9^h04^m pm local time on March 13th, an impressive fireball was seen crossing the sky above Otago and Canterbury. It was caught beautifully on the Allsky7 camera[2] AMS246 (Hankey et al., 2020) and the first eyewitness report was from *Dennis Behan*, who was sitting in his hot tub at the time. Fortuitously, it also was captured by his personal RMS[3] (Vida et al., 2021) meteor camera, NZ0015 (*Figure 2*). Using data from NZ0015, NZ000T

[1] www.fireballs.nz
[2] www.allsky7.net
[3] www.globalmeteornetwork.com

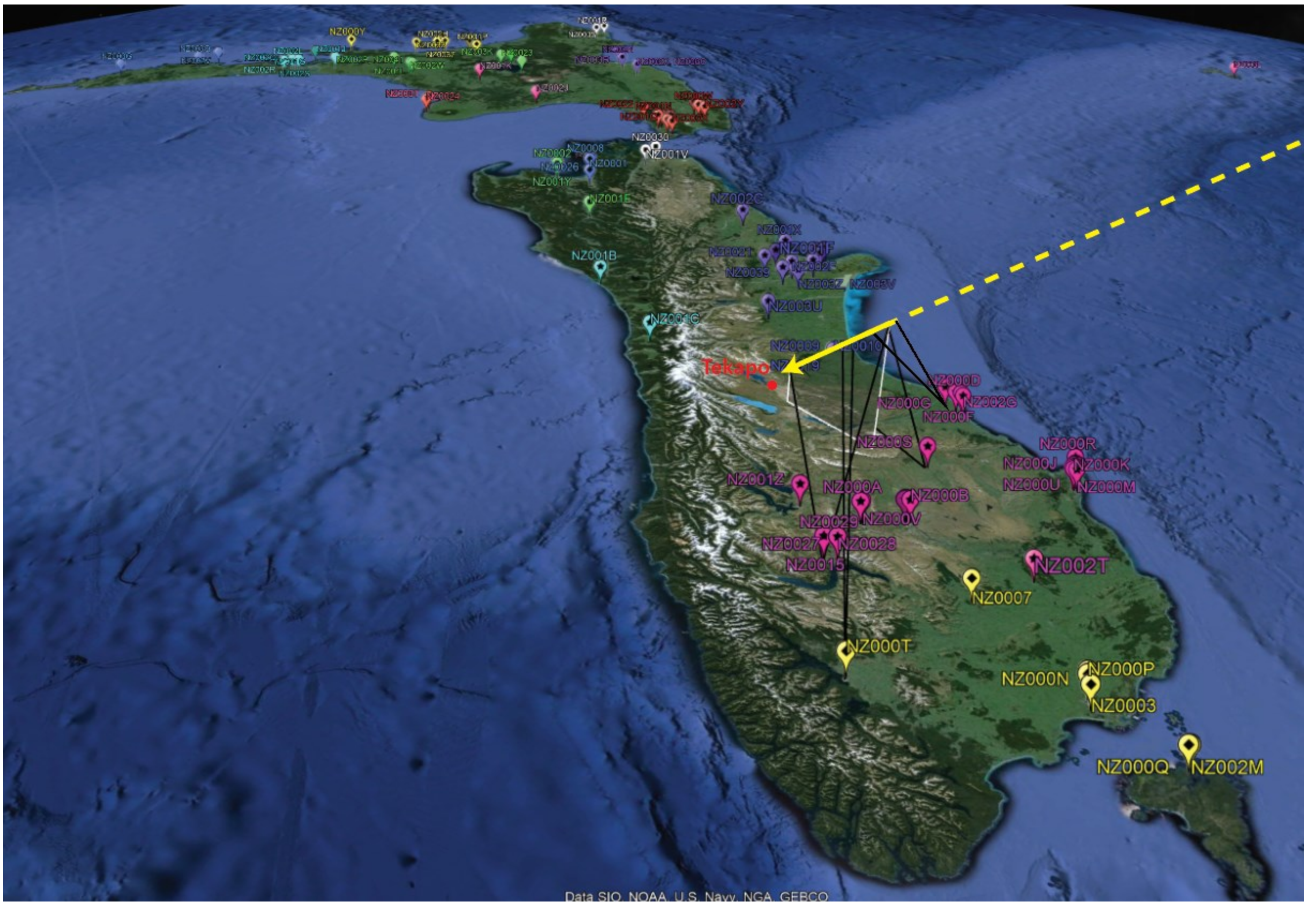

Figure 1 – Distribution of New Zealand's RMS camera network, and location of the fall.

(Fiordland College, Te Anau), NZ000S (Maniototo Area School, Ranfurly), and NZ000D (Oamaru North, Oamaru) the trajectory, velocity and origin of this fireball were determined by McKellar, Stayte and Vida. NZ0044 (Livingstone, Otago) also captured the fireball, but clouds in the region at the time inhibited using this data.

Figure 2 – Fireball captured by NZ0015 at Arthurs Point, Queenstown. This is also the approximate view from the hot tub.

3 Trajectory

Modelling of the trajectory using Skyfit2 indicated that the fireball was visible for 6.72 seconds, during which it descended from 96 km to about 23.3 km elevation (*Figure 3*). It began to rapidly decelerate at 50 km elevation from an initial velocity of about 18 km/s and was traveling at only 5 km/s at 23.3 km. Upon reaching this point, the fireball stage ended and the remaining mass, which was estimated to be between 0.6 to 1.6 kg for an ordinary chondrite-type meteorite, with the nominal mass of 0.9 kg, fell towards the surface of the Earth.

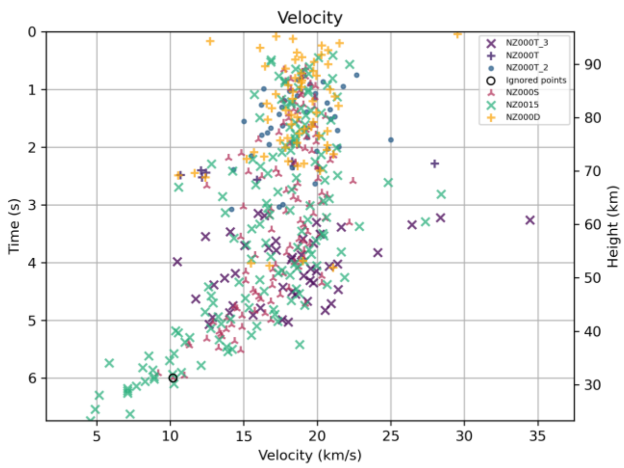

Figure 3 – Velocity and time of the fireball, as determined from NZ000S, D, T and 15.

Using weather station data from Invercargill, a dark flight solution by Vida and Stayte had the rock falling on an old braided river channel associated with the Tekapo River in public Department of Conservation land south of the township of Tekapo. The name of this town is after the adjacent lake, which was known as Takapō by the Maori. This area is famous for its giant salmon, views of New Zealand's highest mountain, and being a location for the Lord of the Rings movie series.

4 Field search

A reconnaissance search of a portion of the strewn-field was undertaken three days later (on the 16th) led by Behan and Palmer. This showed that the prospective area was flat, little vegetated and that the ground was hard-packed as a result of drought. Following a significant media blitz, a public search led by Behan, Palmer and Wyn-Harris set out on the 20th of March and remarkably what is thought to be the main mass meteorite was recovered within 30 minutes of the search initiation within the strewn field. The finder, Jack Weterings from Wellington, noticed the meteorite partially embedded in the ground and immediately recognized it to be distinct from the surround flood-plain greywacke gravels (*Figure 4*). The good cell-phone coverage in the area meant that he could immediately send a photograph to Palmer to examine.

Figure 4 – The meteorite resting in the crater.

The recovered meteorite has a thin black fusion crust and a slightly unusual shape on one flank where it has lost a substantial bit of the rock, possibly late in the fireball stage. The fusion crust was chipped on one surface due to impact with the ground, and reveals a pale interior that – at the time of writing – looks similar to the color and texture of a metamorphosed ordinary chondrite (*Figure 5*). The chipped fragments could not be located. Following positive visual identification, a handheld portable x-ray fluorescence device was used to analyze the rock through a plastic bag. This revealed high Ni concentrations. The rock now awaits further study led by the University of Otago Department of Geology.

Figure 5 – The fusion crust is chipped and displays a pale coloured interior.

5 Discussion and conclusion

This is New Zealand's 10th confirmed meteorite, and the first in 20 years. It is also only the second one in which a fireball was first seen and then the rock rapidly recovered – the other being the CV3 Mokoia (Marriner, 1910). There was a daytime ordinary chondrite fall (Auckland) in 2004 but no fireball was reported (Scott et al., 2023). The largest New Zealand meteorite was the 50 kg Dunganville (Challis 1984) and the previous smallest was the ~1 kg Auckland.

Our calculations show that the object had an Aten-type orbit, with the perihelion just inside the orbit of Venus and the aphelion just outside the orbit of the Earth (*Figure 6*). Only a handful of meteorites are observed to arrive on such orbits. This will be examined in more detail in the future, along with the composition of the rock and its cosmic-ray exposure age, as orbits in this part of the Solar System are not dynamically stable over long periods of time. Thus, the new meteorite, likely to be named Tekapo/Takapō, confirms the ability of the Fireballs Aotearoa meteor camera network to accurately and rapidly aid meteorite recovery, and will hopefully provide further insights into the history of the Solar System.

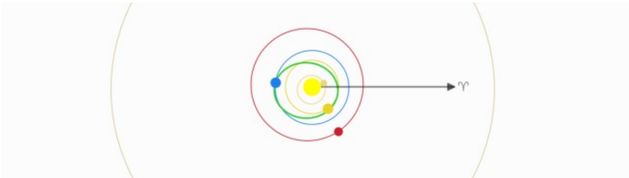

Figure 6 – The calculated Alten-type orbit of the rock that formed the meteor is shown in green. Earth is blue, Venus is yellow.

Acknowledgments

With great thanks, we acknowledge the searchers: *S. Adam, A. Barrajun, D. Behan, M. Behan, W. Chiang, S. Eberlin, E. Gapper, E. Gapper, M. Gapper, Z. Gapper, A. Gilmore P. Kilmartin, T.-Y. Lin, R. McCarthy, M. Midgley, A. Muner, T. Richardson, S. Robb, G. Rocord, P. Silva, M. Stroinigg, J. Weterings, M. Wilkins, H. Wilkins, S. Wilson, S. Wyn-Harris, M. Yi Ying, S. Xiao*.

We also greatly acknowledge all the NZ meteor camera hosts, who have contributed to the project: *M. Anderson, S. Baker Wilson, E. Balks, E. Barraclough, H. Barker, J.-F. Barrois, A. Barron, C. Beaman, D. Behan, T. Bell, M. Boothroyd, R. Brady, A. Brickell, K. Browne, R. Brunton, M. Camilleri, L. Carpenter, R. Carstens, J. Cheetham, M. Clare, F. Cole, D. Colthorpe, S. Cooke-Willis, D. Cowan, K. Christie, J. Critchley, A. Crowther, R. Croy, N. Davies, R. Dickie, L. Dowling, R. Elias-Drago, J. Drummond, A. Emerson, B. Evans, A. Fastier, K. Faure, P. Felhofer, R. Frazer, M. Forbes, A. Fox, A. Fuller, L. Gilbert, D. Godsiff, B. Goodwill, P. Graham, D. Greig, B. Hagen, C. Haines, B. Hasson, J. van Hattum, D. Hickey, L. Holstein, M. Hope, G. Hudson, R. Idaczyk, N. Izsett, P. Jaquiery, C. Jones, C. Jones, A. Johnston, D. Johnson, K. Johnston, M. Kennedy, S. Land, S. Leaske, S. Lewis, J. McCulloch, T. McGirrt, G. McKay, P. McKeller, H. McKinnon, T. McMahon, D. McNamara, S. McMillan, F. McNaught, A. Mason, S.*

Matheson, S. Oosterman, G. Palmer, M. Palmer, G. Parker, J. Parkinson, H. Petelo, N. Peterson, S. Peterson, N. Powell, R. Querel, B. Reid, J. Richards, T. Richardson, A. Robertson, L. Robertson, B. Rowe, J. Russell, C. Sale, C. Sara, A. Scott, Y. Scott, M. Singleton, N. Simmonds, R. Skilton, J. Stayte, P. Stewart, J. Taylor, B. Thomas, J. Thompson, M. Thompson, S. Tonorio, T. Vowles, M. Ward, R. Welch, N. Wiffen, J. Williams, S. Wyn-Harris, C. Young, J. Zani, C. Zink.

We especially acknowledge: *Sirko Molau* and *Mike Hankey* of www.allsky7.net for helping build and then enabling Allsky7 camera 247; a Participatory Science Platform Grant associated with the NZ Curious Minds, which was administered by the Otago Museum; the Royal Astronomical Society of New Zealand; the Geoscience Society of New Zealand; the Raspberry PI Ltd, and two anonymous doners.

References

Challis G. A. (1984). "The Dunganville (New Zealand) meteorite: an iron octahedrite (Note)". *New Zealand Journal of Geology and Geophysics*, **27**, 391–393.

Hankey M., Perlerin V., and Meisel D. (2020). "The all-sky-6 and the Video Meteor Archive system of the AMS Ltd.". *Planetary and Space Science*, **190**, 105005.

Jenniskens P. (2024). "Enhanced iota-Centaurids (ICN#919) activity in 2024". *eMetN*, **9**, 53–54.

Marriner G. R. (1910). "The Mokoia Aerolite; with a few introductory remarks on New Zealand meteoric Phenomena". *Transactions and proceedings of the Royal Society of New Zealand*, **42**, 176–185.

Roggemans P., Vida D., Scott J. M., Jenniskens P., Šegon D., and Rollinson D. (2024). "First observed meteors from comet 46P/Wirtanen (lambda-Sculptorids, LSC)". *eMetN*, **9**, 6–14.

Šegon D., Vida D., Roggemans P., Wood J., Boothroyd M., Fraser R., Hanigan G., Poulton D., Scott G., Scott J. and Zink C. (2023). "2023 activity omega-Carinids (OCR# 1033)". *eMetN*, **8**, 74–76.

Scott J. M., Negrini M., Faure K., Palmer M. C., Knaack D. R., and Leybourne M. I. (2023). "Multi-zone fusion crust formation and classification of the 2004 Auckland meteorite (L6, S5, and W0)". *Meteoritics & Planetary Science*, **58**, 328–340.

Vida D., Scott J. M., Egal A., Vaubaillon J., Ye Q-Z., Rollinson D., Sato M., and Moser D. E. (2024). "Observations of the new meteor shower from comet 46P/Wirtanen." *Astronomy & Astrophysics*, **682**, L20.

Vida D., Šegon D., Gural P. S., Brown P. G., McIntyre M. J. M., Dijkema T. J., Pavletić L., Kukić P., Mazur M. J., Eschman P., Roggemans P., Merlak A., Zubrović D. (2021). "The Global Meteor Network – Methodology and first results". *Monthly Notices of the Royal Astronomical Society*, **506**, 5046–5074.

Enhanced activity of the beta-Tucanids (BTU, #108)

Peter Jenniskens

SETI Institute, 339 Bernardo Ave, Mountain View, CA 94043, USA
pjenniskens@seti.org

Significant activity of beta-Tucanids was detected by CAMS and GMN low-light video camera networks in 2024. This observation adds to two previously recorded outbursts in 2020 and 2021 and further illustrates past activity from now dormant Jupiter-family comet 2006 CS.

1 Introduction

Strong activity of the beta-Tucanids (BTU#108) was detected by SAAMER radar observations in 2020 (Janches et al., 2020). Janches et al. identified the parent body of this shower as minor planet (248590) 2006 CS, which based on the Tisserand parameter with respect to Jupiter is a now dormant Jupiter-family comet.

The shower stands out from the overlapping delta-Mensids meteor shower (IAU #130) by having a lower entry speed of 30.6 km/s on average, as compared to 37.0 km/s for the more diffuse delta-Mensids. The difference corresponds to a Halley-type orbit for the delta-Mensids, but a Jupiter-family type orbit for the beta-Tucanids.

Past observations of the beta-Tucanids are summarized in Jenniskens (2023), where the shower is given as episodic. However, there may be a more diffuse annual activity associated with this shower. Indeed, the shower appears to have been detected by radar as far back as 1969 (Gartrell, 1972; Gartrell and Elford, 1975).

2 2024 observations

The 2024 beta-Tucanids were first detected by CAMS Chile (S. Heathcote and T. Abbott, NOIRLAB/Cerro Tololo; and E. Jehin, University of Liege) on March 12 at 4^h UTC ($N = 5$ Beta Tucanid meteors), then peaked over CAMS New Zealand (coordinated by J. Baggaley, University of Canterbury; and J. Scott, University of Otago) starting at 8^h UTC ($N = 20$), followed by CAMS Australia (H. Devillepoix, Curtin University; and D. Rollinson) starting at 14^h UTC (N = 6). A late shower member was detected by CAMS New Zealand on March 13 at 8^h29^m UTC. The networks in New Zealand (J. Scott) and Australia (D. Rollinson) are part of the Global Meteor Network, coordinated by D. Vida. Note that the network by J. Scott expanded dramatically the number of cameras participating in CAMS New Zealand in 2024. Indeed, the shower was also clearly detected in the Global Meteor Network (*Figure 2*).

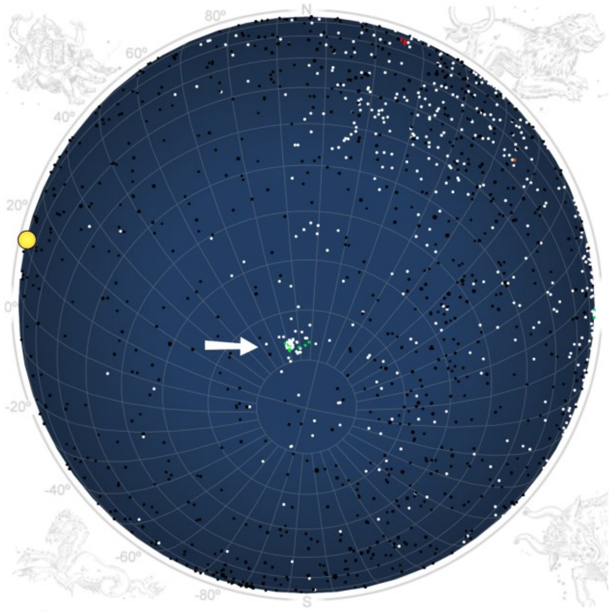

Figure 1 – The plot of the radiants obtained by the CAMS networks for the date of 2024 March 12.

Table 1 – The 2024 orbital elements (Equinox J2000.0) compared to the median 2021 orbit from Jenniskens (2023).

	2021	2024
$\lambda_\odot$ (°)	352.26	352.03 ± 0.03
α_g (°)	62.1	66.2 ± 2.1
δ_g (°)	–77.4	–78.2 ± 0.6
v_g (km/s)	30.6	30.8 ± 0.7
$\lambda - \lambda_\odot$ (°)	304.3	298.1
β (°)	–76.8	–76.4
a (AU)	2.86	2.83 ± 0.45
q (AU)	0.977 ± 0.004	0.9810 ± 0.0016
e	0.658 ± 0.058	0.654 ± 0.046
ω (°)	344.0 ± 2.3	345.3 ± 0.9
Ω (°)	172.3 ± 0.2	172.05 ± 0.24
i (°)	51.0 ± 1.5	51.8 ± 0.7
Π (°)	156.0 ± 2.3	157.7 ± 1.6
T_j	2.23	2.44
N	26	47

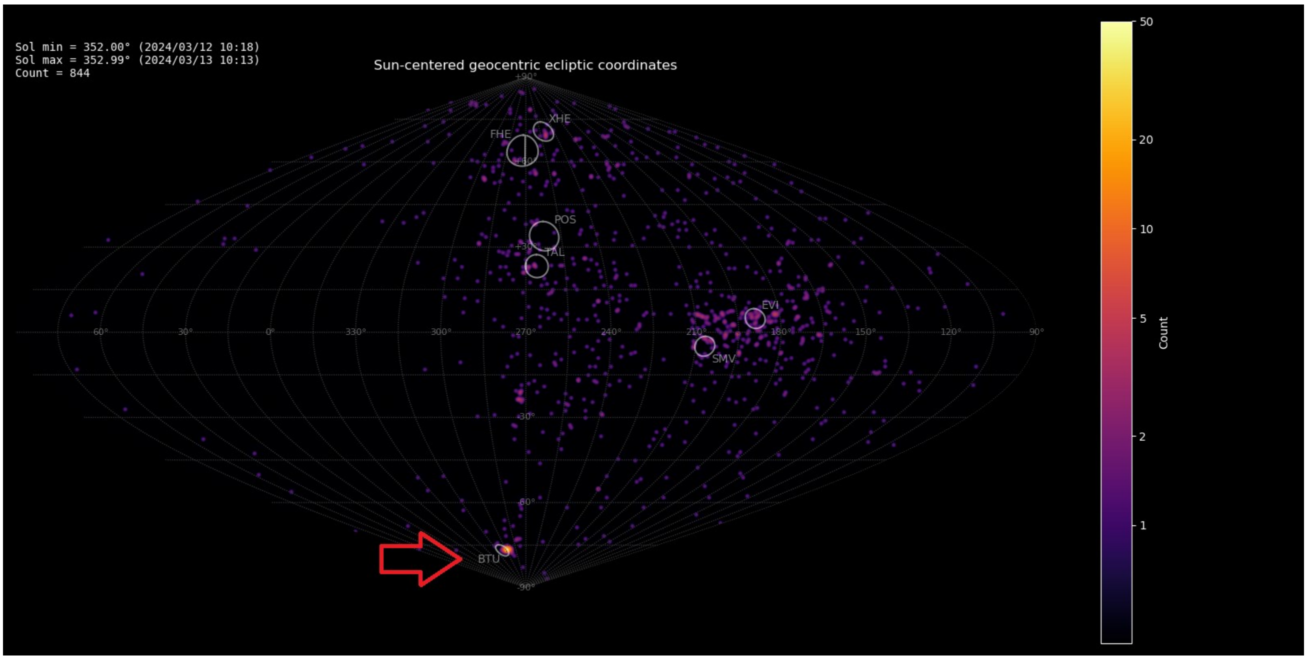

Figure 2 – The beta Tucanid activity in 2024 has been confirmed by the Global Meteor Network.

3 Discussion

In 2020, when SAAMER detected the outburst, CAMS observations showed a compact radiant on March 12, confirming the outburst, but only 7 meteors were triangulated. Since that time, the activity has been variable. In 2021, 38 beta-Tucanids were triangulated on March 12 and 13 (Jenniskens, 2021). In 2022, 12 meteors were triangulated on these dates, but that activity was spread out more in solar longitude. In 2023, only 5 meteors were triangulated on those dates, again spread out. So, it is unclear that there was an outburst in 2022 and 2023.

The peak time of the narrow outburst component changes from year to year. In 2020, the shower peaked at solar longitude = 352.38 ± 0.09 deg (standard error) with full-width-at-half-maximum = 0.76 deg. In 2021, the shower peaked at 352.27 ± 0.04 deg with FWHM = 0.59 deg. In 2024, the shower peaked at solar longitude 352.03 ± 0.03 deg with FWHM = 0.43 deg. The slightly narrower width in 2024 may be on account in part by the higher number of cameras in New Zealand since 2021.

These new observations may help determine when minor planet 2006 CS last disrupted, causing the narrow meteoroid stream that now wanders on occasion in Earth's path.

References

Gartrell G. A. (19721). "Southern Hemisphere Radio Meteor Orbit Survey". Proceedings of the *Astronomical Society of Australia*, **2**, pages 89–90.

Gartrell G., Elford W. G. (1975). "Southern hemisphere meteor stream determinations". *Australian Journal of Physics*, **28**, 591–620.

Janches D., Bruzzone J. S., Weryk R. J., Hormaechea J. L., Wiegert P., Brunini C. (2020). "Observations of an Unexpected Meteor Shower Outburst at High Ecliptic Southern Latitude and Its Potential Origin". *The Astrophysical Journal Letters*, **895**, id.L25, 6 pages.

Jenniskens P. (2021). "Beta Tucanids (BTU #108) meteor outburst in 2021". *eMetN*, **6**, 330–331.

Jenniskens P. (2023). Atlas of Earth's Meteor Showers. Elsevier, USA. pages 766–767.

New shower in Hercules

Denis Vida[1] and Damir Šegon[2]

[1] **Department of Physics and Astronomy, University of Western Ontario, London, Ontario, N6A 3K7, Canada**
dvida@uwo.ca

[2] **Astronomical Society Istra Pula, Park Monte Zaro 2, 52100 Pula, Croatia**
damir@astro.hr

The Global Meteor Network detected a new meteor shower of Halley-type comet origin. The shower activity period occurred in a very narrow time period of only 3.5 hours. The observed geometric radiant was at R.A. = 261.1 deg, Decl. = +47.3 deg, within a circle with a standard deviation of ± 1.1 deg (equinox J2000.0).

1 Introduction

The authors report an outburst of a new meteor shower with a radiant in Hercules. 32 meteors were observed by the Global Meteor Network (Vida et al., 2019, 2020, 2021) low-light video cameras on 2024 April 27[4] in a narrow time range between 20^h00^m – 23^h40^m UTC. *Figure 1* shows the radiant cluster in the Sun-centered ecliptic coordinates.

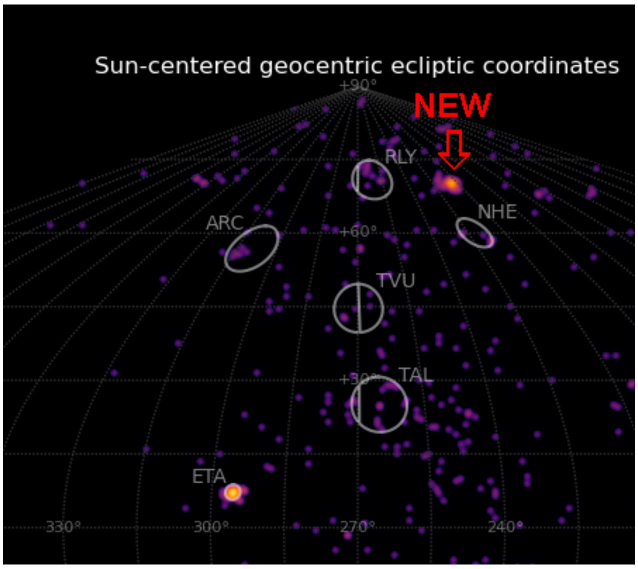

Figure 1 – Radiant plot of the Global Meteor Network data for 2024, April 27–28 in Sun-centered geocentric ecliptic coordinates.

2 The observations

The shower was independently observed by cameras in 11 different European countries (Croatia, Slovenia, the UK, Bulgaria, Greece, the Czech Republic, Poland, Romania, Hungary, Spain, and Slovakia). Meteor shower members were extracted using the method described in Šegon et al. (2023) using the Drummond D criterion (Drummond, 1981). *Figure 2* shows the distribution of the values of the D criterion from the mean orbit, with the bulk of the detected meteors having the value of the Drummond D criterion < 0.05.

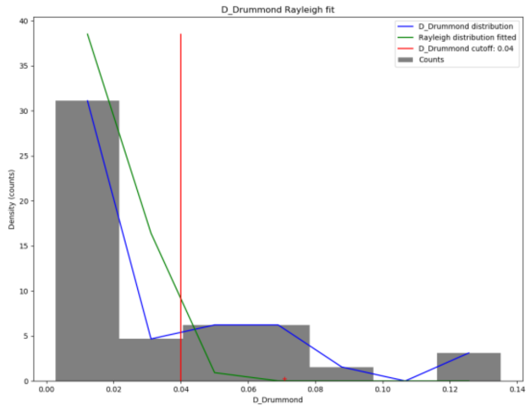

Figure 2 – Rayleigh distribution fit and D_D cutoff.

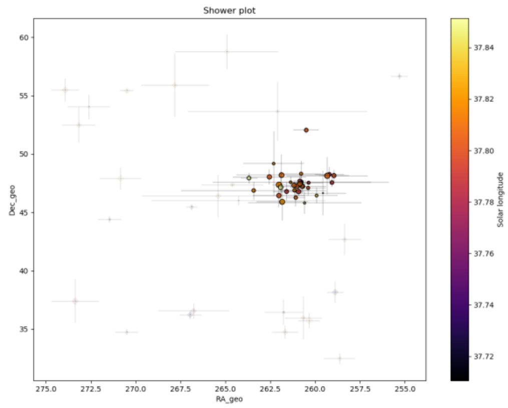

Figure 3 – Meteor shower radiants in geocentric equatorial coordinates, where the sporadic radiants are grayed out.

The shower had a median geocentric radiant with coordinates R.A. = 261.1 deg, Decl. = +47.3 deg, within a circle with a standard deviation of ± 1.1 deg (equinox J2000.0). The radiants are shown in *Figure 3*. The median Sun-centered ecliptic coordinates were $\lambda - \lambda_{\odot} = 214.24$ deg, $\beta = +70.15$ deg. The geocentric velocity was 35.6 ± 0.9

[4] https://globalmeteornetwork.org/data/ for the dates of 2024 April 27

km/s. The meteors were bright, most having peak magnitudes ranging from +1.5 to –3.0.

The orbital elements (equinox J2000.0) are those of a long-period comet:

- $q = 0.95292 \pm 0.00522$ AU;
- $e = 0.968 \pm 0.068$,
- $i = 55.77 \pm 1.02$ deg,
- $\omega = 206.97 \pm 1.55$ deg,
- $\Omega = 37.8190.025$ deg.

All meteors appeared during the solar-longitude interval 37.70 – 37.85 degrees, with a sharp peak at 37.80 deg. The bulk of all meteors, a total of 25, was observed in a narrow interval between $22^h00^m – 22^h45^m$ UTC (solar longitude 37.78 – 37.82 deg), as shown in *Figure 4*.

The parent body search did not return any candidates within the Southworth and Hawkins (1963) D criterion value of < 0.35.

The shower has been added to the IAU list of showers with a temporary name M2024-H1[5].

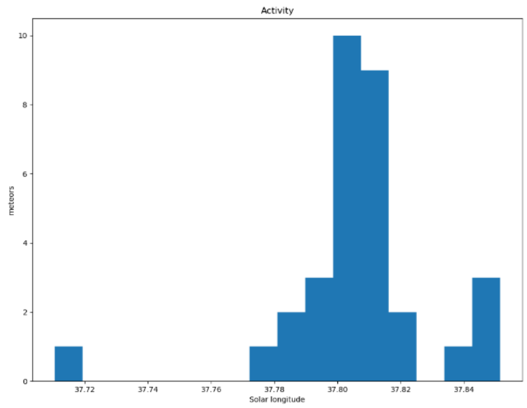

Figure 4 – The activity period with the number of orbits identified as new shower members.

Acknowledgment

This discovery is based on the data of the Global Meteor Network which is released under the CC BY 4.0 license. We thank all the participants in the Global Meteor Network project for their contribution and perseverance, operators whose cameras provided the data used in this work and contributors who made important code contributions The Global Meteor Network results were obtained thanks to the efforts of the following volunteers (list cut-off date as it was at the end of 2023):

Adam Mullins, Aden Walker, Adrian Bigland, Adriana Roggemans, Alain Marin, Alaistar Brickhill, Alan Beech, Alan Maunder, Alan Pevec, Alan Pickwick, Alan Decamps, Alan Cowie, Alastair Emerson, Aled Powell, Alejandro Barriuso, Aleksandar Merlak, Alex Bell, Alex Haislip, Alex Hodge, Alex Jeffery, Alex Kichev, Alex McConahay, Alex Pratt, Alex Roig, Alex Aitov, Alexander Wiedekind-Klein, Alexandre Alves, Alfredo Dal' Ava Júnior, Alison Scott, Amy Barron, Anatoly Ijon, Andre Rousseau, Andre Bruton, Andrea Storani, Andrei Marukhno, Andres Fernandez, Andrew Campbell-Laing, Andrew Challis, Andrew Cooper, Andrew Fiamingo, Andrew Heath, Andrew Moyle, Andrew Washington, Andrew Fulher, Andrew Robertson, Andy Stott, Andy Sapir, Ange Fox, Angel Sierra, Angélica López Olmos, Anna Johnston, Ansgar Schmidt, Anthony Hopkinson, Anthony Pitt, Anthony Kesterton, Anton Macan, Anton Yanishevskiy, Antony Crowther, Anzhari Purnomo, Arie Blumenzweig, Arie Verveer, Arnaud Leroy, Attila Nemes, Barry Findley, Bart Dessoy, Bela Szomi Kralj, Bernard Côté, Bernard Hagen, Bev M. Ewen-Smith, Bill Cooke, Bill Wallace, Bill Witte, Bill Carr, Bill Thomas, Bob Evans, Bob Greschke, Bob Hufnagel, Bob Marshall, Bob Massey, Bob Zarnke, Bob Guzik, Brenda Goodwill, Brendan Cooney, Brendon Reid, Brian Chapman, Brian Murphy, Brian Rowe, Brian Hochgurtel, Wyatt Hochgurtel, Brian Mitchell, Bruno Bonicontro, Callum Potter, Carl Elkins, Carl Mustoe, Carl Panter, Charles Thody, Charlie McCormack, Chris Baddiley, Chris Blake, Chris Dakin, Chris George, Chris James, Chris Ramsay, Chris Reichelt, Chris Chad, Chris O'Neill, Chris White, Chris Jones, Chris Sale, Christian Wanlin, Christine Ord, Christof Zink, Christophe Demeautis, Christopher Coomber, Christopher Curtis, Christopher Tofts, Christopher Brooks, Chuck Goldsmith, Chuck Pullen, Ciaran Tangney, Claude Boivin, Claude Surprenant, Clive Sanders, Colin Graham, Colin Marshall, Colin Nichols, Con Stoitsis, Craig Young, Creina Beaman, Daknam Al-Ahmadi, Damien Lemay, Damien McNamara, Damir Matković, Damir Šegon, Damjan Nemarnik, Dan Klinglesmith, Dan Pye, Daniel Duarte, Daniel J. Grinkevich, Daniela Cardozo Mourão, Danijel Reponj, Danko Kočiš, Dario Zubović, Dave Jones, Dave Mowbray, Dave Newbury, Dave Smith, David Akerman, David Attreed, David Bailey, David Brash, David Castledine, David Hatton, David Leurquin, David Price, David Rankin, David Robinson, David Rollinson, David Strawford, David Taylor, David Rogers, David Banes, David Johnston, David Rees, David Cowan, David Greig, David Hickey, David Colthorpe, Dean Moore, Debbie Godsiff, Denis Bergeron, Denis St-Gelais, Dennis Behan, Derek Poulton, Didier Walliang, Dimitris Georgoulas, Dino Čaljkušić, Dmitrii Rychkov, Dominique Guiot, Don Anderson, Don Hladiuk, Dorian Božičević, Dougal Matthews, Douglas Sloane, Douglas Stone, Dustin Rego, Dylan O'Donnell, Ed Breuer, Ed Harman, Edd Stone, Edgar Mendes Merizio, Edison José Felipe Pérezgómez Álvarez, Edson Valencia Morales, Eduardo Fernandez Del Peloso, Edward Cooper, Ehud Behar, Eleanor Mayers, Emily Barraclough, Enrico Pettarin, Enrique Arce, Enrique Chávez Garcilazo, Eric Lopez, Eric Toops, Errol Balks, Erwin van Ballegoij, Erwin Harkink, Eugene Potapov, Ewan Richardson, Fabricio Borges, Fernando Dall'Igna, Fernando Jordan, Fernando Requena, Filip Matković, Filip

[5] https://www.ta3.sk/IAUC22DB/MDC2022/

Mezak, Filip Parag, Fiona Cole, Florent Benoit, Francis Rowsell, François Simard, Frank Lyter, Frantisek Bilek, Gabor Sule, Gaétan Laflamme, Gareth Brown, Gareth Lloyd, Gareth Oakey, Garry Dymond, Gary Parker, Gary Eason, Gavin Martin, Gene Mroz, Geoff Scott, Georges Attard, Georgi Momchilov, Germano Soru, Gilton Cavallini, Gordon Hudson, Graeme Hanigan, Graeme McKay, Graham Stevens, Graham Winstanley, Graham Henstridge, Graham Atkinson, Graham Palmer, Greg Michael, Greg Parker, Gustav Frisholm, Gustavo Silveira B. Carvalho, Guy Létourneau, Guy Williamson, Guy Lesser, Hamish Barker, Hamish McKinnon, Haris Jeffrey, Harri Kiiskinen, Hartmut Leiting, Heather Petelo, Heriton Rocha, Hervé Lamy, Herve Roche, Holger Pedersen, Horst Meyerdierks, Howard Edin, Hugo González, Iain Drea, Ian Enting Graham, Ian Lauwerys, Ian Parker, Ian Pass, Ian A. Smith, Ian Williams, Ian Hepworth, Ian Collins, Igor Duchaj, Igor Henrique, Igor Macuka, Igor Pavletić, Ilya Jankowsky, Ioannis Kedros, Ivan Gašparić, Ivan Sardelić, Ivica Ćiković, Ivica Skokić, Ivo Dijan, Ivo Silvestri, Jack Barrett, Jacques Masson, Jacques Walliang, Jacqui Thompson, James Davenport, James Farrar, James Scott, James Stanley, James Dawson, Jamie Allen, Jamie Cooper, Jamie McCulloch, Jamie Olver, Jamie Shepherd, Jan Hykel, Jan Wisniewski, Janis Russell, Janusz Powazki, Jason Burns, Jason Charles, Jason Gill, Jason van Hattum, Jason Sanders, Javor Kac, Jay Shaffer, Jean Francois Larouche, Jean Vallieres, Jean Brunet, Jean-Baptiste Kikwaya, Jean-Fabien Barrois, Jean-Louis Naudin, Jean-Marie Jacquart, Jean-Paul Dumoulin, Jean-Philippe Barrilliot, Jeff Holmes, Jeff Huddle, Jeff Wood, Jeff Devries, Jeffrey Legg, Jeremy Taylor, Jesse Stayte, Jesse Lard, Jessica Richards, Jim Blackhurst, Jim Cheetham, Jim Critchley, Jim Fordice, Jim Gilbert, Jim Rowe, Jim Seargeant, Jochen Vollsted, Jocimar Justino, John W. Briggs, John Drummond, John Hale, John Kmetz, John Maclean, John Savage, John Thurmond, John Tuckett, John Waller, John Wildridge, John Bailey, Jon Bursey, Jonathan Alexis Valdez Aguilar, Jonathan Eames, Jonathan Mackey, Jonathan Whiting, Jonathan Wyatt, Jonathon Kambulow, Jorge Augusto Acosta Bermúdez, Jorge Oliveira, Jose Carballada, Jose Galindo Lopez, José María García, José-Luis Martín, Josip Belas, Josip Krpan, Jost Jahn, Juan Luis Muñoz, Jure Zakrajšek, Jürgen Dörr, Jürgen Ketterer, Justin Zani, Karen Smith, Karl Browne, Kath Johnston, Kees Habraken, Keith Maslin, Keith Biggin, Keith Christie, Ken Jamrogowicz, Ken Lawson, Ken Gledhill, Kevin Gibbs-Wragge, Kevin Morgan, Kevin Faure, Klaas Jobse, Korado Korlević, Kyle Francis, Lachlan Gilbert, Larry Groom, Laurent Brunetto, Laurie Stanton, Lawrence Saville, Lee Hill, Leith Robertson, Len North, Leslie Kaye, Lev Pustil'Nik, Lexie Wallace, Lisa Holstein, Llewellyn Cupido, Logan Carpenter, Lorna McCalman, Louw Ferreira, Lovro Pavletić, Lubomir Moravek, Luc Turbide, Lucia Dowling, Luciano Miguel Diniz, Ludger Börgerding, Luis Fabiano Fetter, Maciej Reszelsk, Magda Wisniewska, Manel Colldecarrera, Marc Corretgé Gilart, Marcel Berger, Marcelo Domingues, Marcelo Zurita, Marcio Malacarne, Marco Verstraaten, Margareta Gumilar, Marián Harnádek, Mariusz Adamczyk, Mark Fairfax, Mark Gatehouse, Mark Haworth, Mark McIntyre, Mark Phillips, Mark Robbins, Mark Spink, Mark Suhovecky, Mark Williams, Mark Ward, Marko Šegon, Marshall Palmer, Marthinus Roos, Martin Breukers, Martin Richmond-Hardy, Martin Robinson, Martin Walker, Martin Woodward, Martin Connors, Martyn Andrews, Mary Waddingham, Mary Hope, Mason McCormack, Mat Allan, Matej Mihelčić, Matt Cheselka, Matthew Howarth, Megan Gialluca, Mia Boothroyd, Michael Cook, Michael Mazur, Michael O'Connell, Michael Krocil, Michael Camilleri, Michael Kennedy, Michał Warchoł, Michel Saint-Laurent, Miguel Diaz Angel, Miguel Preciado, Mike Breimann, Mike Hutchings, Mike Read, Mike Shaw, Mike Ball, Milan Kalina, Minesh Patel, Miranda Clare, Mirjana Malarić, Muhammad Luqmanul Hakim Muharam, Murray Forbes, Murray Singleton, Murray Thompson, Myron Valenta, Nalayini Brito, Nawaz Mahomed, Ned Smith, Nedeljko Mandić, Neil Graham, Neil Papworth, Neil Waters, Neil Petersen, Nelson Moreira, Neville Vann, Nial Bruce, Nicholas Hill, Nicholas Ruffier, Nick Howarth, Nick James, Nick Moskovitz, Nick Norman, Nick Primavesi, Nick Quinn, Nick Russel, Nick Powell, Nick Wiffen, Nicola Masseroni, Nigel Bubb, Nigel Evans, Nigel Owen, Nigel Harris, Nikola Gotovac, Nikolay Gusev, Nikos Sioulas, Noah Simmonds, Norman Izsett, Ollie Eisman, Pablo Canedo, Paraksh Vankawala, Pat Devine, Patrick Franks, Patrick Poitevin, Patrick Geoffroy, Patrik Kukić, Paul Cox, Paul Dickinson, Paul Haworth, Paul Heelis, Paul Kavanagh, Paul Ludick, Paul Prouse, Paul Pugh, Paul Roche, Paul Roggemans, Paul Stewart, Paul Huges, Pedro Augusto Hay Day, Penko Yordanov, Pete Graham, Pete Lynch, Peter G. Brown, Peter Campbell-Burns, Peter Davis, Peter Eschman, Peter Gural, Peter Hallett, Peter Jaquiery, Peter Kent, Peter Lee, Peter McKellar, Peter Meadows, Peter Stewart, Peter Triffitt, Peter Leigh, Peter Felhofer, Pető Zsolt, Phil James, Philip Gladstone, Philip Norton, Philippe Schaak, Phillip Wilhelm Maximilian Grammerstorf, Pierre Gamache, Pierre de Ponthière, Pierre-Michael Micaletti, Pierre-Yves Pechart, Pieter Dijkema, Predrag Vukovic, Przemek Nagański, Radim Stano, Rajko Sušanj, Raju Aryal, Ralph Brady, Raoul van Eijndhoven, Raul Truta, Raul Elias-Drago, Reinhard Kühn, Remi Lacasse, Renato Cássio Poltronieri, René Tardif, Richard Abraham, Richard Bassom, Richard Croy, Richard Davis, Richard Fleet, Richard Hayler, Richard Johnston, Richard Kacerek, Richard Payne, Richard Stevenson, Richard Severn, Rick Fischer, Rick Hewett, Rick James, Ricky Bassom, Rob Agar, Rob de Corday Long, Rob Saunders, Rob Smeenk, Robert Longbottom, Robert McCoy, Robert Saint-Jean, Robert D. Steele, Robert Veronneau, Robert Peledie, Robin Boivin, Robin Earl, Robin Rowe, Roel Gloudemans, Roger Banks, Roger Morin, Roland Idaczyk, Rolf Carstens, Romulo Jose, Ron James Jr, Roslina Hussain, Ross Skilton, Ross Dickie, Ross Welch, Russell Jackson, Russell Brunton, Ryan Frazer, Ryan Harper, Salvador Aguirre, Sam Green, Sam Hemmelgarn, Sam Leaske, Sarah Tonorio, Scott Kaufmann, Sebastian Klier, Seppe Canonaco, Seraphin Feller, Serge Bergeron, Sergio Mazzi, Sevo Nikolov, Simon Cooke-Willis, Simon Holbeche, Simon Maidment, Simon McMillan, Simon Minnican, Simon Parsons, Simon Saunders, Simon Fidler, Simon Oosterman, Simon Peterson, Simon lewis, Sofia Ulrich, Srivishal Sudharsan, Stacey Downton, Stan Nelson, Stanislav Korotkiy, Stanislav Tkachenko, Stef Vancampenhout, Stefan Frei, Stephane Zanoni, Stephen Grimes, Stephen Nattrass, Steve Berry, Steve Bosley, Steve Carter, Steve Dearden, Steve Homer, Steve Kaufman, Steve Lamb, Steve Rau, Steve Tonkin, Steve Trone, Steve Welch, Steve Wyn-Harris, Steven Shanks, Steven Tilley, Stewart Doyle, Stuart Brett, Stuart Land, Stuart McAndrew, Sue Baker Wilson, Sylvain Cadieux, Tammo Jan Dijkema, Terry Pundiak, Terry Richardson, Terry Simmich, Terry Young, Thiago Paes, Thomas Blog, Thomas Schmiereck, Thomas Stevenson, Tihomir Jakopčić, Tim Burgess, Tim Claydon, Tim Cooper, Tim Gloudemans, Tim Havens, Tim Polfliet, Tim Frye, Tioga Gulon, Tobias Westphal, Tom Warner, Tom Bell, Tommy McEwan, Tommy B. Nielsen, Torcuill Torrance, Tosh White, Tracey Snelus, Trevor Clifton, Ubiratan Borges, Urs Wirthmueller, Uwe Glässner, Vasilii Savtchenko, Ventsislav Bodakov, Victor Acciari, Viktor Toth, Vincent McDermott, Vladimir Jovanović, Waily Harim, Warley Souza, Washington Oliveira, Wenceslao Trujillo, William Perkin, William Schauff, William Stewart, William Harvey, William Hernandez, Wullie Mitchell, Yakov Tchenak, Yfore Scott, Yohsuke Akamatsu, Yong-Ik Byun, Yozhi Nasvadi, Yuri Stepanychev, Zach Steele, Zané Smit, Zbigniew Krzeminski, Željko Andreić, Zhuoyang Chen, Zoran Dragić, Zoran Knez, Zoran Novak, Asociación de Astronomía de Marina Alta, Costa Blanca Astronomical Society, Perth Observatory Volunteer Group, Royal Astronomical Society of Canada Calgary Centre.

References

Drummond J. D. (1981). “A test of comet and meteor shower associations”. *Icarus*, **45**, 545–553.

Southworth R. B. and Hawkins G. S. (1963). “Statistics of meteor streams”. *Smithsonian Contributions to Astrophysics*, **7**, 261–285.

Šegon D., Vida D., and Roggemans P. (2023). “A possibly new meteor shower in Sagitta”. *eMetN*, **8**, 246–251.

Vida D., Gural P., Brown P., Campbell–Brown M., Wiegert P. (2019). “Estimating trajectories of meteors: an observational Monte Carlo approach – I. Theory”. *Monthly Notices of the Royal Astronomical Society*, **491**, 2688–2705.

Vida D., Gural P., Brown P., Campbell–Brown M., Wiegert P. (2020). “Estimating trajectories of meteors: an observational Monte Carlo approach – II. Results”. *Monthly Notices of the Royal Astronomical Society*, **491**, 3996–4011.

Vida D., Šegon D., Gural P. S., Brown P. G., McIntyre M. J. M., Dijkema T. J., Pavletić L., Kukić P., Mazur M. J., Eschman P., Roggemans P., Merlak A., Zubrović D. (2021). “The Global Meteor Network – Methodology and first results”. *Monthly Notices of the Royal Astronomical Society*, **506**,5046–5074.

GCR #1047 outburst of activity on February 15, 2024

Ivan Sergei

Mira Str.40-2, 222307, Molodechno, Belarus
astroseriv@yandex.by

Comparing CAMS data since 2021 for the date of the maximum activity of the gamma Crucids, the author noticed that the activity of this meteor shower was significant stronger on 15 February 2024 than the same date during the previous 3 years.

1 Gamma Crucids outburst in 2024

While comparing my visual meteor observations for the VMDB (IMO) with CAMS data, I noticed a strong concentration of unclassified radiants in the southern hemisphere at the boundary of the constellations Centauri and Southern Cross. I then contacted *Robert Lunsford* about a likely new shower. It turned out to be the gamma Crucids (GCR, #1024). There is data on this shower in Robert's article[6].

This meteoroid stream was detected by *P. Jenniskens* (2021), More information about this meteor shower can be found in the IAU MDC[7].

Since the maximum shower activity was expected on 15 February 2024, I looked at all the CAMS data since 2021 and concluded that the enhancement in activity on February 15 was the strongest since 2021.

Judging from the trend of the meteor shower activity according to CAMS data, the meteor shower activity is increasing every year, perhaps in 2025 video networks can detect even more meteor activity from this shower than in 2024.

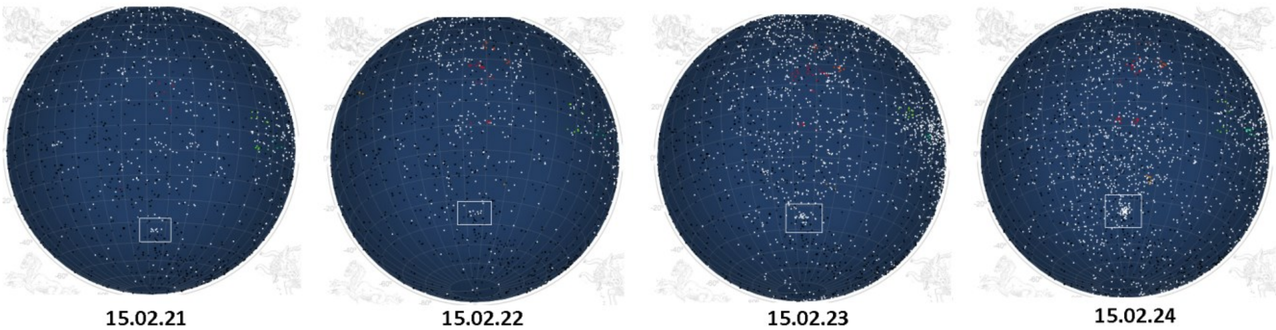

Figure 1 – Location of GCR #1047 radiant on February 15 from 2021 to 2024.

Acknowledgment

Thanks to *Paul Roggemans* for his help in the lay-out and the correction of this article. Thank you *Robert Lunsford* for the information.

References

Jenniskens P. (2021). "Gamma Crucid meteors 2021". CBET 9432. Ed. D. W. E. Green, Central Bureau for Astronomical Telegrams (issued Feb. 15, 2021).

[6] https://www.emeteornews.net/2024/02/09/meteor-activity-outlook-for-10-16-february-2024/
[7] https://www.ta3.sk/IAUC22DB/MDC2022/Roje/pojedynczy_obiekt.php?lporz=01534&kodstrumienia=01047&colecimy=0&kodmin=00001&kodmax=01223&lpmin=00001&lpmax=01712&sortowanie=0

Meteor shower data from video observation Part I Research methods and summary of survey results

Masahiro Koseki

The Nippon Meteor Society, 4-3-5 Annaka Annaka-shi, Gunma-ken, 379-0116 Japan
geh04301@nifty.ne.jp

The "Meteor Shower Database" created using data from the SonotaCo network was revised (Koseki, 2021) and expanded using the Global Meteor Network (GMN) data. The number of meteors used by GMN (Global Meteor Network) was 760874, significantly increasing from the previous 2007–2018 SonotaCo net's 284273 meteors. Furthermore, the number of meteor showers detected increased from 82 to 118 since observations of the southern sky were now included. The summarized data is shown in *Table 7*.

1 Introduction

About three years ago, we published "Meteor Shower Database" using data from the SonotaCo network (Koseki, 2021). Since then, the GMN[8] has become more active, including in the Southern Hemisphere, and meanwhile more than a million meteor orbits have been accumulated (Vida et al., 2019, 2020; 2021). This time, we decided to use GMN's data until February 2023 (downloaded 2023–02–25, at $00^h35^m46.416729^s$ UTC) to revise and expand the previously announced "Meteor Shower Database".

This paper consists of three parts: I. Research methods and survey results, II. Meteor showers that need to be examined carefully, and III. Radiant point distribution map and activity profile. In this Part I, the radiant point, geocentric velocity, and orbital elements at the maximum are shown in *Table 7*. In Part II, we explained meteor showers that may cause misunderstandings when consulted only in Parts I and III, focusing on those that are confusing in IAUMDCSD[9]. Part III will also touch on the differences in the "definitions of meteor showers" between SonotaCo[10] net and GMN[11].

We published in eMeteorNews a 10-level rating for every entry listed in IAUMDCSD (March 29, $20^h00^m00^s$ UTC, 2023 revised edition), and we will focus on those with a rating of 8 or higher. Basically, the average DR is 5 or more and the maximum number of meteors per day is 10 or more. We also considered some of the interesting activities that were below 7. The survey items are the same as last time, but the survey procedure will be explained using the Orionids as an example.

2 Research methods

2.1 Select data that appears to be representative for the IAUMDCSD list

If the described data are in good agreement, such as the Orionids, use the first report.

0008ORI00: $\lambda_\odot = 208.7°$, $\lambda - \lambda_\odot = 246.56°$, $\beta = -7.45°$

If there are discrepancies in the data listed, we use the best 10-level rating created earlier.

2.2 If the position of the radiant point ($\lambda - \lambda_\odot, \beta$) does not change with the solar longitude, we will create a temporary radiant point distribution and activity graph

Figure 1 (left) and *Figure 2* (left) show the radiant point distribution and activity graph using the original data as is. If the radiant point distribution is expressed in equatorial coordinates (α, δ), the drift of the radiant points becomes large, making it difficult to approximate the spherical coordinates of the celestial sphere with a straight line on a plane. By using ($\lambda - \lambda_\odot$, β) coordinates, the amount of movement is small, and a reasonable linear approximation is possible. The radiant point distribution shown here is based on data with an initial value of $\Delta\lambda_\odot = 10°$, that is $\lambda_\odot = 198.7°\sim218.7°$.

[8] https://globalmeteornetwork.org/data/traj_summary_data/
[9] https://www.ta3.sk/IAUC22DB/MDC2022/
[10] https://sonotaco.jp/doc/PDA/J14/
[11] https://globalmeteornetwork.org/projects/2023_gmn_shower_table/

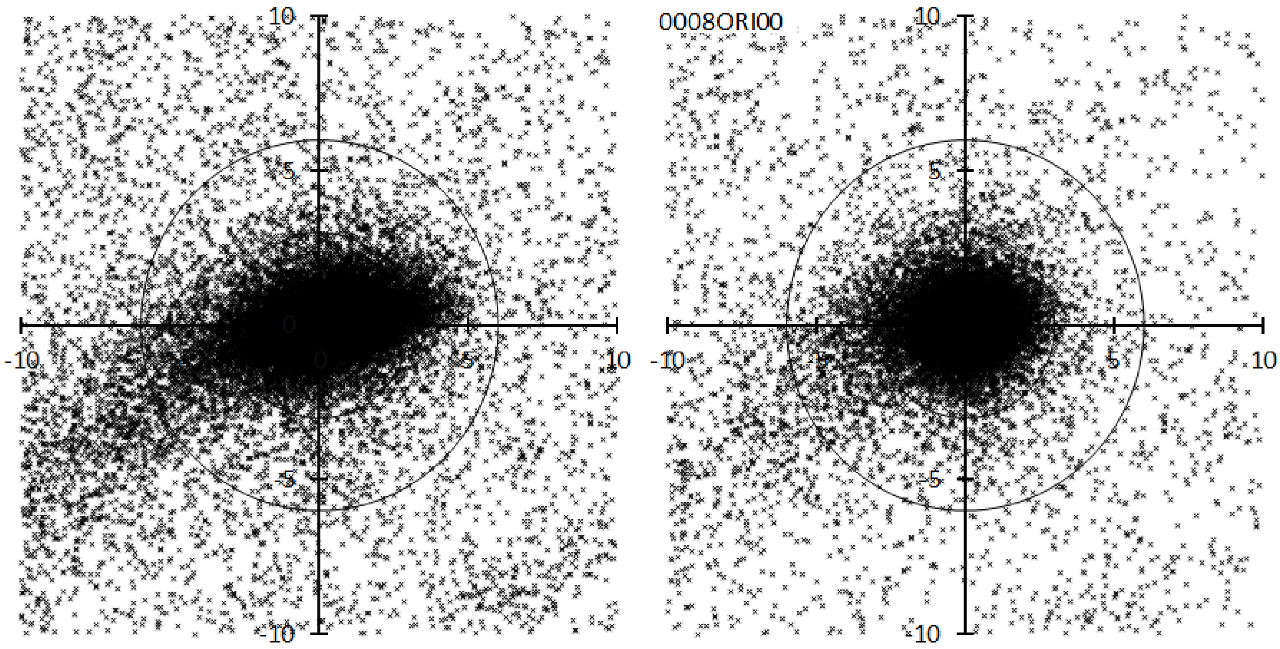

Figure 1 – The left side is the original data, and the right side is the one with the radiant point movement taken into account.

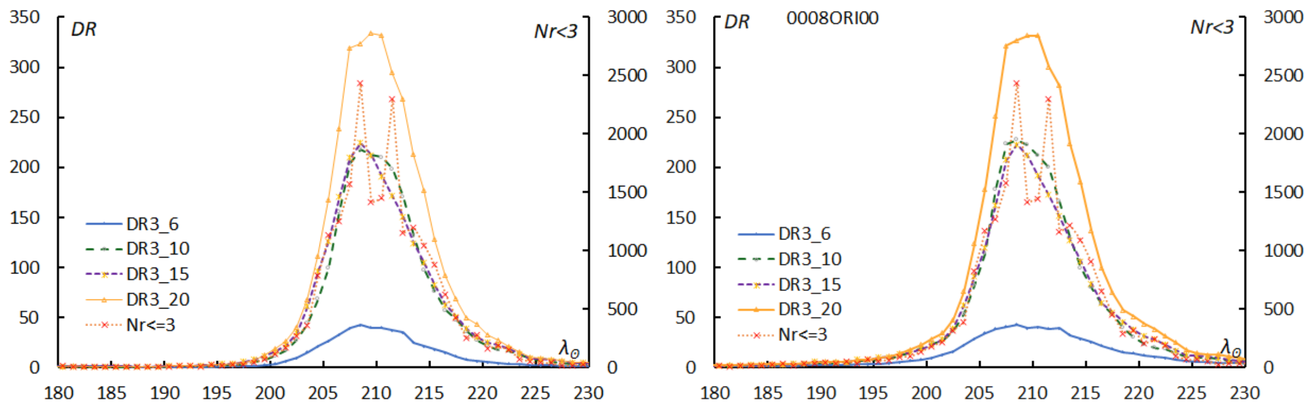

Figure 2 – The left side assumes that the radiant point is fixed in ecliptic coordinates, and the right side assumes that the radiant point moves.

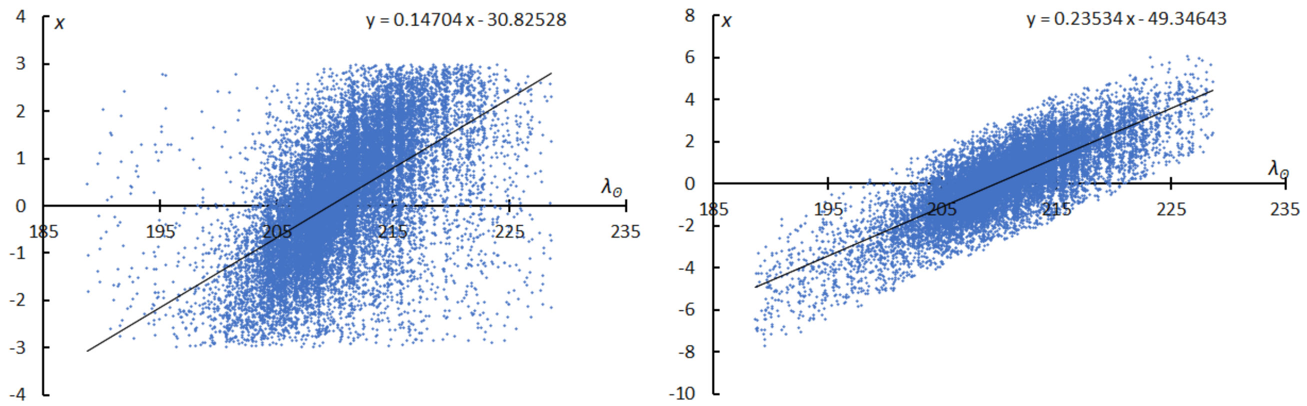

Figure 3 – Changes in the *x*-coordinate of the radiant point depending on the solar ecliptic longitude. The left is the original data, and the right is the converged state of the regression analysis.

2.3 For the activity period estimated from the activity graph, we use a regression analysis to find changes in the position of the radiant point ($\lambda - \lambda_\odot$, β) and the geocentric velocity with the solar ecliptic longitude

Judging from the activity graph, $\Delta\lambda_\odot = 10°$, which we used as the initial value, is appropriate, so we perform a regression analysis for observations in this range. We use data within 3 degrees from the center and ±3 (km/s) from the regression line of the geocentric velocity.

The distribution before the analysis is cut off at the top and bottom because the radius of the radiant point is set to 3 degrees and does not include the entire movement of the radiant point (*Figure 3*, left). After several operations, the regression line converges to a constant value (*Figure 3*, right).

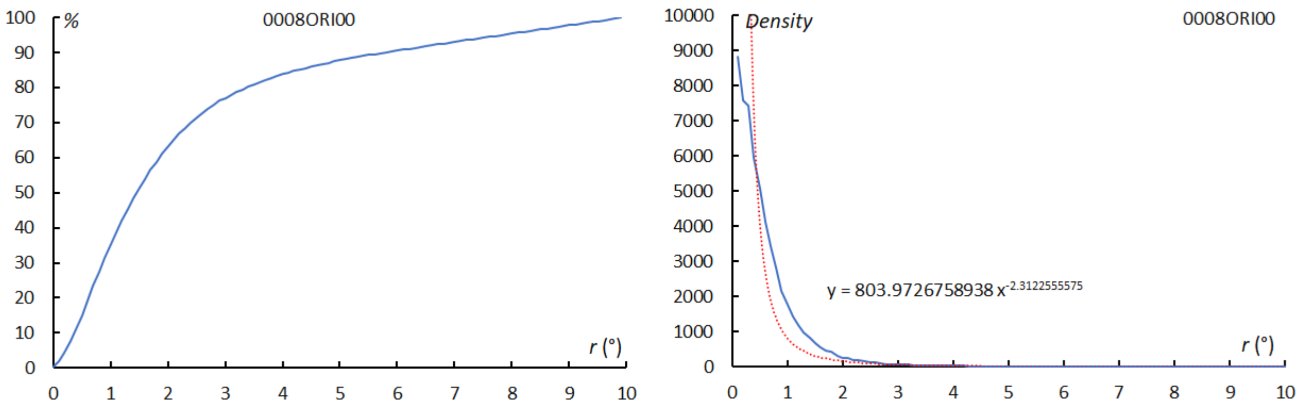

Figure 4 – The total number of radiant points within 10 degrees from the center against the ratio of the number of radiant points to each distance (left). The change in radiant density with the distance in steps of 0.1 degrees (right).

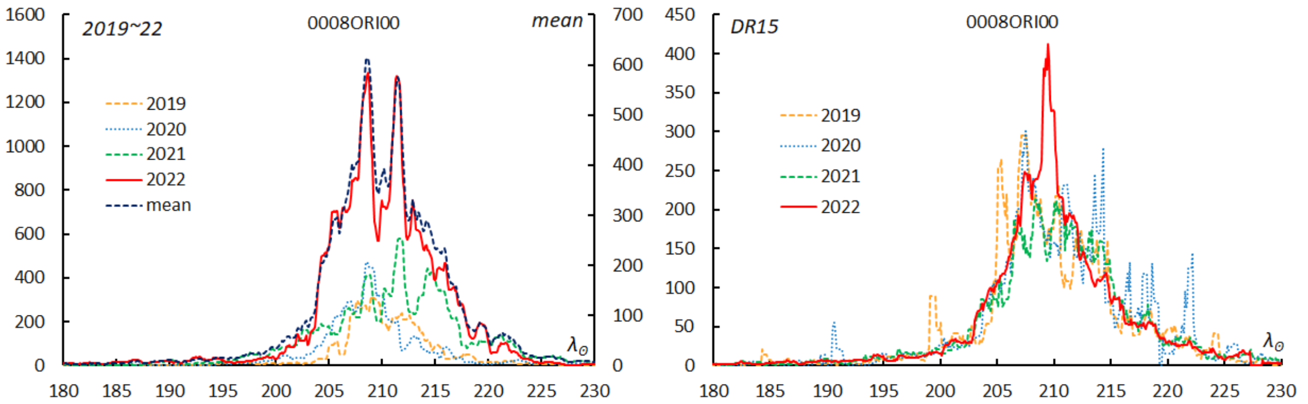

Figure 5 – Activity curve by year. On the left is the change in the number of meteors determined to be part of the Orionid group. The image on the right is corrected by *DR*.

2.4 A radiant point distribution map and activity profile are created based on the determined radiant shift

Figures 1 and 2 (both right) show the recalculations of the radiant distribution and activity curve using the estimates of radiant movement obtained by regression analysis, respectively. The radiant distribution is almost circular, and the so-called "tail of the Orionis" is clearly visible. Furthermore, as shown in *Figure 4* (left), 80% of the radiant points of the Orionids are included within 3.0 degrees, and 90% when included up to 5.6 degrees. This shows the validity of considering radiant points within 3 degrees from the center to belong to a meteor shower.

Figure 4 (right) shows the change in radiant point density with distance from the center, and the change is almost exponential. The structure of radiant points is actually complex, and it is best not simply expressed as an exponential function, but by expressing it in the form of $N = a*r^b$, it is possible to give a certain index of the density and spread of the radiant point distribution; when r is the distance from the radiant, a and b can be indicators of the density of the radiant at the center and how the radiant spreads, respectively.

Although the activity curves in *Figure 2* are similar, it is possible to trace activity even outside the survey period $\lambda_\odot$ =198.7°~218.7°, and the values for *DR* and Nr <= 3 are increasing. It is necessary to consider which of the activity curves in *Figure 2* (right) best represents the activity. Two conditions need to be taken into consideration: one is that if the number of meteors is used as is, it will be affected by observation conditions (weather, etc.), and the other is that even if *DR* is used to alleviate the influence of observation conditions, it will be affected by the influence of the nearby activity of meteor showers.

Figure 5 (left) gives the activity profile based on the number of meteors expressed as a moving mean of 0.1 degrees in 1-degree width in solar longitude. *Figure 5* indicates the cause of the problem in which Nr <= 3 (the number of Orionid meteors), *Figure 2* shows two maxima. *Figure 5* (left) shows that the observations of 2022 dominate the average value among GMN observations. We should be careful that the content of this paper is dominated by the 2022 observations (or 2023 if there are 2023 observations) because the number of GMN observations is increasing exponentially. Observations of the Orionids in 2022 show two maxima in *Figure 5* (left), but a single maximum in *DR15* in *Figure 5* (right). This suggests that the influential Western observations of GMN were obstructed for some reason (probably the weather), and it shows that the two maxima were spurious.

If the number of meteors itself is used carelessly in this way, it will lead to incorrect conclusions, so it is necessary to use *DR* correction together. However, as mentioned earlier, *DR*s are affected by surrounding meteor activity. *Figure 6* shows the change in the number of radiant points within a

0.1-degree wide ring depending on the distance from the center, considering the radiant shift. The number of radiant points of the Orionids decreases when moving away from the center but starts to increase again from around 6 degrees. This is a natural increase due to an increase in the surface of the 0.1-degree wide ring. The slight increase around 15 degrees is due to the EGE meteor shower, and the increase after 45 degrees is due to the STA and NTA radiants. The activity of the Orionids is very strong and is not affected by EGE much, but it is a point that should be taken into consideration when obtaining the activity profile of the weak meteor shower. In the case of the Orionids, it is clear from *Figure 2* (right) that *DR3_6* is inappropriate, and *DR3_10* would be better to avoid the impact of EGE. The area of the ring used for *DR* calculation increases as the distance from the center increases, and therefore the number of radiant points also increases. If the surrounding meteor activity level is low, the larger the number of meteors, the smaller the variation in *DR*. In such a case, *DR3_20* is the most appropriate.

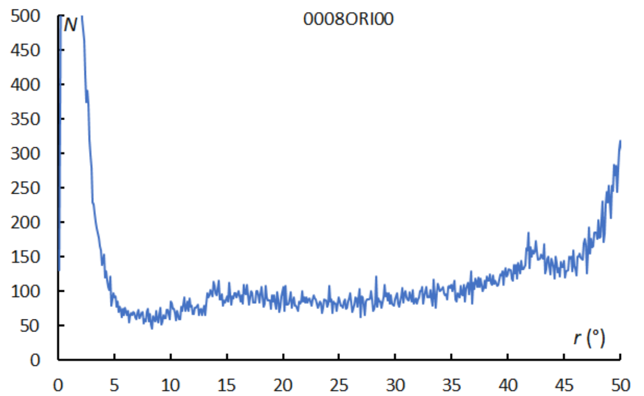

Figure 6 – The change in the number of radiant points every 0.1 degree depends on the distance from the center considering the movement of the radiant point.

Regardless of whether *Nr* <= 3 or *DR* is taken, the activity profile obtained is not smooth because the activity of the meteor shower cannot be constant from year to year, and the observation conditions vary. A simplified model of the structure of meteoroid streams is used to estimate the average activity curve.

The model A: The direction of the perihelion and the size of the orbit are assumed to be constant, the orbital plane of the meteoroid stream rotates around the direction of the perihelion, and the eccentricity changes, so the meteor shower activity can be seen at different solar longitudes.

The rotation model: The size and shape of the orbit (eccentricity) are assumed to be constant, and the orbital plane of the meteor stream rotates along the ecliptic plane (the ecliptic latitude of the perihelion is constant), so the meteor shower is active even at different solar longitudes.

We apply the D-criterion, which is often used to determine the attribution of meteor showers, to these two models. The Southworth-Hawkins D-criterion (1963) is expressed in the following form:

$$D^2 = (\Delta S)^2 + (\Delta V)^2 + (\Delta P)^2 + (\theta)^2$$

Where:

- ΔS is the difference in orbit shape;
- ΔV is the difference in orbit size;
- ΔP is the difference in perihelion direction;
- θ is the intersection angle of mutual orbital planes.

For the A model, the second and third terms are considered constant, so the first and fourth terms are used, and for the rotation model, the first and second terms are considered constant, so the third and fourth terms are used. The coefficient of each term is 1 in the D-criterion, but here we assign coefficients C_1 and C_2 to the terms used, respectively. Also, in the D-criterion, the power of each term is fixed at 2, but the power C_3 is added to the entire sum of two terms. By adjusting the coefficients and powers, almost the same activity profiles for the A model and the Rotation model can be obtained for the Orionids (*Figure 7*). *Table 1* shows the coefficients used in the estimated profiles shown in *Figure 7* for the Orionids. It should be noted that since model A and the rotation model use different terms, it is meaningless to compare C_1 and C_2 between them.

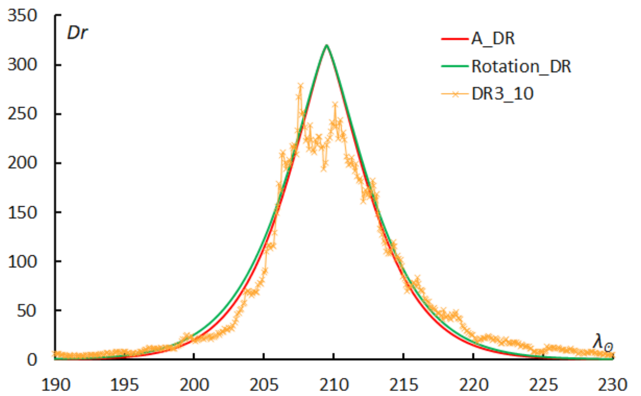

Figure 7 – The Orionid group activity curve according to the different model estimates.

Table 1 – Coefficients used to represent the estimated profile in *Figure 7*.

	C_1	C_2	C_3	$\lambda_\odot$	*Max*
A	37	37	1.3	209.5	320
Rotation	10	10	1.3	209.5	320

2.5 Estimation of the radiant point and orbit calculation

It is easy to convert the movement of the radiant point in (x, y) coordinates to ($\lambda - \lambda_\odot$, β) and then to (α, δ) coordinates, and when combined with the estimated value of the geocentric velocity, orbit changes can also be estimated. Coordinate transformation and orbit calculation methods are also extensively described elsewhere, so they will be omitted here. Changes in the radiant point, geocentric velocity, and orbital elements of the Orionids are shown in *Table 2*.

Table 2 – The radiant point, geocentric velocity, and orbital elements of the Orionids.

$\lambda_\odot$	λ–$\lambda_\odot$	β	α	δ	v_g	e	q	i	ω	Ω	λ_π	β_π	a
190	251.3	–8.8	81.2	14.3	66.9	0.91	0.703	162.6	67.9	10	303	16.1	7.8
191	251.1	–8.8	81.9	14.4	66.9	0.909	0.696	162.7	68.8	11	303.1	16.1	7.69
Omitted													
205	247.7	–7.8	92.7	15.6	65.9	0.913	0.591	163.6	81.5	25	303.8	16.3	6.76
206	247.4	–7.8	93.5	15.6	65.8	0.913	0.583	163.6	82.4	26	303.9	16.2	6.73
207	247.2	–7.7	94.3	15.7	65.7	0.914	0.576	163.7	83.3	27	304	16.2	6.7
208	246.9	–7.6	95.1	15.7	65.7	0.915	0.568	163.7	84.1	28	304.1	16.2	6.68
209	246.7	–7.6	95.9	15.7	65.6	0.916	0.561	163.8	85	29	304.2	16.1	6.66
210	246.5	–7.5	96.6	15.8	65.5	0.917	0.553	163.9	85.9	30	304.3	16.1	6.64
211	246.2	–7.4	97.4	15.8	65.4	0.918	0.546	163.9	86.7	31	304.4	16	6.63
212	246	–7.4	98.2	15.8	65.4	0.919	0.539	164	87.6	32	304.5	16	6.62
213	245.7	–7.3	99	15.9	65.3	0.92	0.531	164.1	88.4	33	304.7	15.9	6.61
214	245.5	–7.2	99.8	15.9	65.2	0.921	0.524	164.1	89.2	34	304.8	15.9	6.6
Omitted													
229	241.8	–6.2	111.5	15.7	64.2	0.94	0.417	165.2	101.2	49	307.4	14.5	6.93
230	241.6	–6.1	112.3	15.7	64.1	0.941	0.41	165.3	102	50	307.6	14.4	6.98

It is noteworthy that the perihelion direction (λ_π, β_π) and the semimajor axis a of the Orionids remain almost constant. There are many cases where the perihelion direction and semi-major axis of the orbit change significantly.

In *Section 2*, we have shown the coordinates of the center used in calculations and the change of the radiant point in (x, y) coordinates and the geocentric velocity, so we will only show the radiant point and trajectory at the estimated maximum.

2.6 Investigation of nearby activities

Figure 8 shows the meteor showers listed in the IAUMDSD under the same conditions as *Figure 1* (right). The red squares are registered as the Orionids and are well concentrated in the center. Among minor meteor showers, even those registered in the IAUMDCSD vary greatly, often in a confusing way. Crosses indicate that other names have been given in IAUMDCSD.

Table 3 – Meteor showers recorded in the IAUMDCSD in the same area as *Figure 1* (right).

Code	$\lambda_\odot$	λ–$\lambda_\odot$	β	v_g	x	y
0718XGM00	206	250.9	–10.6	68.1	–3.37	–2.81
1198XRO00	207.1	245.7	–7.7	50.3	1.47	–0.04
0008ORI03	207.5	247.1	–7.9	66.4	–0.01	–0.18
0008ORI04	207.9	247.5	–7.8	66.2	–0.48	–0.19
0008ORI05	208	247.4	–8.1	65.4	–0.42	–0.5
0008ORI01	208.6	246.6	–7.4	66.2	0.15	0.16
0008ORI00	208.7	246.6	–7.5	66.5	0.21	0.15
0008ORI06	209	246.7	–7.6	66.3	–0.03	–0.04
0008ORI02	209.8	246.3	–7.2	66.4	0.2	0.31

1198XRO is located within 3 degrees from the center (x, y) = (1.47, –0.04). Since it was 15km/s slower than the Orionids, v_g = 50.3, it was probably considered as a different activity. The existence of separate groups has been argued because of the difference in geocentric velocity between the main activity, but neither has been confirmed. This will probably be the same case here. 0718XGM is a member of the so-called "tail of the Orionids" and careful discussion will be necessary as to whether they should be recognized as an independent meteor showers.

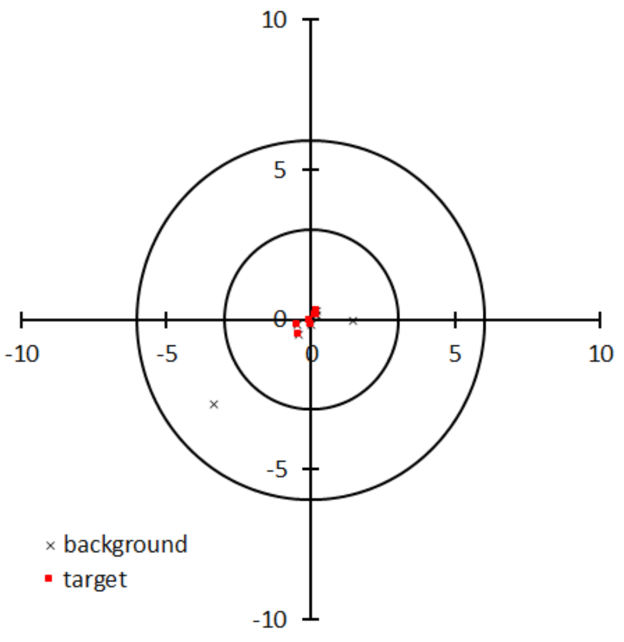

Figure 8 – Meteor showers listed in the IAUMDSD.

3 Summary of survey results

Tables 4 to 7 summarize the results for the 118 meteor showers investigated.

Table 4 gives the data that served as the starting point for the survey and the changes in the radiant point and geocentric velocity depending on the solar longitude. If you have these numbers and the original GMN data, you can reproduce the numbers from *Table 5* onwards. Code represents the IAU numeral code + IAU 3 letter code + AdNo. The reason why Table 4 is not in the order of solar longitude is that it has been adjusted to the order of maximum solar longitude determined by the modeling shown in *Table 7*. $\lambda_\odot$, $\lambda-\lambda_\odot$ and β are the values for radiant points listed in the IAUMDCSD, and the following investigation is conducted using these as the starting point. However, if they are not suitable as the origin, it will be changed and indicated in italics. Δr and $\Delta\lambda_\odot$ are the scope of attribution judgment and investigation period The movement of the radiant point is approximated by a straight line on a coordinate system centered on this origin, with the direction in which the ecliptic longitude decreases along the ecliptic latitude line as the positive x-axis and the direction in which the ecliptic latitude increases along the ecliptic longitude line as the positive y-axis. Then, x_a, x_b, y_a, and y_b are the coefficients and constant terms of the approximate straight line. Similarly, v_a and v_b are coefficients and constant terms that are linear approximations of the geocentric velocity. Please refer to the previous section for the specific examples of the Orionids, including the items in the table below.

Table 4 – Radiation points as the starting point of the survey, survey period, and the change in radiant point and geocentric velocity obtained by regression analysis.

Code	Origin					Radiant shift					
	$\lambda_\odot$	$\lambda-\lambda_\odot$	β	Δr	$\Delta\lambda_\odot$	x_a	x_b	y_a	y_b	v_a	v_b
0647BCO00	*13.3*	175.25	29.14	3	10	0.1114	–0.889	0.3953	–4.1319	–0.0341	27.0738
0040ZCY01	16	300.11	59.08	3	5	–0.0665	0.8988	–0.1696	2.6972	0.0498	42.6984
0841DHE00	19.5	232.08	46.26	3	5	–0.0808	1.6894	–0.1706	3.5906	0.0659	47.9721
0450AED00	20.2	292.83	29.85	3	5	–0.0907	1.5561	0.2029	–3.853	–0.0931	62.4424
0839PSR00	25.1	211.69	34.29	3	5	–0.3084	7.875	–0.2934	7.6928	0.4016	35.135
0021AVB06	27.6	170.32	12.03	3	10	0.4675	–12.7715	0.2377	–6.2633	–0.1712	23.9921
0040ZCY02	32	299.63	57.79	3	5	0.6056	–18.7925	0.1266	–3.6641	–0.2587	49.9125
0006LYR00	32.2	241.39	56.72	3	5	–0.3003	10.0005	–0.3615	11.6821	0.2763	37.6836
0343HVI07	39.2	166.63	–1.2	3	5	0.6749	–25.9303	–0.1702	6.4895	–0.2917	29.7599
0348ARC01	*42*	311.73	56.56	3	5	–0.6159	23.8141	0.0831	–3.3468	–0.2936	52.9007
0519BAQ00	46.3	278.91	13.47	3	5	0.0807	–3.973	–0.006	0.0891	–0.0807	71.8886
0031ETA07	47	293.28	7.68	3	10	0.2451	–11.5905	0.055	–2.4999	0.0423	63.5525
0531GAQ01	49.8	262.44	32.44	3	5	–0.1847	8.8321	–0.0961	5.4252	0.0751	58.38
0854PCY00	53.8	276.79	71.98	3	10	0.2031	–10.4586	–0.0431	1.6777	0.0308	37.8613
0145ELY02	50	256.73	63.97	3	5	0.3748	–18.641	0.0156	–0.2332	0.025	42.6992
0520MBC00	56.8	244.94	4.28	3	10	0.2167	–12.7955	–0.036	2.5228	–0.0625	69.136
0061TAH	68	125	32	3	3	0.5295	–37.0384	5.4157	–371.208	0.326	–11.2406
0860PAN00	71.6	307.92	43.24	2	3	0.275	–19.1996	0.3804	–27.0442	–0.1867	63.8194
0362JMC01	71	324.61	43.4	3	10	–0.1635	12.5697	0.3048	–21.7102	–0.1378	52.6056
0171ARI03	77	331.58	7.34	3	10	0.3638	–27.9298	–0.0141	1.5546	0.0781	34.5427
0458JEC00	82.3	248.13	47.78	3	3	–0.4362	35.3057	–0.2748	22.7932	0.1986	36.3117
0510JRC00	84	262.78	54.43	3	3	0.0372	–2.7745	–0.162	14.5395	0.0859	42.5144
0069SSG03	90	185.16	–4.67	3	10	0.4559	–41.1943	0.0322	–4.6239	–0.1244	36.0361
0170JBO07	89.64	102.98	59.03	3	3	1.3028	–116.749	0.2386	–21.1976	0.1806	–2.3079
0410DPI00	92	280.17	0.75	3	5	0.2026	–18.6893	–0.0231	2.4041	–0.0906	78.0196
0459JEO01	89	155.38	12.42	3	5	0.8038	–71.308	0.3671	–33.0682	–0.1571	28.1574
0431JIP00	94.456	252.88	37.39	3	3	–0.9655	91.2422	–0.5911	56.0458	–0.1943	76.8147
0867FPE00	96.7	254.6	16.38	3	3	0.155	–15.1602	0.8084	–77.8719	–0.4798	112.6566
0372PPS_0	95	283.28	15.27	3	5	0.1076	–10.275	0.1131	–10.3518	0.01	65.3255
0164NZC03	101	209.69	12.71	3	15	0.108	–10.6845	0.0367	–3.9905	–0.1068	49.682
0370MIC00	*100*	209.87	–12.2	3	10	0.1416	–13.3029	–0.0707	9.0276	–0.1032	50.488
1133TCS00	105.1	303.93	52.75	3	5	–0.1759	18.5893	0.1755	–18.4183	–0.1716	64.2561
0411CAN00	*105*	298.06	33	3	10	–0.052	5.3959	0.0934	–10.0424	–0.1091	68.5495
0175JPE02	110.9	244.09	14.49	3	10	0.1214	–13.7635	–0.1099	12.1921	–0.0364	67.7813

Code	Origin					Radiant shift					
	$\lambda_{\odot}$	$\lambda-\lambda_{\odot}$	β	Δr	$\Delta\lambda_{\odot}$	x_a	x_b	y_a	y_b	v_a	v_b
0444ZCS00	113.2	277.79	42.82	3	3	–0.3796	43.0291	–0.3564	40.3444	0.1145	44.1326
0533JXA00	119	282.02	–4.77	3	10	0.2315	–27.8444	0.012	–2.1535	0.0638	61.4211
0623XCS00	*115*	*185*	*8*	1.5	5	0.2066	–24.1731	0.025	–2.5507	–0.0952	36.1377
0372PPS_1	120	278.96	15.98	3	5	0.2976	–36.4379	–0.4713	57.1145	0.1406	49.5335
0184GDR00	125.3	167.84	73.73	3	3	0.3917	–49.0047	0.1612	–20.5705	–0.0961	39.6404
0001CAP06	126.1	179.64	9.72	3	5	0.3548	–43.9871	0.1272	–15.9994	–0.1677	43.393
0005SDA00	127.2	208.56	–7.44	3	5	0.2687	–33.9557	–0.1063	13.5181	–0.1965	65.2986
0191ERI02	137	260.26	–27.26	3	15	–0.0024	0.5483	0.0019	–0.4129	0.0015	63.9874
0465AXC00	135.8	252.41	41.99	3	3	–0.8	108.6428	–0.1896	26.2828	0.3021	14.5402
0007PER00	137	283.15	38.27	3	15	–0.0406	5.5172	–0.0661	9.335	0.0129	56.9855
0012KCG	142	168	74	3	5	–0.3753	54.7644	0.6381	–93.1013	0.2353	–10.8706
0199ADC01	143.1	180.04	2.33	3	3	–0.0479	6.8369	–0.2221	31.8215	0.2127	–6.7381
AXD	*145*	*142.5*	*77.47*	3	5	0.2082	–30.4049	1.0378	–147.406	0.2001	–7.6101
0026NDA10	144.8	207.24	6.81	3	10	0.0682	–9.7592	0.0382	–5.4769	–0.1244	56.4329
ZDR	*155*	*30.19*	*83.82*	3	5	–0.0627	7.5381	–0.8019	124.0229	–0.2273	56.7222
0523AGC00	155.1	263.11	63.51	3	5	–0.1546	23.9816	–0.0714	11.2097	0.0936	29.3975
0206AUR03	159	292.45	15.57	3	5	0.0855	–13.6587	0.1356	–21.2819	–0.022	68.9463
0552PSO01	159	269.53	–24.3	3	10	–0.1719	29.5186	–0.0368	5.9337	–0.0001	65.5639
0694OMG00	164	307.13	16.76	3	10	0.1819	–29.6546	–0.0895	14.9512	0.1782	29.0183
0337NUE00	167.9	259.26	–20.67	3	15	0.1213	–19.9298	0.2203	–37.1078	0.0517	56.8959
0208SPE02	168	248.97	20.79	3	5	0.0415	–7.0712	–0.2061	34.7059	0.036	58.0022
0215NPI04	176	196.75	3.87	3	15	0.1894	–31.67	–0.0021	0.3102	–0.0687	40.1538
0081SLY00	*169*	294.7	32.27	3	5	–0.1719	28.9685	0.2176	–35.7013	–0.183	89.7565
0757CCY00	171.64	142.43	51.4	3	5	0.6923	–118.646	1.3672	–235.88	0.0295	9.5829
0221DSX04	188	331.25	–11.32	3	5	0.1299	–23.8991	–0.2572	48.3283	–0.1272	56.3114
0081SLY01	186	278.78	25.99	3	5	0.1003	–18.0282	–0.1652	29.5384	0.1175	43.8318
0281OCT00	193	279.98	61.97	3	3	1.1864	–229.216	0.1633	–31.4408	–0.9496	228.6515
0924SAN00	196.7	214.37	29.45	3	5	–0.0063	1.188	0.1951	–37.9924	–0.0398	24.7732
0825XIE00	196.1	227.54	–27.12	3	5	–0.0183	3.0992	–0.1149	22.0415	–0.1092	75.846
0002STA_SE	*202.6*	*194.82*	*–4.45*	3	5	0.1977	–40.8473	–0.0345	7.0159	–0.0968	48.2632
0333OCU00	202.1	278.86	46.82	3	5	–0.571	115.4577	–0.0059	1.1627	–0.0587	67.3791
0023EGE00	209.7	253.48	4.2	3	10	0.2135	–44.9085	–0.0613	13.3966	–0.0354	75.9489
0022LMI03	209	297.96	25.93	3	5	–0.023	4.7739	0.1067	–22.0377	–0.0724	76.4444
0480TCA_OML	*210.5*	*283.37*	*13.63*	3	15	0.2173	–45.5829	0.2711	–56.9822	0.0046	66.0806
0008ORI00	208.7	246.56	–7.45	3	10	0.2418	–50.662	0.0682	–14.3876	–0.0714	80.5061
0524LUM00	215	284.08	36.9	3	5	–0.0562	11.8263	–0.2106	45.0985	0.0133	57.6923
0526SLD00	221.6	265.65	53.89	3	3	–0.2732	60.7616	–0.51	112.5384	0.3182	–21.5505
0002STA_SF	*221.5*	*190.7*	*–5*	2	5	0.4893	–110.27	–0.0676	15.4866	–0.3282	101.4279
0445KUM00	225	268.21	29.76	3	5	0.011	–2.2506	–0.1798	40.0375	0.0387	56.2142
0338OER_DGE	*225*	*186.62*	*–18.2*	6	25	0.3021	–67.8047	–0.2913	64.4547	–0.1381	59.5427
0018AND01	228.6	163.43	18.81	3	15	0.4525	–103.95	0.583	–131.503	–0.129	47.1005
0512RPU00	223	266	–43.46	3	10	–0.2728	59.1409	0.2348	–53.2242	0.1975	12.7893
0017NTA03	222.7	192.77	2.85	3	20	0.2493	–55.8429	0.0068	–1.9411	–0.125	56.6041
0013LEO00	235.2	271.83	10.22	3	10	0.3128	–74.3409	–0.1568	37.014	0.0475	58.5456
0394ACA00	247	215.81	–40.29	3	10	–0.0376	8.2361	0.3104	–75.8768	0.1184	15.3703
0246AMO00	239	239.65	–19.91	2	5	0.0288	–6.7519	0.0655	–15.7132	–0.1309	93.095
0488NSU00	241.6	244.91	42.93	3	3	–0.4783	115.4909	–0.3742	90.7317	0.5148	–70.0019
0250NOO06	247	203.59	–8.24	3	10	0.3154	–78.0349	–0.0617	15.4998	–0.154	80.7632

Code	Origin					Radiant shift					
	λ_O	$\lambda-\lambda_O$	β	Δr	$\Delta\lambda_O$	x_a	x_b	y_a	y_b	v_a	v_b
0257ORS03	243	190.78	–4.69	3	5	0.1671	–40.4572	0.0213	–5.2689	–0.0716	45.0609
1096NAC00	246.2	285.89	–19.99	3	5	0.0303	–7.8055	0.1777	–44.3511	0.1128	38.8415
0340TPY00	249.4	261.96	–39.09	3	3	–0.2619	65.8754	0.3503	–87.6017	0.3206	–19.856
0336DKD01	252	243.06	61.66	3	5	–0.3642	91.4251	0.0718	–18.1264	0.068	26.7305
0339PSU01	253	258.89	34.52	3	10	–0.1293	33.2236	–0.1445	37.3849	0.1253	29.367
0334DAD00	256.5	266.12	62.96	3	15	–0.3261	83.5243	0.0121	–3.3008	0.0057	39.1135
0016HYD01	259.1	229.92	–16.76	3	20	0.1092	–28.8909	–0.0107	2.9956	–0.07	76.6474
0502DRV00	252.5	286.95	13.84	3	10	0.1498	–37.4094	0.2763	–69.4976	0.0398	58.0096
0529EHY00	*260.7*	*237.33*	*–14.7*	3	20	0.12	–31.1678	0.0405	–10.472	–0.042	72.8472
0255PUV00	254	258.16	–60.51	3	10	–0.3877	94.6079	–0.1294	31.7667	–0.0332	50.1627
0019MON01	261.5	202.13	–14.81	3	15	0.3146	–81.5491	–0.0659	17.0315	–0.173	86.0296
0004GEM00	261.6	207.94	10.4	3	10	0.1016	–26.6594	–0.0462	12.2033	0.1051	6.3179
0335XVI00	256.7	292.67	–4.56	3	15	0.247	–63.8677	–0.0526	13.2224	0.072	49.1877
0497DAB00	263.9	298.47	33.45	3	5	–0.0514	13.8764	0.3223	–85.6914	–0.1539	99.9159
0340TPY01	264	259.58	–33.53	3	5	–0.0569	15.0139	0.3278	–85.9806	0.2346	1.0001
0020COM03	275.9	242.79	20.53	3	30	0.0465	–12.5646	–0.0698	19.2142	–0.0055	64.2899
0015URS01	271	218.48	72.07	3	5	0.0334	–9.1414	0.5758	–155.805	–0.2288	94.9921
0428DSV00	267.41	293.72	14.78	3	30	0.1307	–35.1538	0.1089	–29.3136	0.0201	60.6018
0784KVE00	276	257.77	–60.48	3	5	–0.6225	170.2818	0.1063	–28.3692	0.2457	–24.2441
0319JLE00	282.5	219.77	10.41	3	5	0.3376	–94.8099	0.0608	–17.3523	–0.4394	175.6707
0010QUA00	283.28	276.97	63.58	3	10	0.1717	–48.5025	0.2691	–76.0478	–0.2153	101.4334
0331AHY00	285.5	206.75	–25.99	3	10	0.2751	–79.1128	–0.0453	12.6156	–0.1425	84.0134
0515OLE00	*290*	207.98	–6.91	3	5	0.2457	–72.0572	–0.2923	83.8488	–0.1049	76.771
0323XCB04	296	306.92	51.36	3	5	0.1063	–31.595	0.1704	–50.7995	–0.0667	65.0871
0341XUM06	298.4	218.3	25.85	3	5	0.4109	–122.504	–0.3088	92.1558	0.1963	–17.6211
0404GUM04	299.7	217.38	74.32	3	5	–0.6969	208.5355	0.1979	–59.1513	0.2712	–51.9283
0429ACB00	309.89	271.81	44.48	3	5	–0.521	160.507	–0.6344	195.3062	0.3573	–52.7269
0110AAN04	312	210.6	–17.67	3	10	0.054	–17.2448	–0.0392	12.517	–0.0408	56.6646
0427FED00	315.1	228.34	76.59	3	5	0.6447	–203.526	–0.0605	18.4312	–0.2357	109.3789
1032FHY00	324.3	161.57	–17.83	3	5	0.3352	–108.279	–0.6002	194.2505	–0.0559	34.306
1166TTR00	331.9	285.23	–44.22	3	5	–0.6675	221.5964	0.2326	–76.9744	–0.0972	88.6073
0915DNO00	333.7	271.99	–24.95	3	5	0.1423	–47.1462	0.0408	–13.5988	–0.0791	93.1613
0571TSB00	344	221.78	36.5	3	5	0.8277	–283.702	0.225	–77.0865	–0.5564	240.642
0346XHE01	350	244.94	70.58	3	5	–0.7215	252.5716	–0.0416	14.8965	0.0511	16.4979
0011EVI06	357.2	186.68	5.39	3	10	0.2417	–86.8488	0.0442	–15.9647	–0.1314	74.294
0893EOP00	358	262.63	6.72	3	10	0.2195	–78.7953	–0.0268	9.5359	–0.0295	81.3416

Table 5 provides an overview of the radiant distribution and activity profile. The radiant density shows the coefficients *a* and *b* when the radiant point distribution density corrected for the radiant shift is approximated by an exponential function $N = a*r^b$ of the distance *r* (degrees) from the center. The columns from *Nr* < =3 to *DR3_20* show the solar longitude at the maximum and the maximum value using five different methods. The activity of a meteor shower is expressed by an increase or decrease in the number of meteors classified as shower members. Most of the attributed meteors are within 3 degrees of the estimated position in many meteor showers. *Nr*< = 3 indicates the maximum solar longitude and its maximum value for meteors within 3 degrees from the estimated radiant. In many cases, this is sufficient, but in some cases, there is a bias in the observation itself, so correction is necessary. In this paper, the correction is made by taking the ratio of the number of meteors within 3 degrees from the center and the number of surrounding meteors. The items following *DR3_6* are based on the ratio of the number of meteors within 3 degrees to the number of surrounding meteors per unit area (square degree). *DR3_6* uses meteors at 3 to 6 degrees from the center, *DR3_10* at 6 to 10 degrees, *DR3_15* at 10 to 15 degrees, and *DR3_20* at 15 to 20 degrees for comparison. It is necessary to use these values depending on the activity of the surrounding meteor

shower. The values shown in *Table 5* are based on a moving average of 3 degrees in solar ecliptic longitude.

Table 5 – Radiant distribution and activity profile.

Code	Radiant density		*Nr*< = 3		*DR3_6*		*DR3_10*		*DR3_15*		*DR3_20*	
	a	*b*	λ_{Θ}	*max*	λ_{Θ}	*max*	λ_{Θ}	*max*	λ_{Θ}	*max*	λ_{Θ}	*max*
BCO	5.66	–0.875	14.5	12	13.5	5.6	14.5	8	15.5	8.5	15.5	5.9
ZCY_0	5.83	–0.746	18.5	20	15.5	2.2	14.5	5.4	12.5	8.5	19.5	9.3
DHE	3.97	–1.137	19.5	23	19.5	8.1	19.5	11.7	19.5	9.4	20.5	5.3
AED	1.96	–1.552	17.5	22	23.5	13.5	21.5	12	18.5	13.3	18.5	12.3
PSR	4.12	–1.112	25.5	27	25.5	5.5	24.5	10	24.5	19.5	24.5	13.5
AVB	14.49	–1.052	17.5	27	23.5	6.5	28.5	9.1	23.5	8.7	28.5	8.4
ZCY_1	6.09	–0.669	32.5	20	29.5	1.5	32.5	4.3	32.5	7.5	32.5	11.2
LYR	122.8	–2.177	32.5	1326	33.5	31.9	32.5	184.7	32.5	214.4	32.5	314.8
HVI	8.93	–1.232	39.5	43	38.5	10.2	39.5	11.5	39.5	15.5	39.5	15.1
ARC	4.52	–1.035	40.5	17	46.5	6	41.5	13.1	41.5	14.2	40.5	12.8
BAQ	4.18	–1.151	43.5	14	42.5	9.3	42.5	9.9	41.5	3.9	50.5	1.2
ETA	148.56	–2.66	44.5	612	45.5	85.8	48.5	400.1	43.5	636.8	45.5	605
GAQ	3.93	–0.773	48.5	18	48.5	6.3	47.5	4.3	47.5	5.1	47.5	6.6
PCY	6.6	–0.68	50.5	14	46.5	4.7	55.5	7.6	54.5	9.2	54.5	6.6
ELY	14.88	–1.36	50.5	142	51.5	15.8	50.5	30.5	50.5	32.8	50.5	50.1
MBC	4.58	–0.945	59.5	12	56.5	7.7	54.5	8.1	53.5	9.3	58.5	7.5
TAH	51.98	–2.375	69.5	1105	70.5	30.6	69.5	439.8	69.5	657.6	68.5	653.9
PAN	3.59	–1.219	71.5	22	72.5	31.5	72.5	10.3	72.5	9.5	71.5	10
JMC	5.48	–1.118	70.5	12	77.5	5.6	75.5	19.5	67.5	28.9	75.5	22.2
ARI	6.15	–1.562	80.9	25	80.3	56.9	81.3	148.9	80.7	316.9	78.1	325.4
JEC	7.86	–1.371	82.5	102	83.5	11.5	81.5	15.9	81.5	12.8	83.5	18
JRC	5.12	–1.067	83.5	46	84.5	6.7	84.5	11.2	84.5	11.6	84.5	15.1
SSG	11.33	–0.851	82.5	20	83.5	5.2	89.5	5.9	89.5	6.2	88.5	9.1
JBO	2.85	–1.132	90.5	18	91.5	9.5	89.5	10.6	89.5	14.2	89.5	11.5
DPI	5.11	–1.22	91.5	26	91.5	14.7	90.5	10.7	90.5	6.2	90.5	9.5
JEO	4.65	–1.259	92.5	20	93.5	12.7	91.5	23.3	92.5	19.4	92.5	10.4
JIP	5.82	–1.257	94.5	63	93.5	15.7	93.5	13.8	93.5	11.7	93.5	10.2
FPE	3.51	–0.919	96.5	21	95.5	4.1	95.5	5.4	95.5	6.1	95.5	6.7
PPS_0	17.26	–1.381	98.5	48	93.5	8.4	94.5	17.7	94.5	18.6	91.5	16.7
NZC	50.43	–1.454	107.5	72	110.5	8.9	110.5	30.3	102.5	34	102.5	34.8
MIC	10.78	–1.296	101.5	29	108.5	12.2	101.5	29.7	102.5	21.2	101.5	14.7
TCS	3.82	–0.909	105.5	14	102.5	3.5	104.5	6.1	104.5	7.3	104.5	2.7
CAN	25.86	–1.141	106.5	64	103.5	9.9	109.5	14.7	98.5	15.5	105.5	14.3
JPE	26.85	–1.355	108.5	80	109.5	16.4	109.5	17.2	109.5	26.3	109.5	25.5
ZCS	23.01	–1.539	113.5	166	113.5	19.3	112.5	24.7	113.5	30.4	113.5	29.6
JXA	7.77	–1.166	116.5	17	111.5	11	110.5	17.7	119.5	14.7	110.5	7.3
XCS	25.3	–1.374	117.5	81	116.5	6.3	118.5	15.7	118.5	21.8	117.5	31.5
PPS_1	8.99	–0.713	115.5	38	122.5	3.3	114.5	5.2	115.5	6.3	114.5	5.9
GDR	16.19	–1.706	125.5	185	125.5	23.3	125.5	40	125.5	46.8	125.5	46.2
CAP	91.85	–2.066	127.5	354	126.5	25.5	125.5	75	127.5	94.5	127.5	122.8
SDA	242.13	–2.408	126.5	996	126.5	32.6	127.5	187.9	126.5	250.2	126.5	357.8
ERI	33.73	–1.184	132.5	53	135.5	11.8	131.5	19.5	131.5	33.3	139.5	29.4
AXC	5.61	–0.907	135.5	41	135.5	7.2	136.5	5.9	135.5	6.7	135.5	5.4
PER	1586.13	–2.298	140.5	6711	140.5	36.3	140.5	561.6	140.5	1102.7	140.5	1169.8
KCG	37.71	–1.22	141.5	105	142.5	5.6	139.5	11.8	140.5	29.5	140.5	36.9

Code	Radiant density		Nr< = 3		DR3_6		DR3_10		DR3_15		DR3_20	
	a	*b*	λ_O	*max*	λ_O	*max*	λ_O	*max*	λ_O	*max*	λ_O	*max*
ADC	8.04	–1.193	143.5	138	142.5	9.1	144.5	11.5	144.5	16	142.5	17.6
AXD	11.96	–0.424	146.5	41	147.5	2.7	148.5	3.7	144.5	7	146.5	15.5
NDA	47.32	–1.128	152.5	73	152.5	5.3	140.5	15.3	144.5	12.5	150.5	15
ZDR	8.87	–0.705	153.5	33	156.5	3.2	154.5	5.4	154.5	6	149.5	7.8
AGC	10.92	–0.87	156.5	48	157.5	4.7	155.5	9.4	155.5	8.6	155.5	8.4
AUR	16.35	–1.232	158.5	74	157.5	7.4	159.5	9.5	157.5	8.2	158.5	8.2
PSO	16.01	–0.462	160.5	43	164.5	2.3	160.5	3.4	160.5	7.5	160.5	9.5
OMG	10.22	–1.01	163.5	24	169.5	6	162.5	11.5	164.5	5.7	164.5	6.7
NUE	35.48	–0.625	164.5	46	174.5	2.9	164.5	4.4	166.5	7.2	164.5	9.3
SPE	42.26	–1.514	166.5	235	166.5	21.9	166.5	29.8	166.5	34.1	166.5	37.2
NPI	46.66	–0.577	163.5	51	165.5	3.3	165.5	4.1	167.5	6.5	167.5	13.3
SLY_0	12.96	–1.159	169.5	48	168.5	8.6	169.5	11.6	168.5	10.1	169.5	11.1
CCY	11.23	–1.386	173.5	41	172.5	7.3	171.5	18.3	172.5	23	172.5	19.5
DSX	3.99	–1.399	188.5	13	192.5	36	186.5	134.7	190.5	179.1	188.5	111.7
SLY_1	9.83	–0.606	189.5	37	190.5	3.2	190.5	3.9	185.5	5.3	185.5	4.9
OCT	10.52	–1.411	192.5	223	192.5	14.3	193.5	20.1	192.5	21.9	193.5	20.7
SAN	2.48	–1.147	197.5	14	196.5	3.7	197.5	6.7	196.5	6.3	197.5	4.7
XIE	3.5	–0.982	195.5	11	197.5	10.7	195.5	6.6	195.5	5.5	197.5	5.6
STA_SE	111.61	–1.393	204.5	301	203.5	9.5	200.5	17.5	201.5	41.8	206.5	70.1
OCU	16.46	–1.291	202.5	158	202.5	15.9	202.5	30.6	202.5	32	202.5	21.3
EGE	36.12	–0.97	208.5	61	212.5	6	207.5	6.8	199.5	2.7	212.5	3
LMI	28.61	–1.909	208.5	126	210.5	28.9	210.5	61.4	207.5	53.8	209.5	29.9
TCA	33.21	–0.901	211.5	38	196.5	7.4	208.5	8.1	210.5	7.7	202.5	4.9
ORI	803.97	–2.312	208.5	2436	208.5	43.1	208.5	227.9	208.5	222.8	210.5	331.8
LUM	8.98	–1.106	214.5	45	215.5	9.4	214.5	12.8	214.5	9.8	214.5	6.4
SLD	7.96	–1.06	221.5	77	222.5	6.2	221.5	7.1	221.5	6.9	221.5	9.8
STA_SF	211.97	–1.438	219.5	608	223.5	11.7	217.5	12.6	219.5	55.9	218.5	95.5
KUM	19.35	–1.158	222.5	155	223.5	10.8	223.5	10.8	223.5	11.3	223.5	10.6
OER	38.74	–0.778	217.5	36	246.5	4.7	235.5	11.8	247.5	9.1	247.5	3.2
AND	45.03	–1.313	239.5	103	239.5	20	239.5	41.3	243.5	39.9	240.5	43.5
RPU	5.75	–0.933	222.5	13	218.5	6.7	223.5	7.8	225.5	8.4	227.5	6.7
NTA	405.55	–1.474	222.5	420	229.5	18.9	228.5	10.7	225.5	48.2	224.5	90.9
LEO	155.21	–1.96	236.5	479	235.5	40.5	235.5	110	236.5	98.4	236.5	93
ACA	5.64	–0.976	243.5	17	238.5	4.3	242.5	10.2	239.5	12.8	238.5	12.8
AMO	9.78	–0.851	239.5	58	239.5	5.5	239.5	6.4	239.5	7.2	239.5	8.5
NSU	5.18	–0.903	241.5	29	241.5	4.5	241.5	5.4	241.5	5.3	242.5	4.1
NOO	120.81	–1.509	248.5	257	246.5	18.3	246.5	33.8	247.5	26.2	246.5	20
ORS	32.29	–1.018	247.5	82	246.5	4.4	247.5	2.4	238.5	5.2	247.5	10.8
NAC	4.04	–0.807	246.5	18	245.5	5	247.5	4.9	245.5	6.1	245.5	5.6
TPY_0	5.98	–1.258	249.5	25	249.5	5.7	249.5	8.8	249.5	12.4	249.5	8.8
DKD	24.5	–1.183	250.5	144	251.5	8	251.5	19.4	250.5	33.8	251.5	45.3
PSU	17.84	–0.854	251.5	42	252.5	7.7	251.5	10	251.5	9.8	251.5	8
DAD	25.92	–0.535	243.5	36	243.5	3.2	242.5	6.2	256.5	8.5	257.5	13.3
HYD	200.53	–1.668	254.5	356	250.5	37.9	250.5	56.9	255.5	111.5	255.5	122.1
DRV	11.12	–0.793	253.5	23	252.5	6.3	252.5	4.4	254.5	7.2	258.5	6.7
EHY	42.56	–1.021	263.5	40	271.5	3.1	272.5	2.7	255.5	9.8	256.5	17.5
PUV	14.72	–1.33	259.5	22	249.5	6.3	256.5	18	253.5	33.2	260.5	44.7
MON	85.89	–1.291	258.5	149	258.5	21.3	259.5	30.8	255.5	57.1	258.5	38.3

Code	Radiant density		$Nr<=3$		$DR3\_6$		$DR3\_10$		$DR3\_15$		$DR3\_20$	
	a	*b*	λ_O	*max*	λ_O	*max*	λ_O	*max*	λ_O	*max*	λ_O	*max*
GEM	1479.18	–2.934	262.5	13471	263.5	73.9	261.5	1139.6	261.5	4129	261.5	2326.3
XVI	16.3	–1.407	261.5	25	255.5	24.5	262.5	20.1	256.5	17.8	257.5	8.3
DAB	5.15	–1.299	263.5	27	261.5	26.2	263.5	14.4	263.5	16.8	263.5	6
TPY_1	5.05	–0.975	265.5	19	263.5	7.6	264.5	5.8	264.5	5.5	264.5	6
COM	198.34	–1.533	264.5	221	270.5	25.4	266.5	38.1	265.5	33.4	267.5	56.2
URS	38.25	–1.834	270.5	590	269.5	24.6	270.5	88.5	269.5	109.7	269.5	119.6
DSV	46.64	–1.133	274.5	33	269.5	11.2	274.5	12.3	273.5	13.5	270.5	19.4
KVE	4.56	–1.053	276.5	19	277.5	4.2	275.5	9.6	274.5	20.4	277.5	16.4
JLE	3.57	–0.985	281.5	13	282.5	13.2	282.5	4.6	280.5	3.4	280.5	3
QUA	156.55	–1.495	283.5	1689	283.5	12.4	283.5	94.2	282.5	271.8	282.5	380.1
AHY	19.69	–1.632	284.5	37	284.5	12.2	287.5	51.7	286.5	44.3	284.5	23.6
OLE	7.75	–1.013	288.5	32	288.5	5.8	288.5	13.4	288.5	9.9	288.5	6.7
XCB	6.36	–1.277	296.5	28	297.5	11.4	296.5	30.9	296.5	17.2	296.5	15.6
XUM	11.72	–1.596	298.5	90	298.5	21.1	298.5	65	298.5	24.6	298.5	22.9
GUM	11.2	–1.292	300.5	72	298.5	12	300.5	16.3	299.5	17.7	299.5	17.8
ACB	12.33	–1.07	307.5	109	308.5	12.3	307.5	10.2	308.5	10.9	308.5	13
AAN	7.28	–1.079	311.5	17	314.5	13.7	313.5	14.2	312.5	5.9	314.5	7.6
FED	3.49	–0.724	315.5	26	315.5	6.7	314.5	7.6	314.5	9.9	314.5	8.6
FHY	3.9	–1.042	324.5	14	325.5	7.7	325.5	6.5	325.5	6.1	326.5	5.8
TTR	2.41	–1.023	331.5	11	335.5	18	333.5	11.3	328.5	6.7	332.5	8.9
DNO	3.1	–0.991	334.5	13	335.5	13.5	338.5	9.5	333.5	7.1	333.5	6.8
TSB	3.46	–0.913	343.5	13	342.5	4.4	344.5	9.1	344.5	6.6	344.5	6.4
XHE	5.02	–0.942	350.5	26	351.5	9.9	351.5	8.7	351.5	8.5	351.5	12.4
EVI	16.98	–0.967	358.5	57	359.5	7.9	358.5	7.5	358.5	13.3	359.5	20.3
EOP	3.22	–0.997	363.5	11	358.5	12	355.5	11.3	356.5	7	356.5	6.5

Table 6 shows an overview of meteor shower activity. "Meteors per year" shows the number of meteors that fall within 3 degrees of the estimated position of the radiant in each year during the survey period shown in *Table 4*. The number of meteors in many meteor showers appears to increase each year because the number of GMN observations increases almost exponentially. However, it should be noted that 2019 is the year when observations began, so there are large variations, and 2023 uses data up to February, so there are many cases that are displayed as 0. The next six items are related to the activity profile. "Profile" is the observation curve that was used as the basis for drawing the estimated profile. Those using lowercase letters are moving averages every third degree, and those using uppercase letters are moving averages every one degree. C_1 and C_2 represent the spread of activity, and C_3 represents the maximum sharpness. λ_O and *max* are estimated values based on the estimated profile and indicate the maximum solar longitude and maximum value. The values below the decimal point for the maximum solar ecliptic longitude are obtained from the graph and are for reference only. This estimated curve is shown in part III, "*Radiant point distribution map and activity profile*" along with the activity curve shown in the "Profile" column.

Table 6 – Annual changes in the number of shower meteors and indices of the modelled activity profile.

Code	Meteors per year					Indices of the modelled activity profile					
	2019	2020	2021	2022	2023	Profile	C_1	C_2	C_3	$\lambda_{\odot}$	*max*
BCO	7	22	43	68	0	dr3_15	10	10	2	13	8
ZCY_0	3	20	39	72	0	dr3_15	5	5	3	16	10
DHE	0	5	16	46	0	DR3_15	45	45	2	19.6	19
AED	3	24	36	58	0	dr3_15	16	16	2	20	15
PSR	1	10	27	26	0	DR3_15	45	45	2	24.7	29
AVB	7	89	101	112	0	dr3_15	15	15	2	25	8
ZCY_1	4	24	40	55	0	dr3_15	8	8	2	31.5	8
LYR	40	599	863	1216	0	DR3_15	35	35	1.5	32.3	402
HVI	15	166	11	10	0	dr3_15	110	110	1.7	39	16
ARC	1	9	26	61	0	dr3_15	10	10	2	39.5	16
BAQ	3	6	26	47	0	dr3_10	18	18	2	44	10.5
ETA	167	482	1302	2425	0	DR3_15	55	55	1.5	44.3	850
GAQ	3	7	46	41	0	dr3_15	4.5	4.5	2	48	5
PCY	3	24	38	90	0	dr3_20	1.5	1.5	1.7	49.5	9.5
ELY	7	41	146	203	0	DR3_20	10	10	2	50.2	85
MBC	5	18	34	33	0	dr3_15	50	50	2	55	10
TAH	0	0	0	1269	0	Nr3	5500	3500	0.45	69.45	12000
PAN	0	4	12	30	0	DR3_15	60	60	2	72	18.6
JMC	1	18	50	53	0	DR3_20	10	10	1.8	72	40
ARI	10	20	46	50	0	DR3_20	10	10	1.8	79.5	350
JEC	5	40	62	43	0	DR3_20	40	40	1.8	82.6	40
JRC	1	14	42	52	0	DR3_20	8	8	2	84	22
SSG	13	59	53	107	0	DR3_20	14	14	2	87	9
JBO	1	3	1	34	0	DR3_15	40	40	3	90.3	75
DPI	1	10	17	49	0	DR3_20	350	350	1.2	91.2	14
JEO	38	14	4	41	0	DR3_15	90	90	1.4	92	26
JIP	2	16	12	67	0	DR3_10	80	80	2	94.1	50
FPE	3	13	4	40	0	DR3_10	180	180	2	95.8	16
PPS_0	21	98	51	216	0	DR3_15	4	4	1.6	98.5	27
NZC	51	259	229	570	0	DR3_20	4	4	1.8	101	40
MIC	11	46	67	156	0	DR3_10	19	19	0.7	101.3	65
TCS	3	4	16	44	0	DR3_10	19	19	1.8	104.6	11
CAN	14	114	168	383	0	DR3_20	9	9	1.4	105	19
JPE	17	110	165	289	0	DR3_15	25	25	1	109.6	45
ZCS	14	92	194	267	0	DR3_20	10	10	1	113.6	45
JXA	6	44	51	75	0	dr3_20	13	13	2	115	8
XCS	17	87	113	251	0	Nr	75	75	1.5	116.3	6.8
PPS_1	3	39	64	109	0	DR3_15	4.5	4.5	1.7	117.5	9.5
GDR	8	135	71	185	0	DR3_20	37	37	1.5	125.5	95
CAP	86	586	455	1110	0	DR3_20	25	35	1.6	126.9	140
SDA	256	1257	1185	3029	0	DR3_20	15	17	1.2	126.9	440
ERI	56	155	224	416	0	DR3_20	3	3	1.8	132.3	36
AXC	6	18	40	68	0	DR3_20	25	25	1.2	135.5	9
PER	1296	6487	11913	16054	0	DR3_20	20	20	2	140.5	1500
KCG	4	9	749	11	0	DR3_20	8	8	1.3	141.5	52
ADC	4	11	11	144	0	DR3_15	110	110	3	143.65	65

Code	Meteors per year					Indices of the modelled activity profile					
	2019	2020	2021	2022	2023	Profile	C_1	C_2	C_3	$\lambda_\odot$	*max*
AXD	22	83	85	106	0	Nr3	3.4	3.4	1.7	147.2	45
NDA	58	289	278	470	0	DR3_20	3	3	2.2	149	17
ZDR	23	29	68	89	0	Nr3	8	8	1.8	153.2	37
AGC	14	43	63	150	0	DR3_20	8	8	3	155.4	9.3
AUR	31	46	109	147	0	DR3_10	120	120	2	158.4	19
PSO	22	48	143	195	0	DR3_20	4	4	2	160.4	11
OMG	14	33	80	102	0	DR3_10	6	6	2	163.2	11.5
NUE	64	152	241	360	0	DR3_20	2.5	3	2	165.5	11
SPE	93	212	421	259	0	DR3_20	70	70	2	166.9	61
NPI	117	239	357	419	0	DR3_20	2.3	2.3	1.8	167.2	12
SLY_0	12	76	117	84	0	DR3_20	10	10	2	169.5	12
CCY	0	223	6	7	0	DR3_20	14	14	1.8	173.4	25
DSX	5	3	21	40	0	DR3_20	15	15	2	188.5	230
SLY_1	8	26	69	131	0	DR3_10	3.5	3.5	2	191.5	6
OCT	27	9	55	154	0	DR3_20	55	55	3	192.55	65
SAN	2	3	22	6	0	Nr	27	27	1.8	196.8	1.4
XIE	11	12	21	16	0	DR3_6	18	18	1.8	198.2	30
STA_SE	235	519	918	935	0	DR3_15	12.5	12.5	1.7	201.5	48
OCU	38	49	147	127	0	DR3_15	30	30	2	202.5	65
EGE	71	87	199	358	0	DR3_10	4.3	4.3	2	203.7	9
LMI	85	113	160	341	0	DR3_20	12	12	1.5	209.2	40
TCA	59	63	213	283	0	dr3_10	6.5	6.5	1.6	209.5	7.5
ORI	2165	2641	4574	10035	0	DR3_10	37	37	1.3	209.5	320
LUM	13	8	67	109	0	DR3_10	21	21	1.5	214.8	23
SLD	14	16	63	63	0	DR3_20	21	21	1.3	221.5	15
STA_SF	285	190	767	3273	0	DR15_2022	22	22	1.3	222.2	157
KUM	25	70	152	132	0	DR3_20	9	9	1.4	222.8	19.5
OER	100	120	233	372	0	Nr3	8	3	1.8	223	32
AND	53	104	635	255	0	Nr_2021	20	20	2	224.5	23
RPU	11	32	40	47	0	DR3_20	3.7	3.7	2	226.2	7
NTA	1051	1548	3040	3538	0	DR3_20	19	19	1.3	226.5	112
LEO	305	741	1075	1697	0	DR3_10	17	13	0.9	235.4	140
ACA	17	13	35	60	0	dr3_20	4	4	1.5	239.5	12
AMO	26	29	46	85	0	DR3_20	65	65	0.8	239.6	17
NSU	12	16	25	53	0	DR3_6	35	35	1.3	241.7	8.5
NOO	277	310	959	1092	0	DR3_10	5	5	1.4	246.1	40
ORS	64	84	169	369	0	DR3_20	23	23	1.6	246.2	13
NAC	11	4	36	27	0	DR3_20	8	8	1.6	246.5	8
TPY_0	15	6	41	37	0	DR3_20	15	15	2	249.4	11
DKD	99	25	261	114	0	DR3_20	23	23	1.7	251	72
PSU	44	46	173	108	0	DR3_15	12	12	0.9	251.5	13.7
DAD	60	86	267	271	0	dr3_20	2	2	2	253.5	13
HYD	457	628	1832	1636	0	DR3_20	7	7	1.2	255.4	190
DRV	25	31	101	89	0	DR3_15	9	9	1.8	255.6	8
EHY	77	129	280	366	5	DR3_20	14	14	1.4	256.2	22
PUV	10	11	93	144	0	DR3_15	1.8	1.8	2.2	256.5	150
MON	168	304	752	678	0	DR3_20	12	12	1.7	258.1	45

Code	Meteors per year					Indices of the modelled activity profile					
	2019	2020	2021	2022	2023	Profile	C_1	C_2	C_3	λ_Θ	*max*
GEM	2375	6746	11150	16924	0	DR3_15	37	37	1.7	261.85	7300
XVI	47	73	121	145	0	dr3_10	21	21	2	262.8	21
DAB	5	14	21	51	0	DR3_10	19	19	2	263.1	18
TPY_1	11	17	31	50	0	DR3_20	8	8	1.8	264.3	7.5
COM	321	730	941	2114	440	DR3_20	12	12	1	267.5	67
URS	87	265	177	353	0	DR3_20	47	47	1.2	270.65	470
DSV	76	127	255	439	86	dr3_20	6	6	1.3	271.5	18
KVE	0	1	25	71	0	DR3_15	11	11	0.9	274.9	36
JLE	0	12	8	23	12	DR3_6	14	14	1.4	281.6	40
QUA	16	543	1239	1089	902	DR3_20	42	42	1.8	283.25	1150
AHY	12	48	83	219	73	dr3_15	6.6	6.6	1.4	283.8	47
OLE	0	8	14	33	19	Nr	23	23	1	288.3	2.2
XCB	0	14	27	38	62	DR3_10	9	9	1.9	294.8	31
XUM	0	26	32	58	155	Nr3	27	27	1.7	298.6	97
GUM	0	30	17	47	151	DR3_20	15	15	1.8	299.8	26
ACB	6	25	19	114	125	DR3_20	45	45	2	307.5	21
AAN	3	22	13	73	58	DR3_20	4.5	4.5	1.7	312.5	7.5
FED	3	9	5	39	18	DR3_15	70	70	1	314.84	58
FHY	0	2	7	5	47	DR3_6	180	180	0.8	325.4	25
TTR	0	0	0	6	28	DR3_20	15	15	0.8	332.1	21
DNO	0	1	2	10	33	DR3_20	20	20	0.8	334.2	13
TSB	2	6	11	36	0	DR3_15	62	62	1	343.7	15
XHE	0	10	23	77	0	DR3_20	10	10	1.6	351.9	16
EVI	3	19	194	124	0	DR3_15	38	38	1	358	15
EOP	0	14	21	23	0	dr3_6	24	24	1.5	358.2	12

Table 7 shows the radiant point geocentric velocity, and orbital elements corresponding to the maximum of the meteor shower estimated in *Table 6*. This table summarizes this paper. It should be noted that these values are different from the commonly used average value for all observed meteors and are values corresponding to the maximum.

Table 7 – Radiant points and orbital elements at the maximum of the meteor shower.

Code	Radiant point						Orbital elements							
	λ_Θ	$\lambda\text{–}\lambda_\Theta$	β	α	δ	v_g	e	q	i	ω	Ω	λ_Π	β_Π	a
BCO	13	174.6	30.1	199.6	24.5	26.6	0.945	0.696	22.7	248	13	259.4	-21	12.74
ZCY	16	300.4	59.1	299.2	40.2	43.5	0.867	0.909	74.3	143.4	16	184.6	35.1	6.84
DHE	19.6	231.9	46.5	256.2	23.9	49.3	0.944	0.749	85.1	241.2	19.6	208.4	-60.9	13.44
AED	20	293.1	30.1	307.2	12	60.6	0.949	0.734	121.4	116.8	20	245.9	49.7	14.37
PSR	24.7	211.4	34.7	241.7	14.6	45.1	0.985	0.439	67.9	277.7	24.7	314.4	-66.7	29.15
AVB	25	171.4	11.7	199.6	4.4	19.7	0.725	0.709	7	252.4	25	277.3	-6.7	2.57
ZCY	31.5	299.1	58.1	308.6	42.5	41.8	0.721	0.904	73.7	139.4	31.5	198	38.6	3.25
LYR	32.3	240.8	56.7	272.1	33.3	46.6	0.951	0.919	79.4	214.6	32.3	219.5	-33.9	18.64
HVI	39	166.2	-1.3	202.9	-11	18.4	0.739	0.758	0.7	65.2	219	284.2	0.7	2.91
ARC	39.5	312.7	56.5	323.8	47.3	41.3	0.852	0.834	69.6	128.8	39.5	196.1	46.9	5.66
BAQ	44	279.3	13.3	321.3	-1.2	68.3	0.914	0.929	156.5	146.6	44	255.1	12.7	10.86
ETA	44.3	294	7.6	337.1	-1.4	65.4	0.949	0.564	163.7	95.4	44.3	308.6	16.2	11.06
GAQ	48	262.5	33.3	304.1	14.5	62	0.911	0.984	122.8	198.8	48	217.5	-15.7	11
PCY	49.5	278.1	71.5	296.6	53.4	39.4	0.93	1.007	65.4	173.8	49.5	226.9	5.7	14.42

Code	Radiant point						Orbital elements							
	$\lambda_\odot$	$\lambda-\lambda_\odot$	β	α	δ	v_g	e	q	i	ω	Ω	λ_Π	β_Π	a
ELY	50.2	256.3	64.5	290.7	43.7	44	0.955	1	74.4	191.6	50.2	233.4	-11.1	21.99
MBC	55	245.8	4.8	302	-15.3	65.7	0.932	0.565	169.7	265.1	55	150	-10.3	8.29
TAH	69.45	125.3	36.9	208.9	28	11.4	0.641	0.991	10.5	199.5	69.5	268.7	-3.5	2.76
PAN	72	307.1	43.6	355.3	46.6	50.4	0.963	0.713	89.6	113.3	72	251	66.7	19.54
JMC	72	323.5	43.6	10.7	53.2	42.7	0.912	0.6	69.5	98.3	72	184.6	68	6.85
ARI	79.5	330.6	7.8	45.3	25.2	40.8	0.97	0.071	30.1	27.3	79.5	103.6	13.3	2.37
JEC	82.6	249.2	47.9	315.3	33.7	52.7	0.949	0.921	95.5	216	82.6	258.6	-35.8	18.02
JRC	84	262.2	55.4	320.7	44.5	49.7	0.938	1.007	88.2	190.6	84	264.3	-10.6	16.16
SSG	87	186.7	-6.5	274.2	-29.9	25.2	0.777	0.462	6.2	104.3	267	11.4	6	2.07
JBO	90.3	101.2	59.4	221.1	48.5	14	0.68	1.015	18.4	184.7	90.3	274.8	-1.5	3.17
DPI	91.2	280.4	1	10.2	5.5	69.8	0.962	0.919	178.1	143.5	91.2	307.7	1.1	24.12
JEO	92	152.7	13.1	245.1	-8.2	13.7	0.659	0.889	5	226.8	92	318.7	-3.7	2.61
JIP	94.1	252.4	37.8	331.7	29.3	58.5	0.955	0.898	112.4	220.4	94.1	256.1	-36.8	20.17
FPE	95.8	254.9	15.9	345.2	11	66.7	0.936	0.843	150.7	229.6	95.8	230.1	-21.9	13.17
PPS_0	98.5	282.9	16.1	13.3	23.2	66.3	0.876	0.879	150.8	135.2	98.5	319.4	20.1	7.06
NZC	101	209.5	12.4	309.6	-5.6	38.9	0.942	0.11	38.3	327	101	74	-19.7	1.9
MIC	101.3	208.8	-10.3	315.7	-27.6	40	0.958	0.094	34.9	148.7	281.3	74.8	17.3	2.24
TCS	104.6	303.6	52.7	13.7	65.4	46.3	0.893	0.858	80.9	131.9	104.6	274.6	47.3	8.03
CAN	105	298.1	32.8	27	46.5	57.1	0.918	0.684	112.9	108.5	105	334.4	60.9	8.35
JPE	109.6	244.6	14.6	348.8	11.1	63.8	0.949	0.574	148.6	263.9	109.6	206.7	-31.2	11.34
ZCS	113.6	277.9	42.7	7.5	50.8	57.1	0.934	0.996	107.6	163.5	113.6	298.7	15.7	15.02
JXA	115	283.2	-5.5	37.7	9	68.8	0.937	0.865	169.9	313.7	295	340.8	-7.3	13.73
XCS	116.3	185.1	8.4	301.8	-11.7	25.1	0.791	0.486	7.7	280.5	116.3	36.9	-7.5	2.32
PPS_1	117.5	280.5	17.7	29.1	30.8	66.1	0.842	0.926	148.3	143.8	117.5	329.4	18.1	5.86
GDR	125.5	167.3	73.4	280.1	50.7	27.6	0.978	0.978	40.4	202.1	125.5	322.7	-14.1	44.39
CAP	126.9	178.6	9.9	305.4	-9.3	22.1	0.759	0.599	7.2	267.1	126.9	33.9	-7.2	2.49
SDA	126.9	208.4	-7.4	340	-16.4	40.4	0.968	0.079	26.8	151.1	306.9	100.7	12.6	2.47
ERI	132.3	260	-27.4	39.5	-13.5	64.2	0.942	0.951	132.2	29.4	312.3	291.6	21.4	16.31
AXC	135.5	252.1	42.6	3.8	49.1	55.5	0.914	0.909	104.2	218.5	135.5	304.5	-37.1	10.56
PER	140.5	283.4	38.3	49.2	58.1	58.8	0.923	0.945	113	149.4	140.5	333.5	27.9	12.3
KCG	141.5	162.9	71.1	286.4	49.6	22.4	0.724	0.971	33.9	205.8	141.5	343.3	-14	3.51
ADC	143.6	180.1	2.2	325.3	-11.5	23.8	0.81	0.552	1.8	270.9	143.7	54.6	-1.8	2.91
AXD	147.2	140.6	82.8	274.3	59.7	21.8	0.654	1.006	34.8	189.4	147.2	334.9	-5.3	2.91
NDA	149	206.8	7	353.4	4.8	37.9	0.95	0.105	20.4	327.2	149	117.9	-10.9	2.09
ZDR	153.2	52.7	84.6	258.9	63.8	21.9	0.647	1.01	35	176.7	153.2	330.5	1.9	2.86
AGC	155.4	263.2	63.6	358	76.6	43.9	0.892	1.005	75.6	188.1	155.4	337.4	-7.8	9.28
AUR	158.4	292.6	15.8	91.2	39.2	65.5	0.961	0.667	148.2	108	158.4	47.5	30.1	16.93
PSO	160.4	267.4	-24.3	69.8	-2.4	65.5	0.874	1.002	138.3	9.5	340.4	333.3	6.3	7.96
OMG	163.2	307.1	17.1	115.2	38.8	58.1	0.948	0.3	130.8	63.7	163.2	110.3	42.7	5.72
NUE	165.5	259.1	-21.3	66.4	0.1	65.4	0.866	0.912	141.9	37.3	345.5	314.6	22	6.78
SPE	166.9	249.1	21.1	47.4	39.6	64	0.944	0.718	138.7	245.9	166.9	287.6	-37.1	12.76
NPI	167.2	196.7	3.8	2.1	5.1	28.7	0.83	0.287	5.1	305.2	167.2	112.5	-4.2	1.68
SLY_0	169.5	294.9	33.5	111.7	55.8	58.7	0.928	0.752	114.6	118.4	169.5	27.1	53.1	10.47
CCY	173.4	140.1	52.6	300.2	33.6	14.7	0.651	0.958	18.3	208.4	173.4	20.6	-8.6	2.74
DSX	188.5	330.6	-11.5	156.5	-2.5	32.3	0.869	0.147	24.3	213.4	8.5	219.5	-13.1	1.12
SLY_1	191.5	277.5	23.9	115.2	45.7	66.3	0.919	0.966	138.5	158.4	191.5	28	14.1	11.97
OCT	192.6	281.6	62	167.6	78.6	45.8	0.946	0.991	77.9	169.1	192.6	10.2	10.7	18.44
SAN	196.8	214.4	29.8	37.9	46.5	16.9	0.516	0.396	21.4	320.5	196.8	159.3	-13.4	0.82

Code	Radiant point						Orbital elements							
	$\lambda_{\odot}$	$\lambda-\lambda_{\odot}$	β	α	δ	v_g	e	q	i	ω	Ω	λ_{Π}	β_{Π}	a
XIE	198.2	228.1	-27.8	69.1	-6.1	54.2	0.981	0.383	103	104.1	18.2	240	70.9	19.75
STA_SE	201.5	195.8	-4.4	36.4	9.8	28.8	0.831	0.301	5.7	122.6	21.5	144.2	4.8	1.78
OCU	202.5	279.1	46.8	145.7	64.2	55.5	0.942	0.979	100.7	164.2	202.5	25.5	15.5	16.87
EGE	203.7	254.9	5.1	99.7	28.3	68.7	0.917	0.789	170.4	235.7	203.7	328.4	-7.9	9.52
LMI	209.2	298	26.2	160.3	36.8	61.3	0.959	0.616	124.5	102.8	209.2	97.3	53.4	15.15
TCA	209.5	283.4	13.4	139.7	29.8	67	0.808	0.843	155.1	131.2	209.5	75.5	18.5	4.39
ORI	209.5	246.6	-7.5	96.3	15.8	65.5	0.916	0.557	163.8	85.4	29.5	304.3	16.1	6.65
LUM	214.8	284.4	36.8	158.2	49.2	60.5	0.952	0.915	115.1	146.9	214.8	50.3	29.6	18.91
SLD	221.5	265.2	53.5	161.6	68	48.9	0.741	0.986	88.5	189.8	221.5	41.8	-9.8	3.81
STA_SF	222.2	192.3	-4.5	53.2	14.5	28.5	0.837	0.351	5.4	114.7	42.2	157	4.9	2.16
KUM	222.8	268	29.7	144.4	45.8	64.8	0.933	0.988	129.2	186.9	222.8	38.4	-5.3	14.81
OER	223	187.1	-18.7	52.6	-0.3	28.7	0.874	0.472	19.1	97.1	43	140.5	18.9	3.74
AND	224.5	165.9	18.2	21.2	28.5	18.1	0.751	0.763	9.4	242.4	224.5	106.6	-8.3	3.06
RPU	226.2	269.6	-43.5	125.1	-25.5	57.5	0.902	0.99	106.3	2.2	46.2	45.6	2.1	10.14
NTA	226.5	192.1	2.4	55.8	22.2	28.3	0.833	0.352	2.9	294.7	226.5	161.2	-2.6	2.11
LEO	235.4	272.5	10.3	153.9	21.8	69.7	0.829	0.984	162	171.6	235.4	63.4	2.6	5.74
ACA	239.5	216.8	-41.8	95	-18.5	43.7	0.917	0.553	70	85.4	59.5	136.3	69.5	6.69
AMO	239.6	239.5	-19.9	117.2	0.8	61.7	0.963	0.469	133.3	94	59.6	323.7	46.5	12.74
NSU	241.7	245.1	43.2	148.9	59.4	54.4	0.925	0.813	98.9	230.8	241.7	51	-49.9	10.88
NOO	246.1	204	-7.9	90.1	15.5	42.9	0.992	0.111	24.6	141.4	66.1	210.2	15	13.22
ORS	246.2	190.1	-4.7	75.6	18	27.4	0.82	0.392	5.1	109.7	66.2	175.9	4.8	2.18
NAC	246.5	286.2	-20.5	165	-16	66.6	0.934	0.812	141.8	309.3	66.5	110.3	-28.6	12.31
TPY_0	249.4	261.2	-39.3	138.3	-25.5	60.1	0.951	0.955	112.5	20.7	69.4	61.2	19.1	19.52
DKD	251	243	61.5	186.1	70.5	43.8	0.91	0.929	73.2	208.6	251	79.9	-27.3	10.28
PSU	251.5	258	35.6	168.1	44.2	60.9	0.896	0.917	117.2	211.4	251.5	55.9	-27.6	8.78
DAD	253.5	264.2	62.7	204.6	62.2	40.6	0.604	0.981	72	188.5	253.5	76.1	-8.1	2.48
HYD	255.4	231	-16.5	124.7	2.7	58.8	0.982	0.255	129.1	119.7	75.4	303.2	42.4	14.27
DRV	255.6	286	15	187.5	13.1	68.2	0.935	0.795	152	126.8	255.6	125.3	22.1	12.16
EHY	256.2	237.8	-14.8	132.2	2.4	62.1	0.964	0.375	142.3	105.1	76.2	327.3	36.2	10.31
PUV	256.5	268.3	-61.6	134.7	-49.2	41.6	0.612	0.984	74.1	3.2	76.5	77.4	3	2.53
MON	258.1	202.5	-14.8	100.4	8.3	41.4	0.983	0.185	35.3	129.8	78.1	213.6	26.4	10.71
GEM	261.8	208	10.5	113.3	32.4	33.8	0.889	0.146	22.9	324.1	261.9	228.1	-13.2	1.31
XVI	262.8	291.6	-5.2	191.3	-10.5	68.1	0.95	0.624	169.4	284.4	82.8	158.2	-10.3	12.45
DAB	263.1	298.1	32.6	212.1	21.9	59.4	0.972	0.675	113.5	111.2	263.1	128.9	58.7	24.18
TPY_1	264.3	259.6	-32.9	152	-23.9	63	0.936	0.929	122.5	27.9	84.3	68.4	23.2	14.46
COM	267.5	242.9	21.1	161	30.9	62.8	0.943	0.557	134.2	263.9	267.5	6.2	-45.5	9.77
URS	270.6	218.8	72.1	219.4	75.4	33.1	0.814	0.94	52.8	205.6	270.7	106.8	-20.2	5.06
DSV	271.5	293.4	15	208.5	4.4	66.1	0.95	0.612	148.8	103	271.5	166.4	30.3	12.23
KVE	274.9	259.4	-59.6	142.3	-50.5	43.3	0.657	0.969	76.8	15.4	94.9	98.5	15	2.82
JLE	281.6	219.5	10.2	147	24.1	51.9	0.991	0.049	103.6	335.3	281.6	287.8	-23.9	5.67
QUA	283.2	276.7	63.8	230	49.7	40.4	0.64	0.98	70.9	172	283.3	100.6	7.5	2.72
AHY	283.8	207.9	-26.2	127.1	-8	43.6	0.969	0.285	58.1	116.2	103.8	236.8	49.6	9.28
OLE	288.3	209.2	-7.3	137.7	8.6	46.5	0.995	0.052	37.4	154	108.3	267.1	15.4	10.11
XCB	294.8	307.3	50.8	250.2	29.3	45.4	0.826	0.775	78.1	122	294.8	96.5	56	4.45
XUM	298.6	218.1	25.8	169.5	32.8	41	0.853	0.221	67.2	313.2	298.6	276.2	-42.2	1.5
GUM	299.8	218.8	74.5	229.7	67.3	29.4	0.654	0.954	48.2	202.7	299.8	135.4	-16.7	2.75
ACB	307.5	271.4	44.7	231.3	27.9	57.2	0.918	0.984	104.5	176.5	307.5	128.4	3.4	11.97
AAN	312.5	211	-17.4	158.1	-9.6	43.9	0.957	0.138	56.6	139.3	132.5	287.2	33	3.19

Code	Radiant point						Orbital elements							
	$\lambda_{\odot}$	λ–$\lambda_{\odot}$	β	α	δ	v_g	e	q	i	ω	Ω	λ_{Π}	β_{Π}	a
FED	314.8	230.6	76	239.3	61.8	35.2	0.947	0.97	55.3	194.6	314.8	143.2	-11.9	18.28
FHY	325.4	160.7	-18.9	123.9	0.4	16.1	0.693	0.823	8.4	53.6	145.4	198.7	6.8	2.68
TTR	332.1	285.4	-43.9	247	-66.4	56.3	0.939	0.916	103	328	152.1	160.1	-31.1	14.94
DNO	334.2	271.5	-24.9	237.8	-45.7	66.7	0.918	0.987	137.3	354.2	154.2	158.5	-4	11.99
TSB	343.7	220.8	36.7	216.7	24.6	49.4	0.987	0.497	82	270.2	343.7	255.1	-82	37.88
XHE	351.9	249	70.8	255.9	48.8	34.5	0.629	0.982	59.3	194.1	351.9	179.2	-12.1	2.65
EVI	358	187	5.3	186.7	2.8	27.2	0.818	0.439	5.4	284	358	282	-5.2	2.42
EOP	358.2	262.8	6.7	260.7	-16.5	70.8	0.937	0.954	168.4	204	358.2	154.6	-4.7	15.23

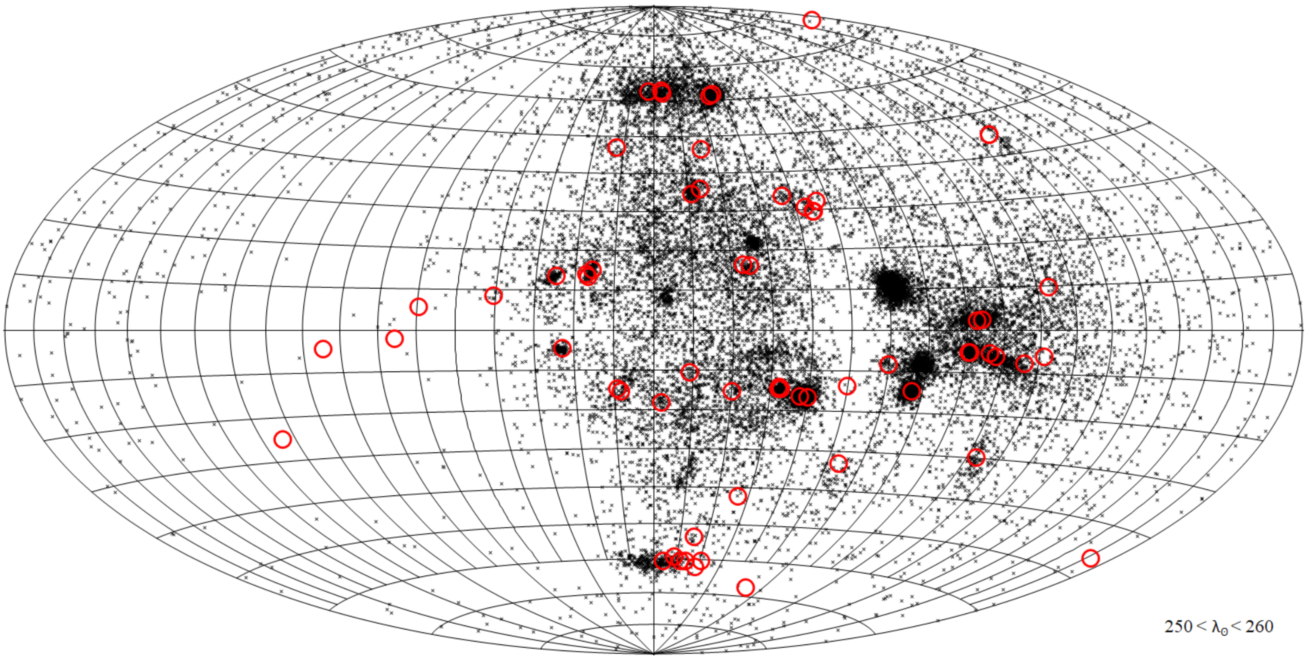

Figure 9 – Radiats observed in GMN with $\lambda_{\odot}$ = 250~260 expressed in (λ–$\lambda_{\odot}$, β) coordinate system, point distribution. The center is (λ–$\lambda_{\odot}$, β) = (270, 0).

4 Comparison with the previous meteor shower table

Many of those that appeared for the first time had weak activity, so it was not possible to clearly capture their activity in the previous paper. Also, some meteor showers in the southern sky are now included. On the other hand, those not covered in this article include 0027KSE, 0152NOC, 0183PAU, 0388CTA, 0097SCC, and 0096NCC. In the case of KSE, this is because KSE03, which was the previous origin, has been deleted from the IAUMDCSD. For more information, please refer to part II. "*Meteor showers that require attention*". The other four activities did not meet the criteria when applied this time. We also explained SCC and NCC in detail in part II.

The survey method is the same as in the previous paper, but the only difference is that to determine whether a meteor belongs to a meteor shower, we exclude meteors that are more than ±3 km/s away from the regression line of the geocentric velocity. This is because many meteor showers appear not so frequently as sporadic meteors, so it is necessary to exclude those that may be sporadic meteors. This difference does not have a large effect on the meteor showers discussed in the previous article. The major difference between the previous paper and this paper is in the database used, so we will explain the differences between the SonotaCo net data and GMN. There are four points.

The first is the difference in the number of meteors. The number of GMN meteors used here was more than twice that of the previous one, and as a result, even weaker meteor showers were detected. However, the number of GMN observations is increasing exponentially, and care must be taken when considering annual changes in meteor showers. Also, it must be noted that this often depends on observations in 2022, and observation conditions in 2022 have a large influence.

The second difference is the observation period. In the previous paper, we used SonotaCo net observations from 2007 to 2018, but the GMN observations used in this paper are from 2019 to February 2023. As a result, we were unable to discuss the activity of the Orionids, which became active from 2007 to 2009, but on the other hand, we obtained data on the outbursts of the Andromedids in 2021 and the 73P/Schwassmann-Wachmann 3 comet-related event in 2022.

The third difference is that the observation points are spread out in longitude. Observations were mainly made in Western Europe and North America, but we were able to obtain continuous observations for almost half a day, making it possible to capture meteor showers whose peaks last for only a short period. This is also why GMN captures the outbursts mentioned above. However, since the number of observation points differs depending on the longitude, it is natural that an increase or decrease in the number of meteors does not necessarily indicate a change in the activity of the meteor shower, so care must be taken.

Finally, GMN includes observations of the southern sky. Although the number of observations is still small, it is now possible to capture activity in the southern sky, as shown in *Figure 9*. In this paper, we were able to investigate meteor showers with declinations south of –40 degrees, such as 0255PUV00, 0784KVE00, 1166TTR00, and 0915DNO00. It is expected that future developments will lead to the discovery of new meteor showers and provide useful knowledge about meteor showers, which had previously been discussed only through visual observation.

Acknowledgment

This paper would not have been possible without the dedicated efforts of the observers, and the author would like to express his heartfelt gratitude to the members of SonotaCo net and GMN.

References

Koseki M. (2021). “The activity of meteor showers recorded by SonotaCo Net video observations 2007–2018”. *eMetN*, **6**, 91–246.

Southworth R. B. and Hawkins G. S. (1963). “Statistics of meteor streams”. *Smithsonian Contributions to Astrophysics*, **7**, 261–285.

Vida D., Gural P., Brown P., Campbell–Brown M., Wiegert P. (2019). “Estimating trajectories of meteors: an observational Monte Carlo approach – I. Theory”. *Monthly Notices of the Royal Astronomical Society*, **491**, 2688–2705.

Vida D., Gural P., Brown P., Campbell–Brown M., Wiegert P. (2020). “Estimating trajectories of meteors: an observational Monte Carlo approach – II. Results”. *Monthly Notices of the Royal Astronomical Society*, **491**, 3996–4011.

Vida D., Šegon D., Gural P. S., Brown P. G., McIntyre M. J. M., Dijkema T. J., Pavletić L., Kukić P., Mazur M. J., Eschman P., Roggemans P., Merlak A., Zubrović D. (2021). “The Global Meteor Network – Methodology and first results”. *Monthly Notices of the Royal Astronomical Society*, **506**, 5046–5074.

February 2024 report CAMS-BeNeLux

Carl Johannink

Am Ollenkamp 4, 48599 Gronau, Germany
c.johannink@t-online.de

A summary of the activity of the CAMS-BeNeLux network during the month of February 2024 is presented. This month was good for a total of 2739 multi-station meteors resulting in 990 orbits. One of the lowest results in February since the start of the CAMS-BeNeLux network in March 2012.

1 Introduction

Meteor activity is relatively low at our latitudes in February. Still, thanks to the long nights, quite a nice number of orbits can be collected in these long nights when it is completely clear.

2 February 2024 statistics

Off course we must get clear sky during these long nights in order to collect a large number of orbits in this winter month.

This year, February in the Netherlands was the warmest February but very cloudy month since measurements of sunshine began in 1901. This is not a good situation to get clear skies. It was therefore a downright gloomy and rainy month. Mean temperatures this month were nearly as high as in April normally.

During five nights no orbits at all were obtained. In addition, there were six other nights in which the number of collected orbits was lower than five. Further on, there were only two nights in which we have obtained more than 100 orbits: February 1–2 (124 orbits) and February 12–13 (252 orbits). This last night accounted for 25% of the monthly score.

The fact that in almost 40% of all nights this month less than 5 meteors per night were recorded shows that the most important feature of this month was the cloudy atmosphere. Only three February months were less sunny than this February since the start of the measurements in 1901.

CAMS-BeNeLux collected only 2739 multi-station meteors this month, resulting in 990 orbits. Together with the results in January 2021, this is the lowest score in seven years.

The number of orbits collected from more than two stations was only 42%. This is also a very low number when compared with other months in the last five years.

130 different cameras were active this month. Most cameras, 123 were active on February 1–2, the lowest number of active cameras, 105, were active on February 25–26. The number of cameras participating in our network is still growing.

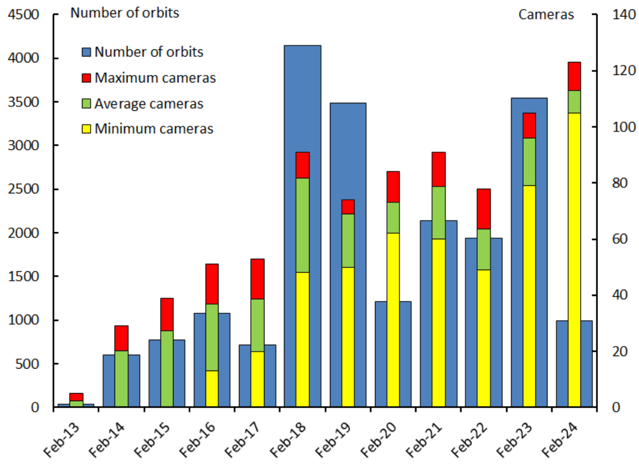

Figure 1 – Comparing February 2024 to previous months of February in the CAMS-BeNeLux history. The blue bars represent the number of orbits, the red bars the maximum number of cameras capturing in a single night, the green bars the average number of cameras capturing per night and the yellow bars the minimum number of cameras.

Table 1 – Number of orbits and active cameras in CAMS-BeNeLux during the month of February in the period 2013–2024.

Year	Nights	Orbits	Stations	Max. Cams	Min. Cams	Mean Cams
2013	9	38	6	5	–	2.3
2014	21	601	12	29	–	20.3
2015	21	777	14	39	–	27.4
2016	24	1075	17	51	13	36.9
2017	16	717	18	53	20	38.6
2018	26	4147	22	91	48	81.7
2019	24	3485	18	74	50	68.8
2020	24	1215	22	84	62	73.1
2021	25	2136	26	91	60	78.6
2022	23	1939	24	78	49	63.7
2023	21	3543	37	105	79	95.9
2024	24	990	45	123	105	112.9
Total	258	20663				

This month, a new station in Germany could be added to our network. At Bruchhausen Vilsen, *Romke Schievink* now operates two RMS cameras.

3 Conclusion

Results for February 2024 are meager when compared to other February months since the start of the CAMS-BeNeLux network in March 2012, despite the still growing number of stations/cameras.

Acknowledgment

Many thanks to all participants in the CAMS-BeNeLux network for their dedicated efforts. The CAMS-BeNeLux team was operated by the following volunteers during the month of February 2024:

Stéphane Barré (Colombey-Les-Belles, France, RMS 3907), *Hans Betlem* (Woold, Netherlands, Watec 3071, 3072, 3073, 3074, 3075, 3076, 3077 and 3078), *Felix Bettonvil* (Utrecht, Netherlands, Watec 376), *Jean-Marie Biets* (Wilderen, Belgium, Watec 3180, 3181, 3182 and 3183), *Ludger Boergerding* (Holdorf, Germany, RMS 3801), *Günther Boerjan* (Assenede, Belgium, RMS 3823), *Martin Breukers* (Hengelo, Netherlands, Watec 320, 321, 322, 323, 324, 325, 326 and 327, RMS 319, 328 and 329), *Jean Brunet* (Fontenay le Marmion, France, RMS 3911), *Seppe Canonaco* (Genk, RMS 3818 and 3819), *Pierre de Ponthiere* (Lesve, Belgium, RMS 3816 and 3826), *Bart Dessoy* (Zoersel, Belgium, Watec 804, 805, 806), *Tammo Jan Dijkema* (Dwingeloo, Netherlands, RMS 3199), *Jürgen Dörr* (Wiesbaden, Germany, RMS 3810), *Isabelle Ansseau, Jean-Paul Dumoulin, Dominique Guiot* and *Christian Wanlin* (Grapfontaine, Belgium, Watec 814, 815, RMS 3817, 3843, 3844 and 3845), *Uwe Glässner* (Langenfeld, Germany, RMS 3800), *Roel Gloudemans* (Alphen aan de Rijn, Netherlands, RMS 3197), *Luc Gobin* (Mechelen, Belgium, Watec 3890, 3891, 3892 and 3893), *Tioga Gulon* (Nancy, France, Watec 3900 and 3901), *Tioga Gulon* (Chassignolles, France, RMS 3910), *Robert Haas* (Alphen aan de Rijn, Netherlands, Watec 3160, 3161, 3162, 3163, 3164, 3165, 3166 and 3167), *Robert Haas* (Texel, Netherlands, Watec 811 and 812), *Kees Habraken* (Kattendijke, Netherlands, RMS 3780, 3781, 3782 and 3783), *Klaas Jobse* (Oostkapelle, Netherlands, Watec 3030, 3031, 3032, 3033, 3034, 3035, 3036 and 3037), *Carl Johannink* (Gronau, Germany, Watec 3100, 3101, 3102), *Reinhard Kühn* (Flatzby, Germany, RMS 3802), *Hervé Lamy* (Dourbes, Belgium, Watec 394 and 395, RMS 3825 and 3841), *Hervé Lamy* (Humain, Belgium, RMS 3821 and 3828), *Hervé Lamy* (Ukkel, Belgium, Watec 393 and 817), *Hartmut Leiting* (Solingen, Germany, RMS 3806), *Arnoud Leroy* (Gretz-Armainvielliers, France, RMS3909), *Horst Meyerdierks* (Osterholz-Scharmbeck, Germany, RMS 3807), *Koen Miskotte* (Ermelo, Netherlands, Watec 3051, 3052, 3053 and 3054), *Pierre-Yves Péchart* (Hagnicourt, France, RMS 3902, 3903, 3904, 3905, 3906 and 3908), *Holger Pedersen* (Otterup, Denmark, RMS 3501), *Eduardo Fernandez del Peloso* (Ludwigshafen, Germany, RMS 3805), *Tim Polfliet* (Gent, Belgium, Watec 396, RMS 3820 and 3840), *Steve Rau* (Oostende, Belgium, RMS 3822), *Steve Rau* (Zillebeke, Belgium, Watec 3850 and 3852, RMS 3851 and 3853), *Paul and Adriana Roggemans* (Mechelen, Belgium, RMS 3830 and 3831, Watec 3832, 3833, 3834, 3835, 3836 and 3837), *Jim Rowe* (Eastbourne, England, RMS 3703), *Philippe Schaack* (Roodt-sur-Syre, Luxemburg, RMS 3952), *Romke Schievink* (Bruchhausen Vilsen, Germany, RMS 3808 and 3809),*Hans Schremmer* (Niederkruechten, Germany, Watec 803), *Rob Smeenk* (Assen, Netherlands, RMS 3196), *Rob Smeenk* (Kalenberg, Netherlands, RMS 3192, 3193, 3194 and 3195), *Erwin van Ballegoij* (Heesh, Netherlands Watec 3148 and 3149), *Andy Washington* (Clapton, England, RMS 3702).

March 2024 report CAMS-BeNeLux

Carl Johannink

Am Ollenkamp 4, 48599 Gronau, Germany

c.johannink@t-online.de

A summary of the activity of the CAMS-BeNeLux network during the month of March 2024 is presented. This month was good for 7783 multi-station meteors resulting in 2462 orbits, compared to other years a good result for March.

1 Introduction

Meteor activity in March is now reaching the lowest level for northern latitudes. This month continued the weather pattern of the previous months with many partly clouded nights. Since the number of active cameras was higher compared to other years, the results could have been better.

2 March 2024 statistics

As already noted, the number of complete clear nights in this month was low. Yet there were only 2 nights (March 10–11 and March 29–30) in which we couldn't collect any orbit at all.

That means that many nights had clear spells, but off course not necessary all over our regions. That reduces the chances for collecting multi-station meteors significantly.

More than 50% of all orbits were achieved in the first 10 days of March, when the weather for astronomical observations was better. After this first period, we could collect more than 100 orbits per night only on March 16–17, 27–28 and March 28–29.

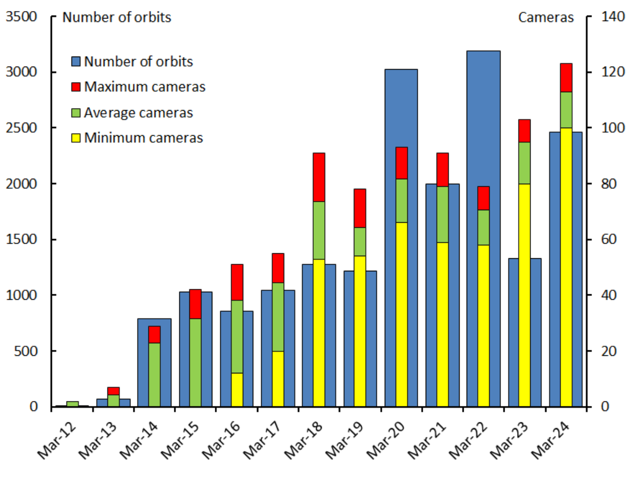

Figure 1 – Comparing March 2024 to previous months of March in the CAMS-BeNeLux history. The blue bars represent the number of orbits, the red bars the maximum number of cameras capturing in a single night, the green bars the average number of cameras capturing per night and the yellow bars the minimum number of cameras.

CAMS-BeNeLux collected a total of 7783 muti-station meteors this month, resulting in 2462 orbits. The third best result for this month. 50,1% of all orbits were captured by more than 2 stations.

Meteors were captured on 56% of the active cameras during this month. Both numbers show that the unstable character of this month. On average 113 cameras were active during the nights this month. This number is much higher than last year.

Table 1 – Number of orbits and active cameras in CAMS-BeNeLux during the month of March in the period 2012–2024.

Year	Nights	Orbits	Stations	Max. Cams	Min. Cams	Mean Cams
2012	2	12	2	2	–	2.0
2013	10	69	6	7	–	4.2
2014	24	793	12	29	–	22.8
2015	23	1033	14	42	–	31.7
2016	23	856	16	51	12	38.2
2017	26	1048	19	55	20	44.4
2018	25	1280	22	91	53	73.5
2019	29	1215	20	78	54	64.4
2020	27	3026	25	93	66	81.7
2021	28	1998	27	91	59	78.9
2022	29	3189	24	79	58	70.6
2023	25	1328	37	103	80	95.0
2024	29	2462	45	123	100	113.0
Total	300	18309				

3 Conclusion

The results for March 2024 were mainly achieved during the first 10 nights of this month.

Acknowledgment

Many thanks to all participants in the CAMS-BeNeLux network for their dedicated efforts. The CAMS-BeNeLux team was operated by the following volunteers during the month of March 2024:

Stéphane Barré (Colombey-Les-Belles, France, RMS 3907), *Hans Betlem* (Woold, Netherlands, Watec 3071,

3072, 3073, 3074, 3075, 3076, 3077 and 3078), *Felix Bettonvil* (Utrecht, Netherlands, Watec 376), *Jean-Marie Biets* (Wilderen, Belgium, Watec 3180, 3181, 3182 and 3183), *Ludger Boergerding* (Holdorf, Germany, RMS 3801), *Günther Boerjan* (Assenede, Belgium, RMS 3823), *Martin Breukers* (Hengelo, Netherlands, Watec 320, 321, 322, 323, 324, 325, 326 and 327, RMS 319, 328 and 329), *Jean Brunet* (Fontenay le Marmion, France, RMS 3911), *Seppe Canonaco* (Genk, RMS 3818 and 3819), *Pierre de Ponthiere* (Lesve, Belgium, RMS 3816 and 3826), *Bart Dessoy* (Zoersel, Belgium, Watec 804, 805, 806), *Tammo Jan Dijkema* (Dwingeloo, Netherlands, RMS 3199), *Jürgen Dörr* (Wiesbaden, Germany, RMS 3810), *Isabelle Ansseau, Jean-Paul Dumoulin, Dominique Guiot* and *Christian Wanlin* (Grapfontaine, Belgium, Watec 814, 815, RMS 3817, 3843, 3844 and 3845), *Uwe Glässner* (Langenfeld, Germany, RMS 3800), *Roel Gloudemans* (Alphen aan de Rijn, Netherlands, RMS 3197), *Luc Gobin* (Mechelen, Belgium, Watec 3890, 3891, 3892 and 3893), *Tioga Gulon* (Nancy, France, Watec 3900 and 3901), *Tioga Gulon* (Chassignolles, France, RMS 3910), *Robert Haas* (Alphen aan de Rijn, Netherlands, Watec 3160, 3161, 3162, 3163, 3164, 3165, 3166 and 3167), *Robert Haas* (Texel, Netherlands, Watec 811 and 812), *Kees Habraken* (Kattendijke, Netherlands, RMS 3780, 3781, 3782 and 3783), *Klaas Jobse* (Oostkapelle, Netherlands, Watec 3030, 3031, 3032, 3033, 3034, 3035, 3036 and 3037), *Carl Johannink* (Gronau, Germany, Watec 3100, 3101, 3102), *Reinhard Kühn* (Flatzby, Germany, RMS 3802), *Hervé Lamy* (Dourbes, Belgium, Watec 394 and 395, RMS 3825 and 3841), *Hervé Lamy* (Humain, Belgium, RMS 3821 and 3828), *Hervé Lamy* (Ukkel, Belgium, Watec 393 and 817), *Hartmut Leiting* (Solingen, Germany, RMS 3806), *Arnoud Leroy* (Gretz-Armainvielliers, France, RMS3909), *Horst Meyerdierks* (Osterholz-Scharmbeck, Germany, RMS 3807), *Koen Miskotte* (Ermelo, Netherlands, Watec 3051, 3052, 3053 and 3054), *Pierre-Yves Péchart* (Hagnicourt, France, RMS 3902, 3903, 3904, 3905, 3906 and 3908), *Holger Pedersen* (Otterup, Denmark, RMS 3501), *Eduardo Fernandez del Peloso* (Ludwigshafen, Germany, RMS 3805), *Tim Polfliet* (Gent, Belgium, Watec 396, RMS 3820 and 3840), *Steve Rau* (Oostende, Belgium, RMS 3822), *Steve Rau* (Zillebeke, Belgium, Watec 3850 and 3852, RMS 3851 and 3853), *Paul and Adriana Roggemans* (Mechelen, Belgium, RMS 3830 and 3831, Watec 3832, 3833, 3834, 3835, 3836 and 3837), *Jim Rowe* (Eastbourne, England, RMS 3703), *Philippe Schaack* (Roodt-sur-Syre, Luxemburg, RMS 3952), *Romke Schievink* (Bruchhausen Vilsen, Germany, RMS 3808 and 3809),*Hans Schremmer* (Niederkruechten, Germany, Watec 803), *Rob Smeenk* (Assen, Netherlands, RMS 3196), *Rob Smeenk* (Kalenberg, Netherlands, RMS 3192, 3193, 3194 and 3195), *Erwin van Ballegoij* (Heesh, Netherlands Watec 3148 and 3149), *Andy Washington* (Clapton, England, RMS 3702).

Radio meteors February 2024

Felix Verbelen

Vereniging voor Sterrenkunde & Volkssterrenwacht MIRA, Grimbergen, Belgium
felix.verbelen@gmail.com

An overview of the radio observations during February 2024 is given.

1 Introduction

The graphs show both the daily totals (*Figure 1 and 2*) and the hourly numbers (*Figure 3 and 4*) of "all" reflections counted automatically, and of manually counted "overdense" reflections, overdense reflections longer than 10 seconds and longer than 1 minute, as observed here at Kampenhout (BE) on the frequency of our VVS-beacon (49.99 MHz) during the month of February 2024.

The hourly numbers, for echoes shorter than 1 minute, are weighted averages derived from:

$$N(h) = \frac{n(h-1)}{4} + \frac{n(h)}{2} + \frac{n(h+1)}{4}$$

Local interference and unidentified noise remained low for most of the month, but almost daily several strong solar outbursts made the observations even more interesting. *Figure 5* is an example of a strong outburst on February 9th.

Quite strong lightning activity occurred on February 22th and faint activity on the 18th and the 23rd.

Only minor meteor showers were observed this month, and the numbers of reflections remained very low as expected at this time of the year.

Quite a number of the reflections appeared in fairly dense groups (*Figures 6 to 12*). Taking into account the time intervals between the members of the groups, it is obvious that the possible fragmentation didn't occur in the Earth's atmosphere but must have taken place earlier. It would be interesting to further investigate this.

Over the entire month, 6 reflections longer than 1 minute were recorded. A selection of these, along with some other interesting reflections is included (*Figures 13 to 18*). More of these are available on request.

In addition to the usual graphs, you will also find the raw counts in cvs-format[12] from which the graphs are derived. The table contains the following columns: day of the month, hour of the day, day + decimals, solar longitude (epoch J2000), counts of "all" reflections, overdense reflections, reflections longer than 10 seconds and reflections longer than 1 minute, the numbers being the observed reflections of the past hour.

[12] https://www.emeteornews.net/wp-content/uploads/2024/03/202402_49990_FV_rawcounts.csv

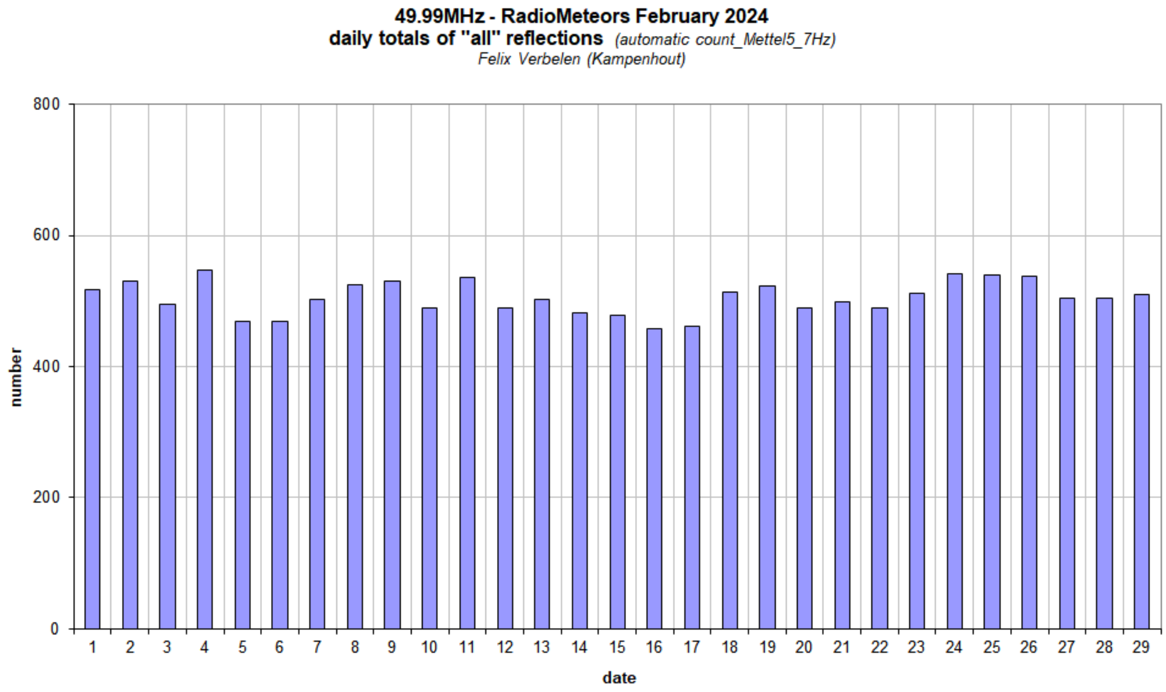

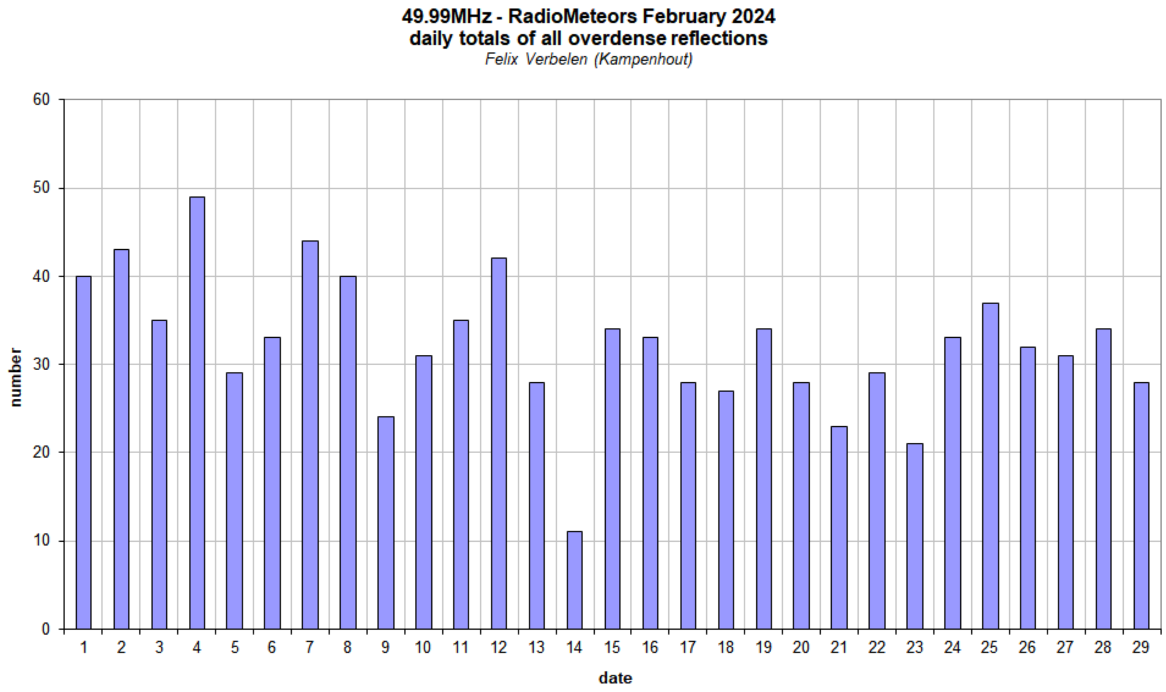

Figure 1 – The daily totals of "all" reflections counted automatically, and of manually counted "overdense" reflections, as observed here at Kampenhout (BE) on the frequency of our VVS-beacon (49.99 MHz) during February 2024.

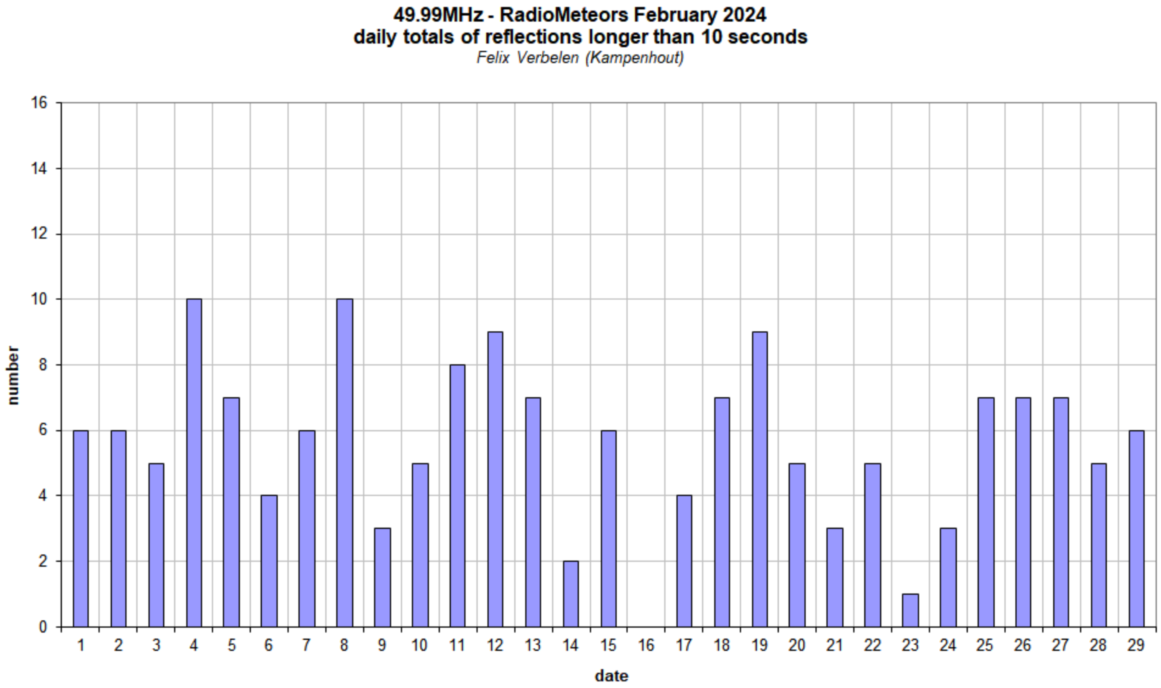

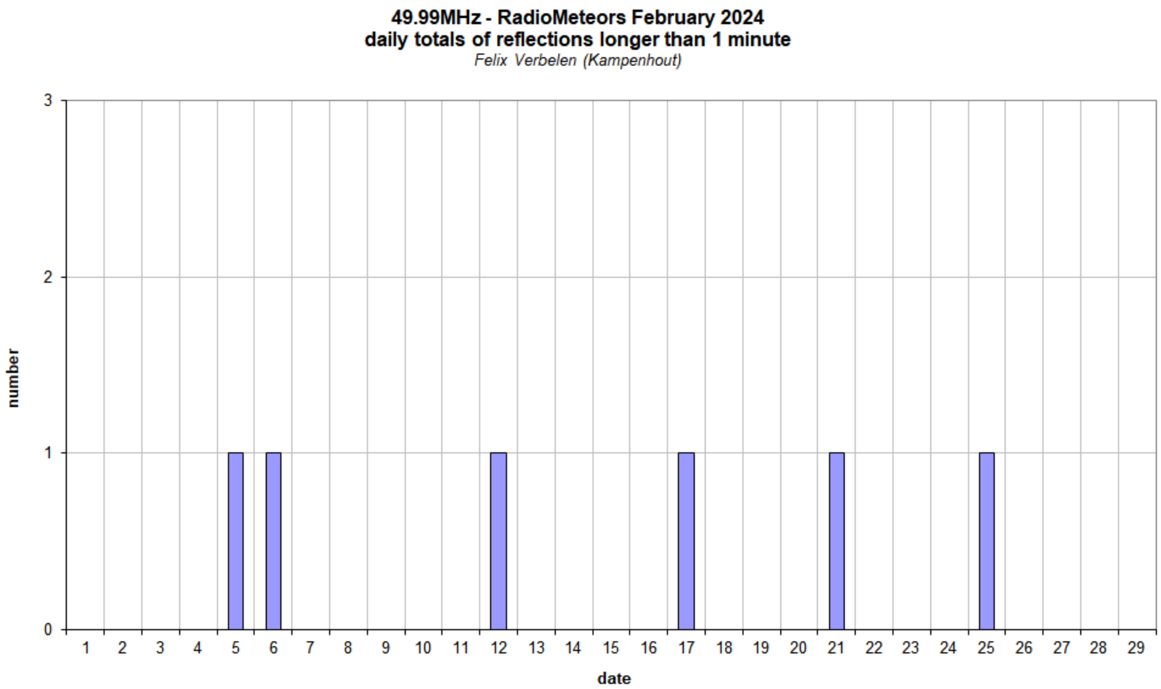

Figure 2 – The daily totals of overdense reflections longer than 10 seconds and longer than 1 minute, as observed here at Kampenhout (BE) on the frequency of our VVS-beacon (49.99 MHz) during February 2024.

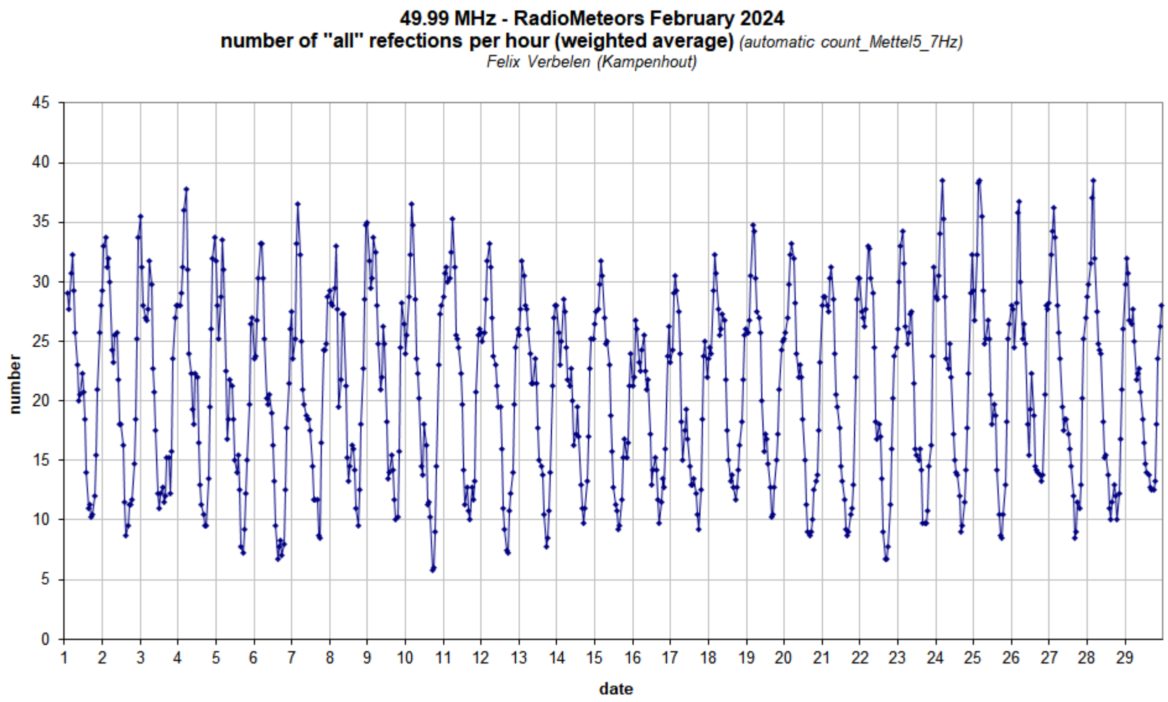

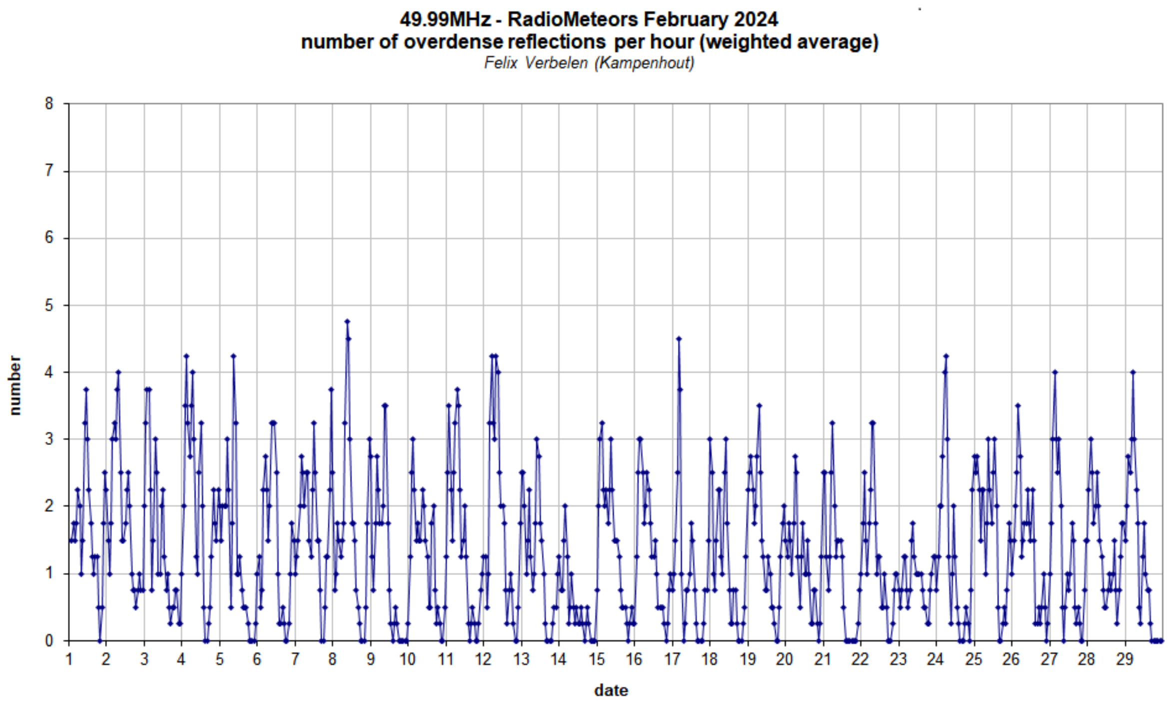

Figure 3 – The hourly numbers of "all" reflections counted automatically, and of manually counted "overdense" reflections, as observed here at Kampenhout (BE) on the frequency of our VVS-beacon (49.99 MHz) during February 2024.

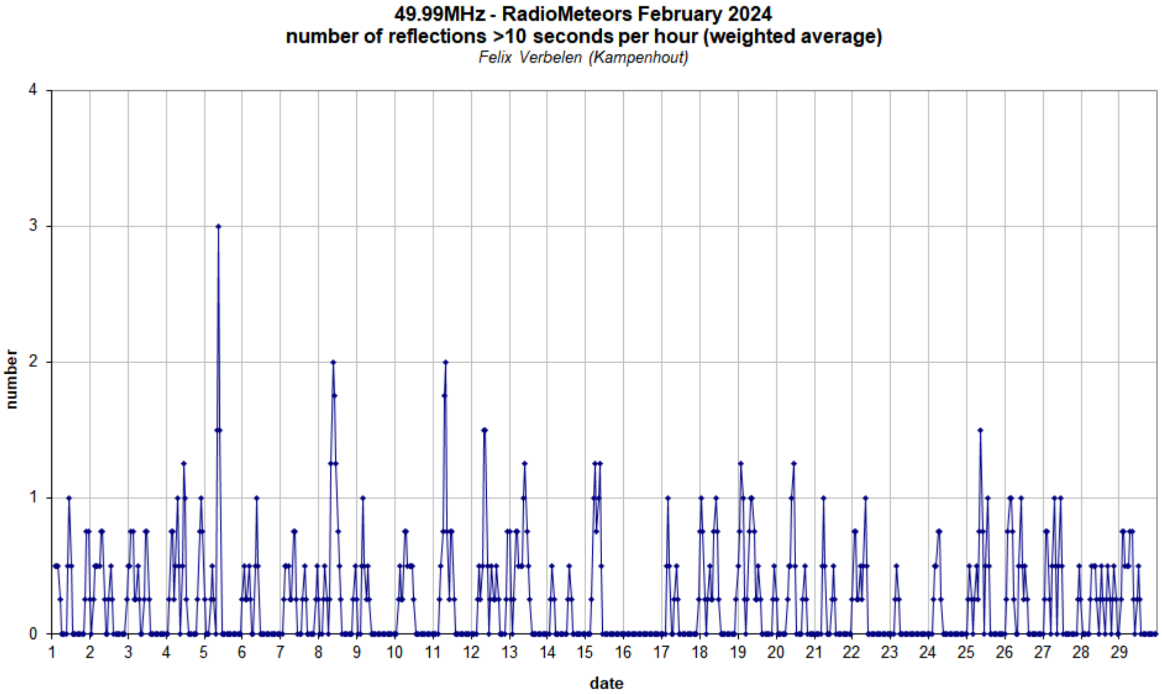

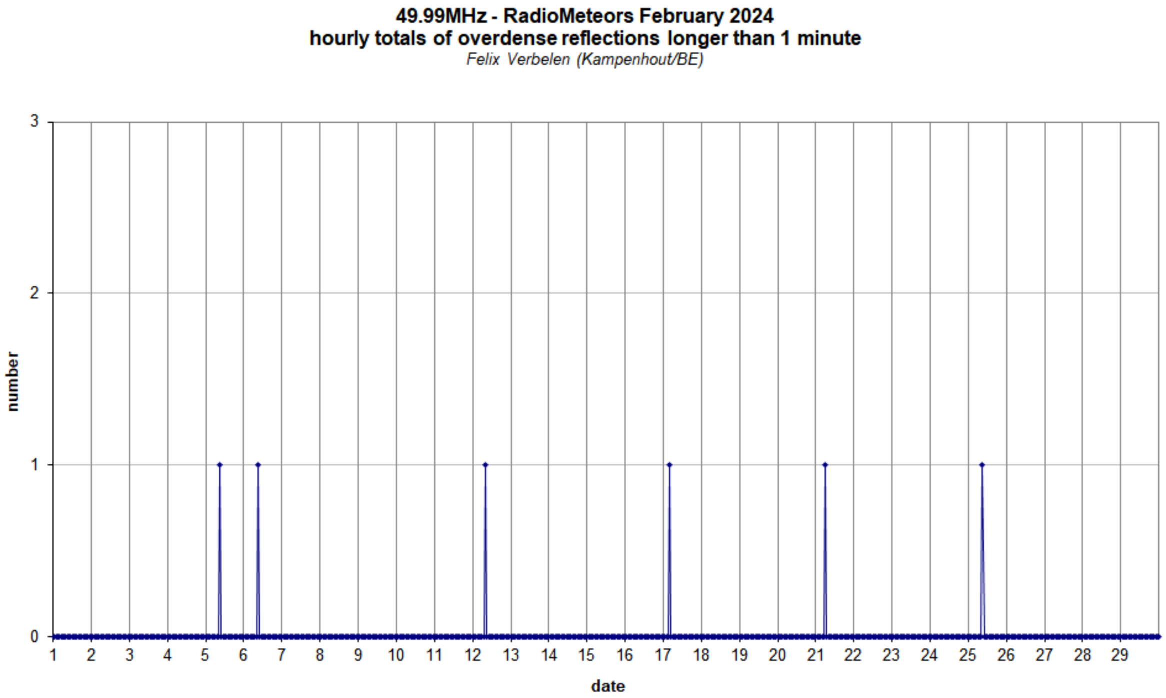

Figure 4 – The hourly numbers of overdense reflections longer than 10 seconds and longer than 1 minute, as observed here at Kampenhout (BE) on the frequency of our VVS-beacon (49.99 MHz) during February 2024.

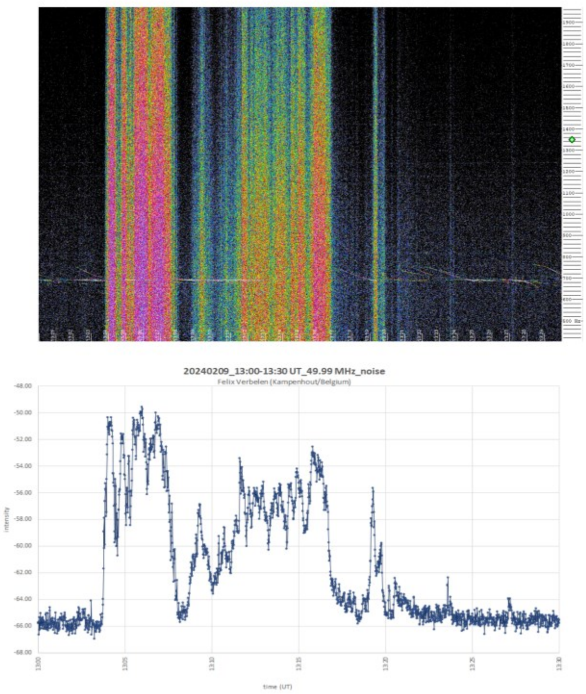

Figure 5 – Strong solar outbursts on February 9th.

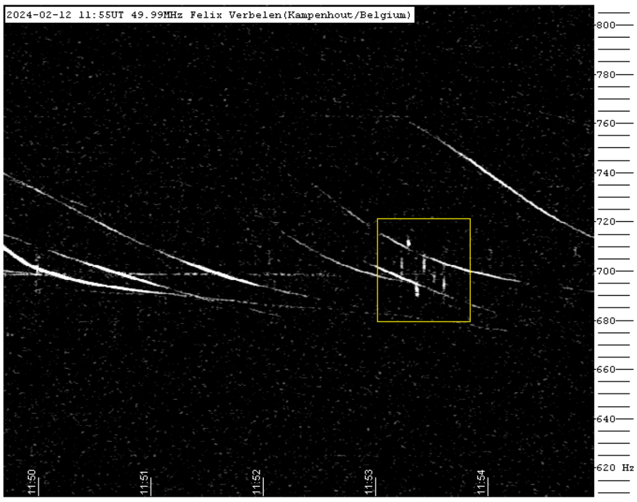

Figure 6 – Meteor echoes February 12, 11^{h}55^m UT.

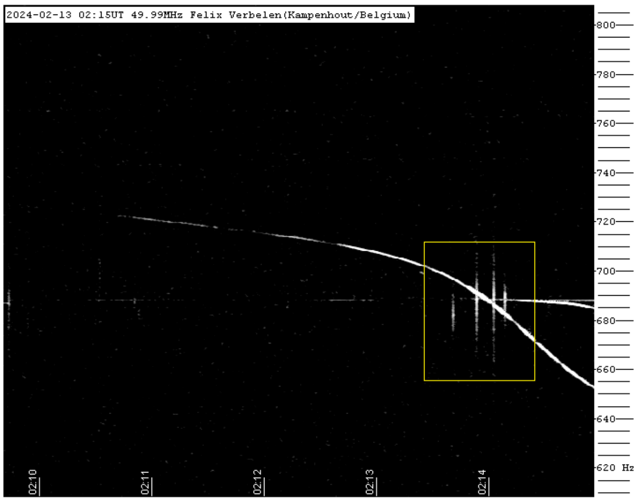

Figure 7 – Meteor echoes February 13, 2^{h}15^m UT.

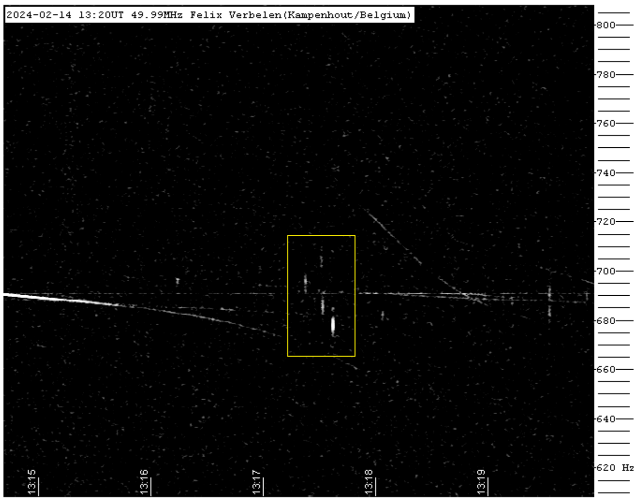

Figure 8 – Meteor echoes February 14, 13^{h}20^m UT.

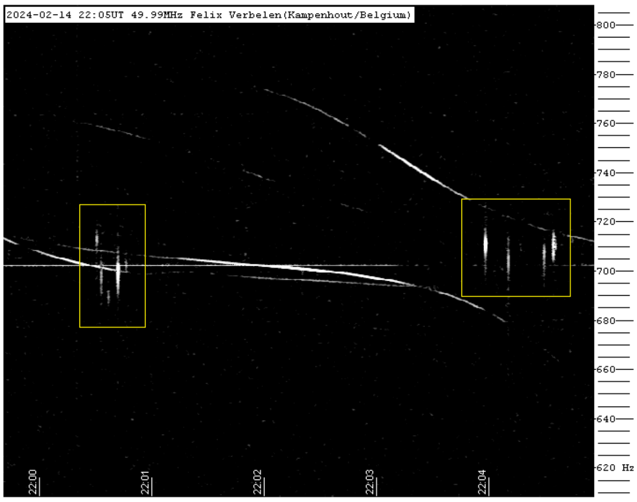

Figure 9 – Meteor echoes February 14, 22^{h}05^m UT.

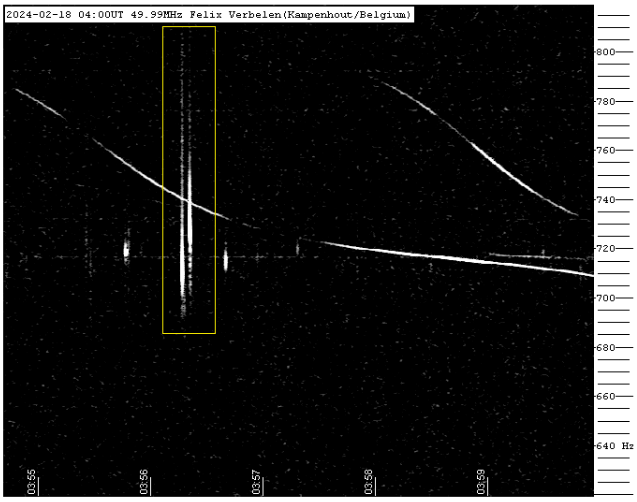

Figure 10 – Meteor echoes February 18, 4^{h}00^m UT.

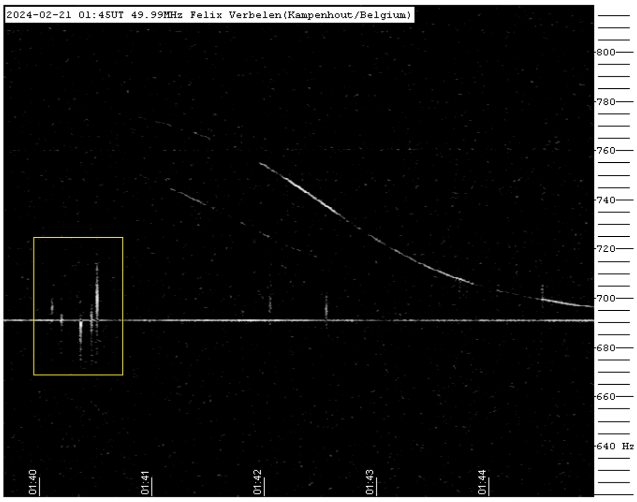

Figure 11 – Meteor echoes February 21, 1^h45^m UT.

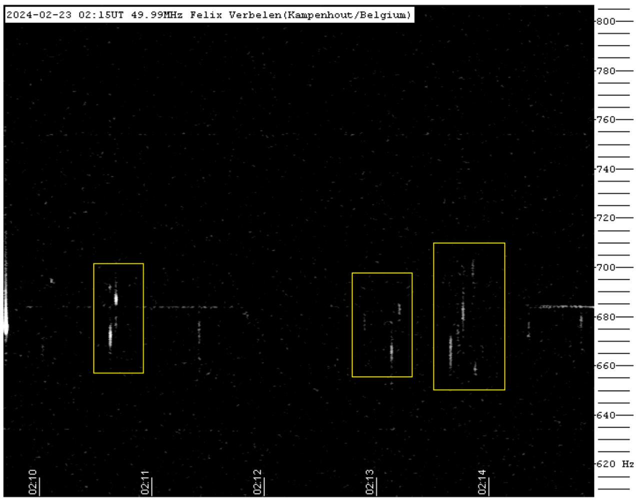

Figure 12 – Meteor echoes February 23, 2^h15^m UT.

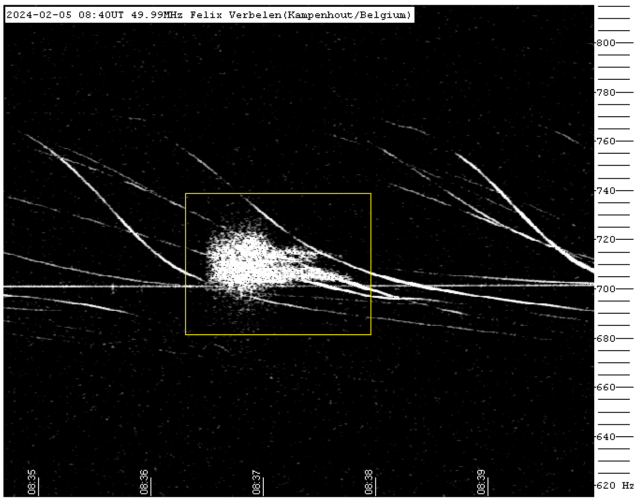

Figure 13 – Meteor echoes February 5, 8^h40^m UT.

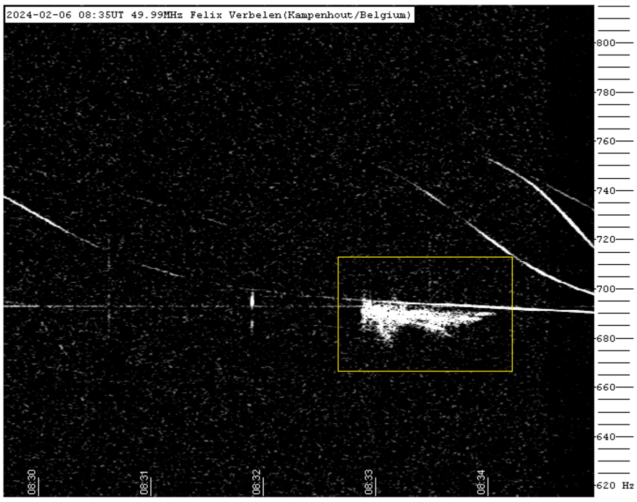

Figure 14 – Meteor echoes February 6, 8^h35^m UT.

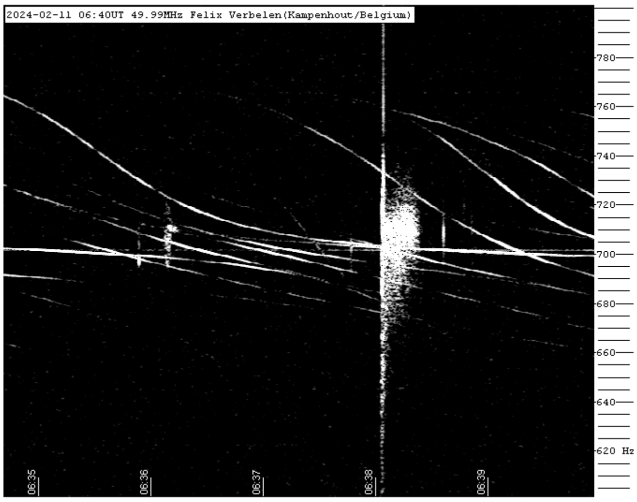

Figure 15 – Meteor echoes February 11, 6^h40^m UT.

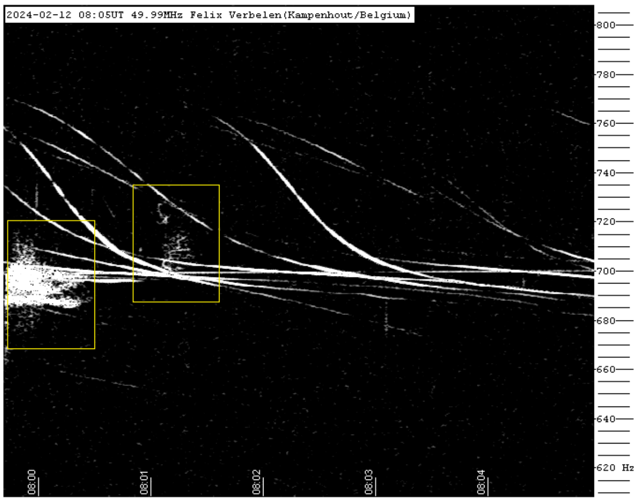

Figure 16 – Meteor echoes February 12, 8^h05^m UT.

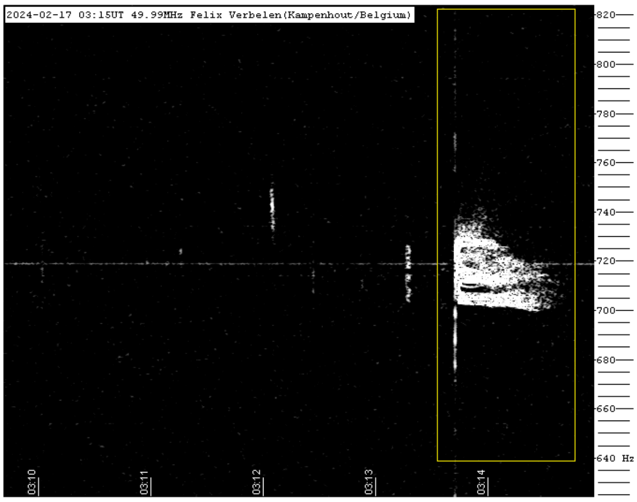

Figure 17 – Meteor echoes February 17, 3^h15^m UT.

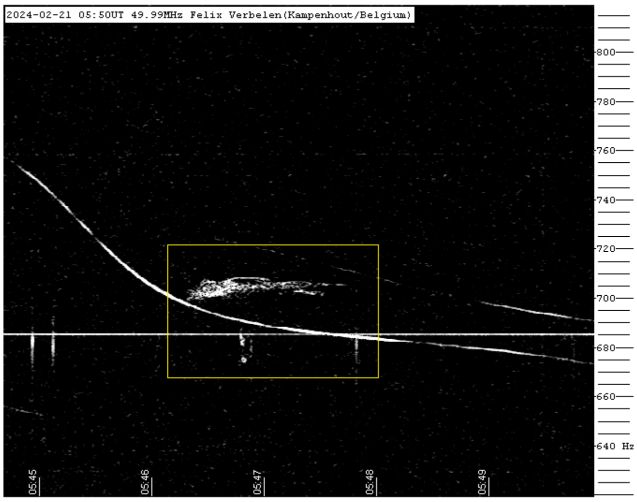

Figure 18 – Meteor echoes February 21, 5^h50^m UT.

Radio meteors March 2024

Felix Verbelen

Vereniging voor Sterrenkunde & Volkssterrenwacht MIRA, Grimbergen, Belgium
felix.verbelen@gmail.com

An overview of the radio observations during March 2024 is given.

1 Introduction

The graphs show both the daily totals (*Figure 1 and 2*) and the hourly numbers (*Figure 3 and 4*) of "all" reflections counted automatically, and of manually counted "overdense" reflections, overdense reflections longer than 10 seconds and longer than 1 minute, as observed here at Kampenhout (BE) on the frequency of our VVS-beacon (49.99 MHz) during the month of March 2024.

The hourly numbers, for echoes shorter than 1 minute, are weighted averages derived from:

$$N(h) = \frac{n(h-1)}{4} + \frac{n(h)}{2} + \frac{n(h+1)}{4}$$

Local interference and unidentified noise remained low for most of the month. Weak to moderate lightning activity was only detected on March 15 and 23, but solar activity caused numerous powerful outbursts at the frequency of our beacon as shown for example in *Figures 5 and 6*, especially during the second half of the month.

As expected, the overall meteor activity remained low, with no real eye-catchers, but with nonetheless some interesting minor shower activity, as shown by the overdense reflections graphs.

During the entire month, only 1 reflection longer than 1 minute was recorded. A selection of some interesting reflections is included (*Figures 7 to 17*). More are available upon request. More of these are available on request.

In addition to the usual graphs, you will also find the raw counts in cvs-format[13] from which the graphs are derived. The table contains the following columns: day of the month, hour of the day, day + decimals, solar longitude (epoch J2000), counts of "all" reflections, overdense reflections, reflections longer than 10 seconds and reflections longer than 1 minute, the numbers being the observed reflections of the past hour.

[13] https://www.emeteornews.net/wp-content/uploads/2024/04/202403_49990_FV_rawcounts.csv

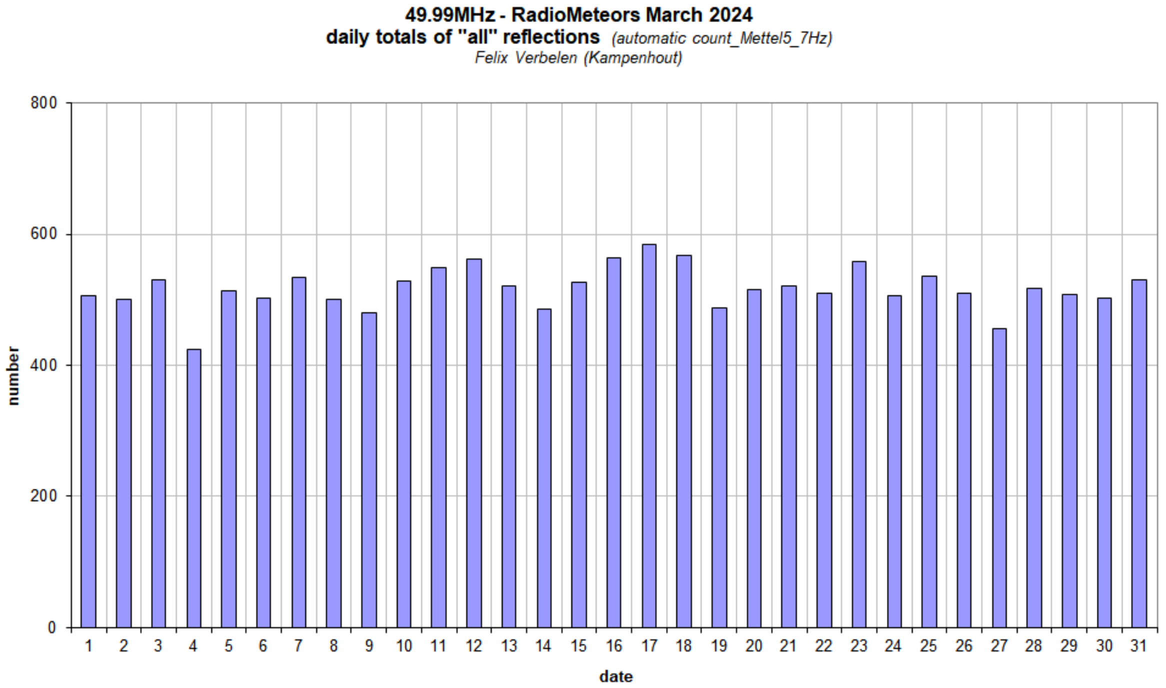

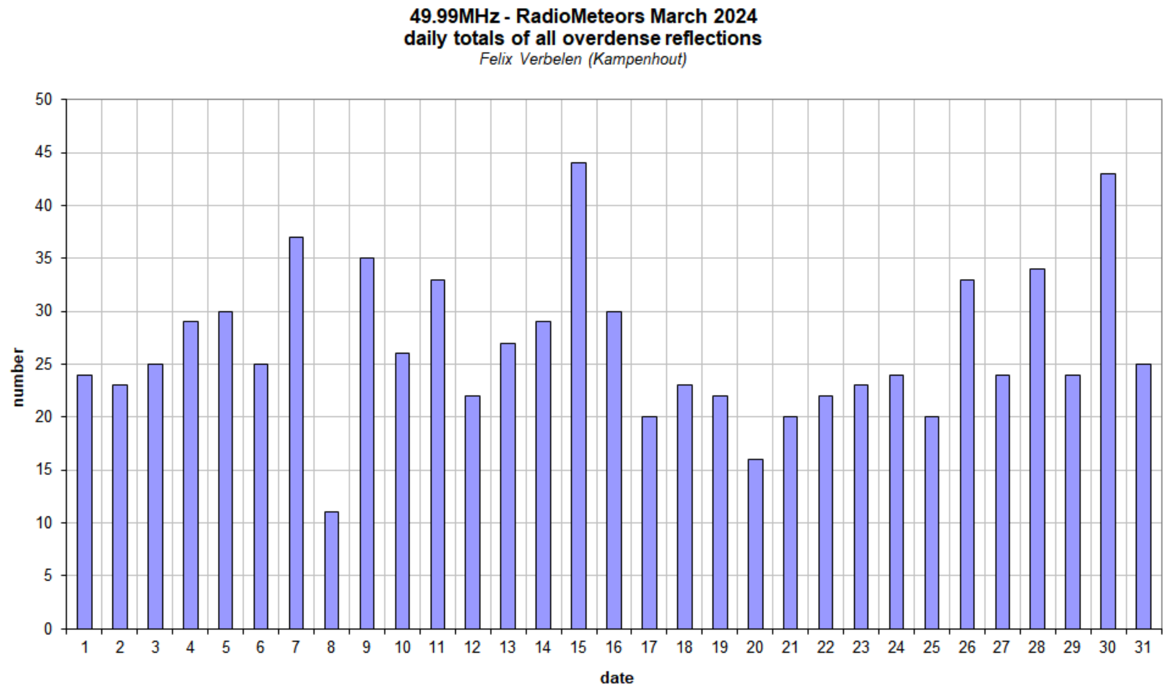

Figure 1 – The daily totals of "all" reflections counted automatically, and of manually counted "overdense" reflections, as observed here at Kampenhout (BE) on the frequency of our VVS-beacon (49.99 MHz) during March 2024.

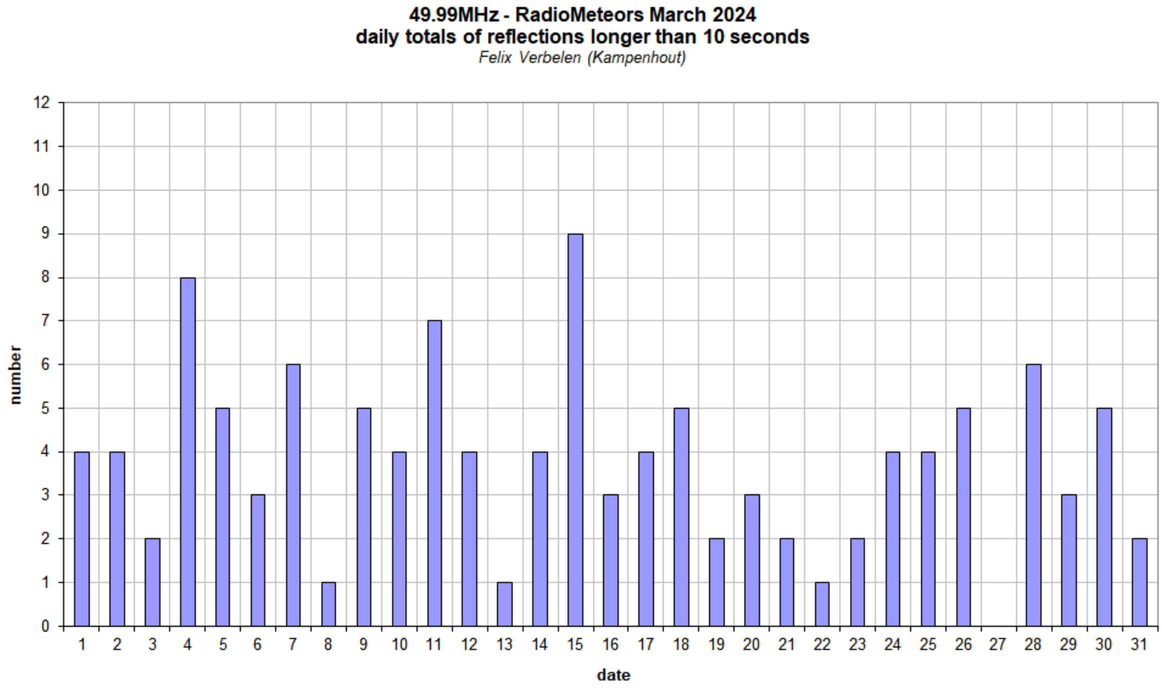

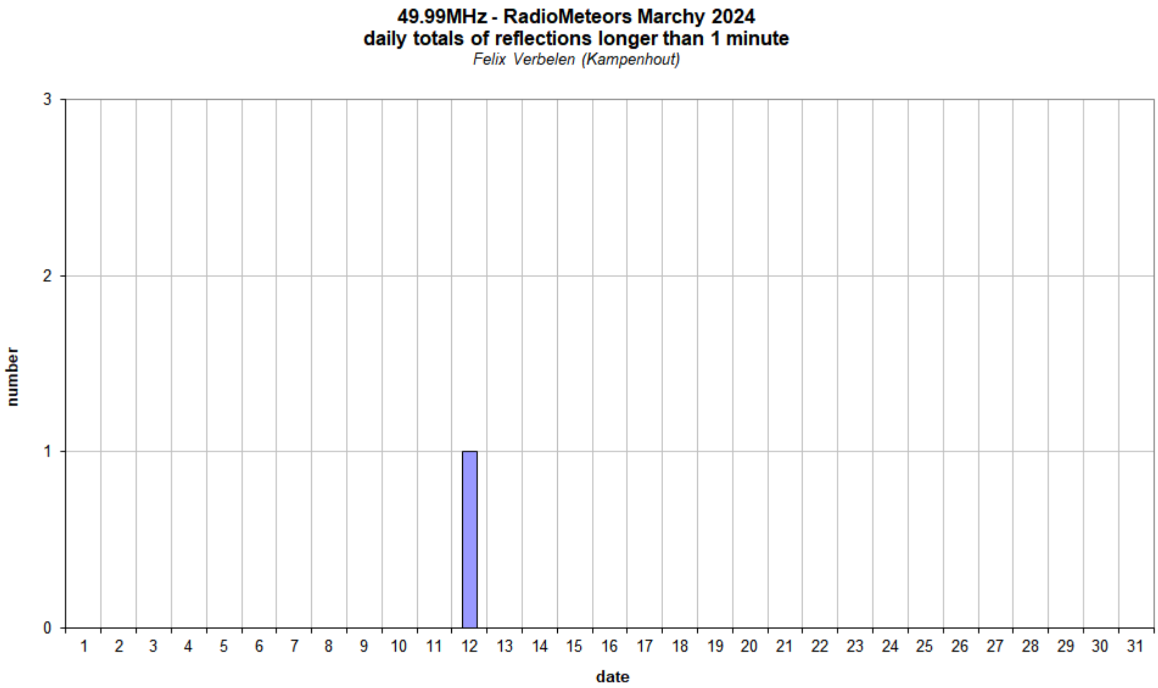

Figure 2 – The daily totals of overdense reflections longer than 10 seconds and longer than 1 minute, as observed here at Kampenhout (BE) on the frequency of our VVS-beacon (49.99 MHz) during March 2024.

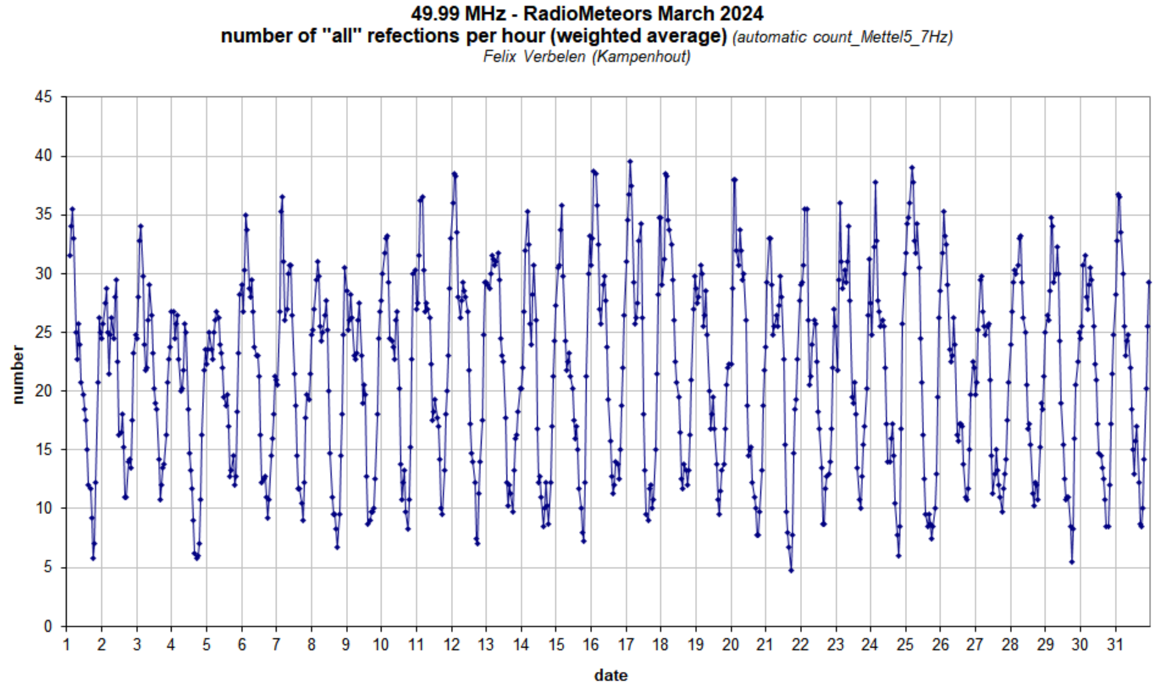

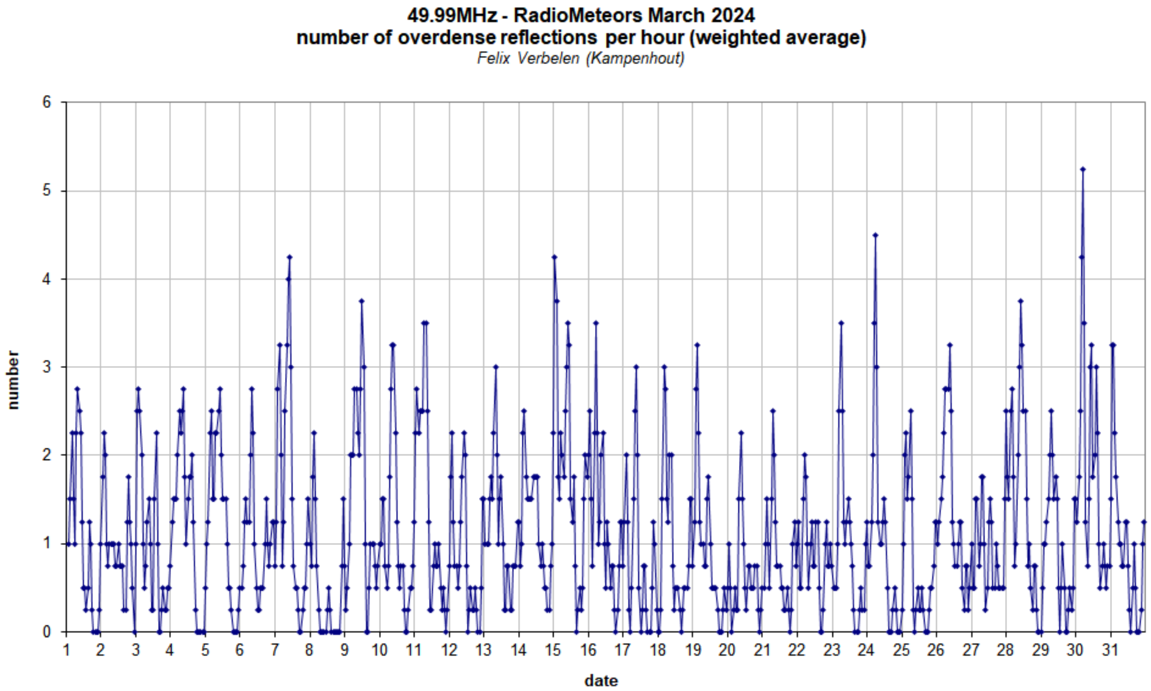

Figure 3 – The hourly numbers of "all" reflections counted automatically, and of manually counted "overdense" reflections, as observed here at Kampenhout (BE) on the frequency of our VVS-beacon (49.99 MHz) during March 2024.

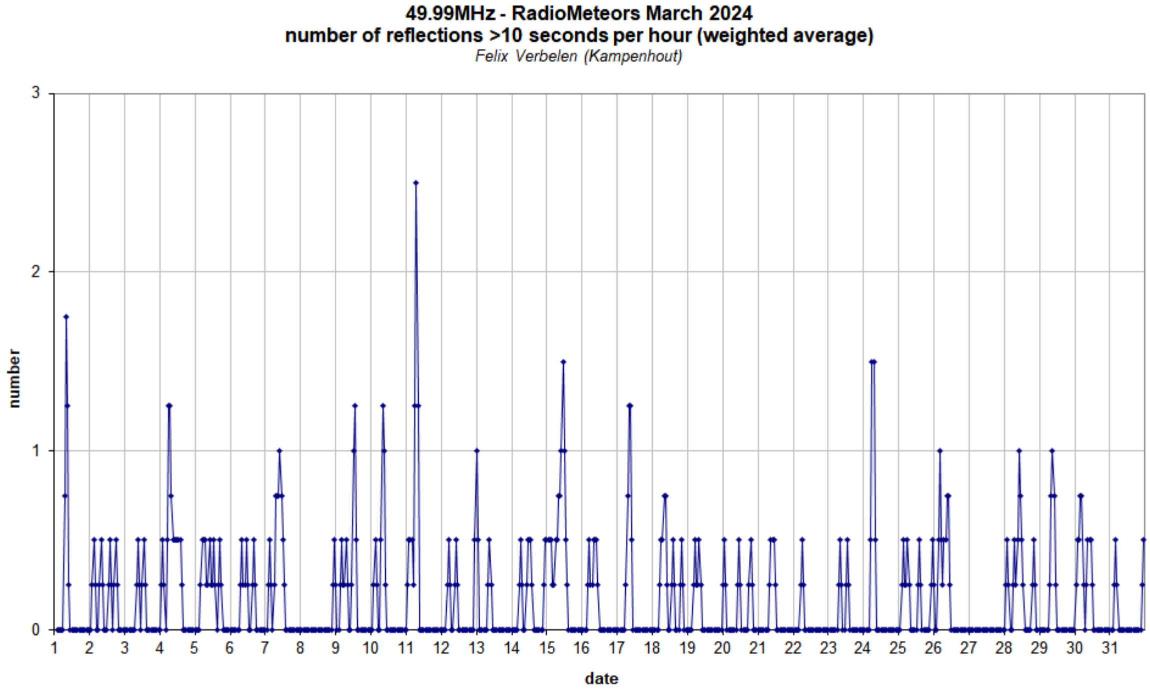

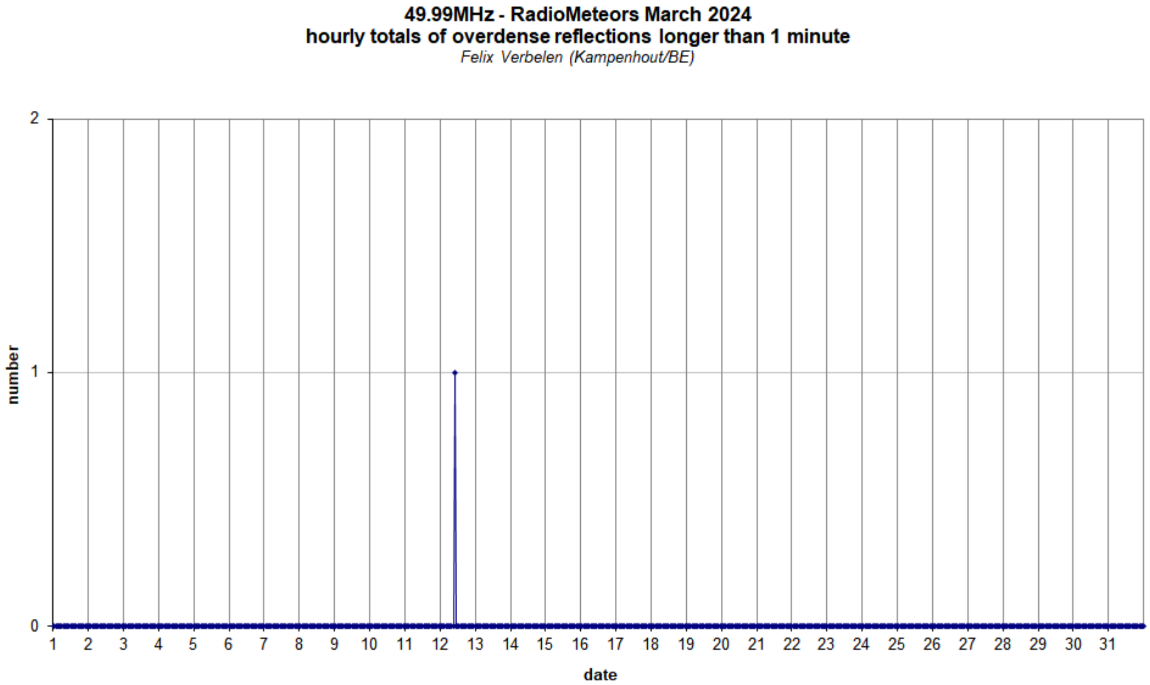

Figure 4 – The hourly numbers of overdense reflections longer than 10 seconds and longer than 1 minute, as observed here at Kampenhout (BE) on the frequency of our VVS-beacon (49.99 MHz) during March 2024.

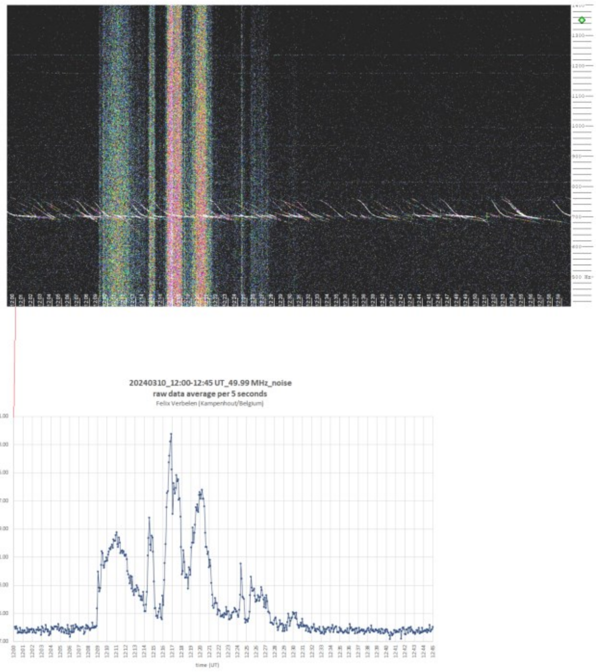

Figure 5 – Strong solar outbursts on March 10th.

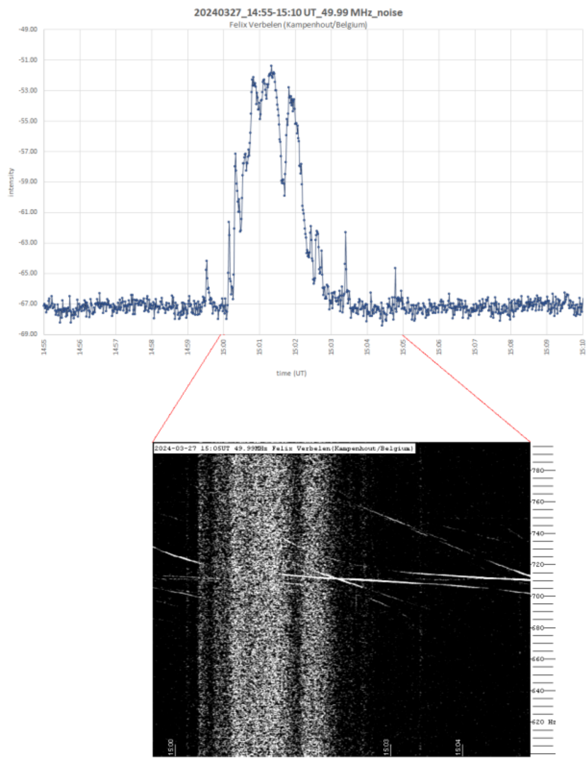

Figure 6 – Strong solar outbursts on March 27th.

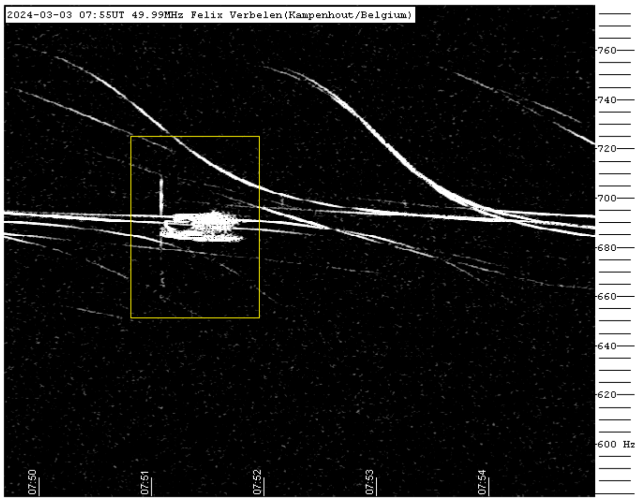

Figure 7 – Meteor echoes March 3, 7h55m UT.

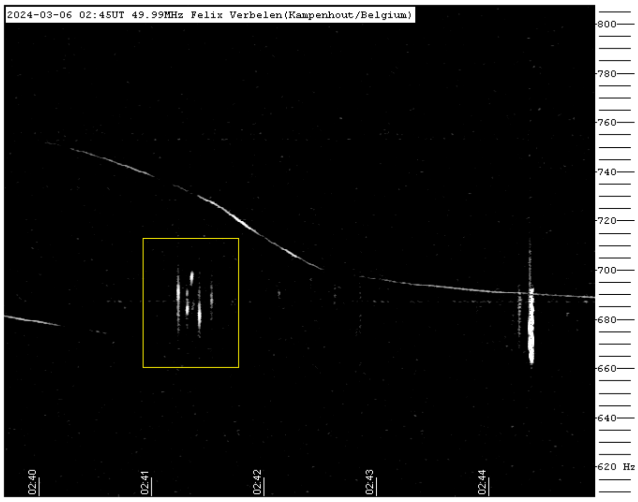

Figure 8 – Meteor echoes March 6, 2h45m UT.

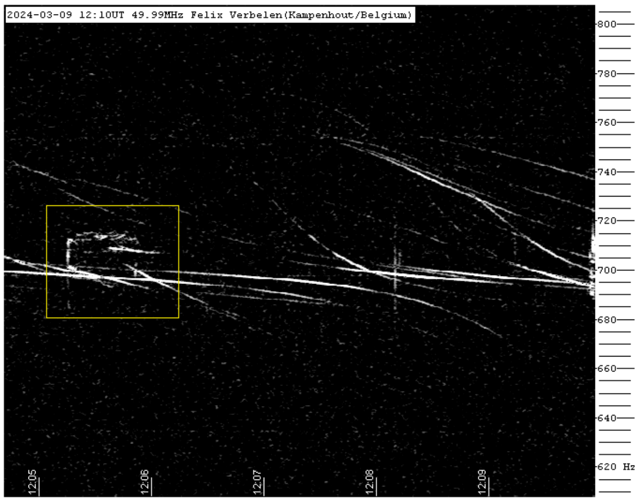

Figure 9 – Meteor echoes March 9, 12h10m UT.

Figure 10 – Meteor echoes March 11, 1^{h}40^{m} UT.

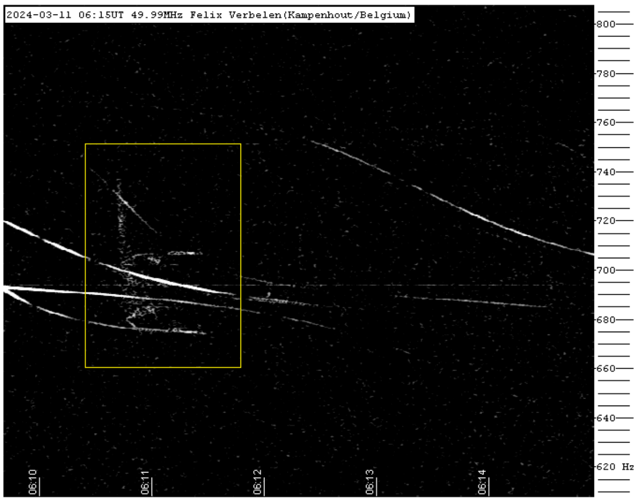

Figure 11 – Meteor echoes March 11, 6^{h}15^{m} UT.

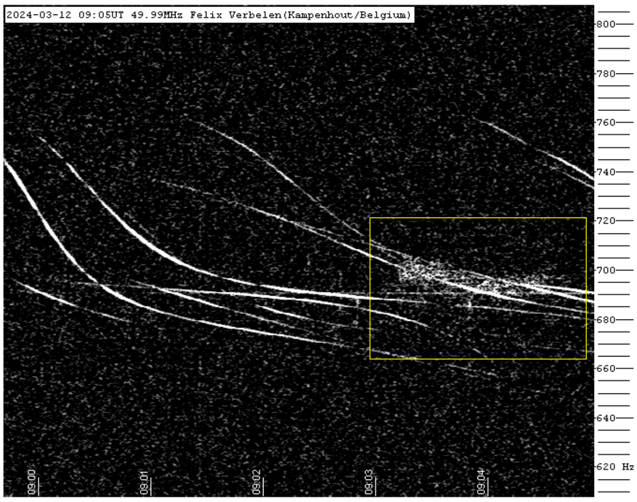

Figure 12 – Meteor echoes March 12, 9^{h}05^{m} UT.

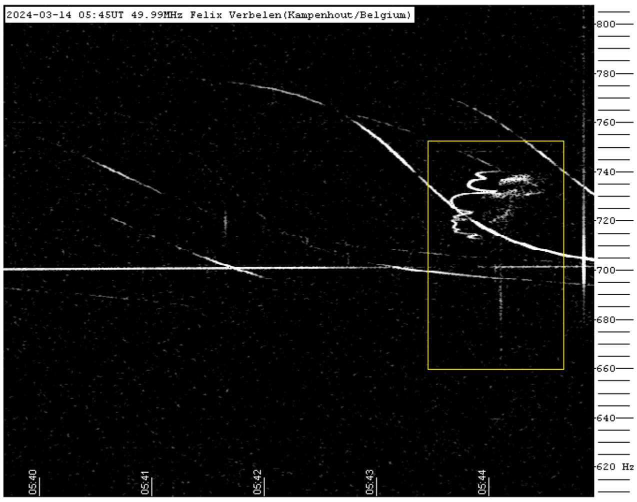

Figure 13 – Meteor echoes March 14, 5^{h}45^{m} UT.

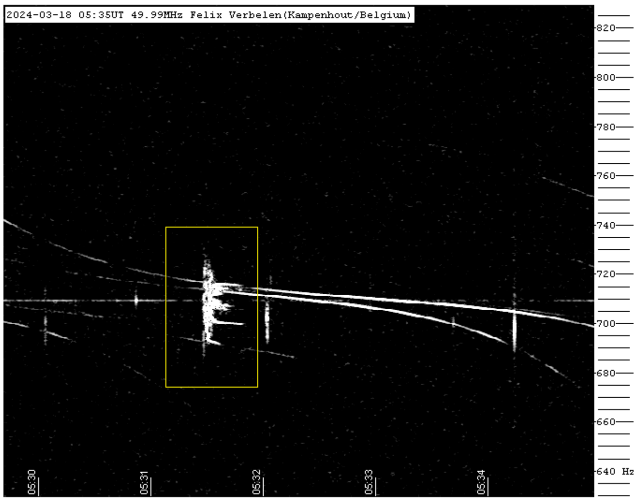

Figure 14 – Meteor echoes March 18, 5^{h}35^{m} UT.

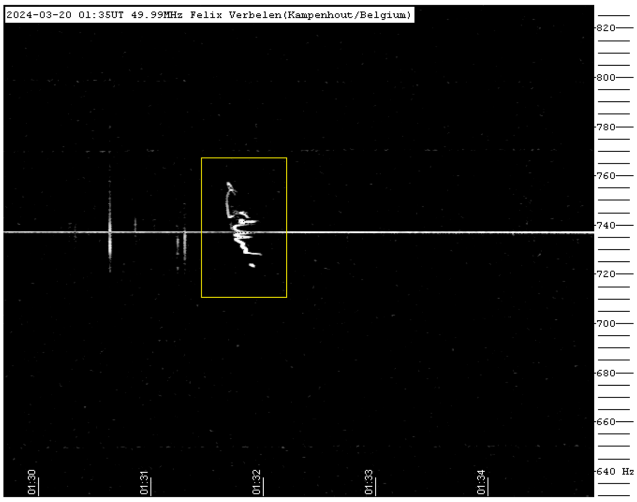

Figure 15 – Meteor echoes March 20, 1^{h}35^{m} UT.

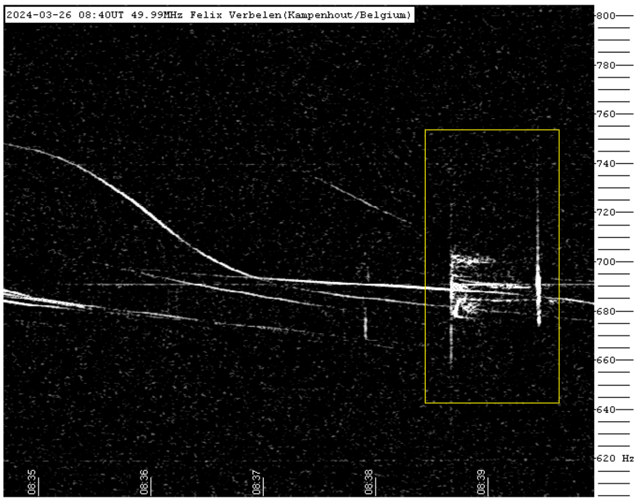

Figure 16 – Meteor echoes March 26, 8^h40^m UT.

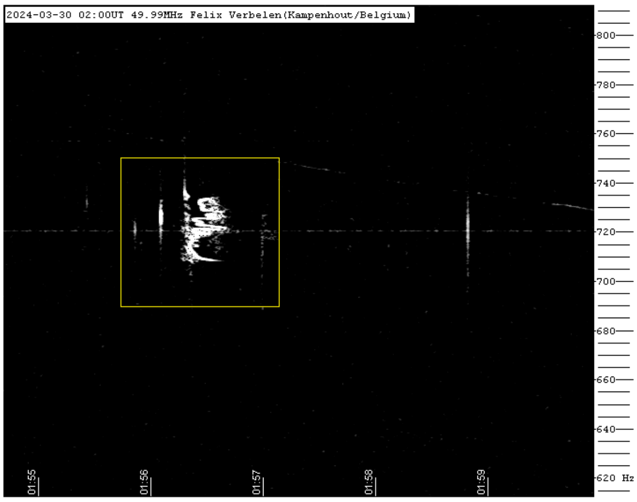

Figure 17 – Meteor echoes March 30, 2^h00^m UT.

The mission of eMetN Meteor Journal is to offer fast meteor news to a global audience, a swift exchange of information in all fields of active amateur meteor work without editing constraints. eMetN Meteor Journal is freely available without any fees. Articles are abstracted and archived with ADS Abstract Service:
https://ui.adsabs.harvard.edu/search/q=eMetN

You are welcome to contribute to eMetN Meteor Journal on a regular or casual basis, if you wish to. Anyone can become an author or editor, send an email to us. For more info read: https://www.emetn.net/writing-content-for-emetn/

Contributors:

- Behan D.
- Boothroyd M. R.
- Burgin D. L.
- Campbell-Burns P.
- Grieg D.
- Jenniskens P.
- Johannink C.
- Koseki M.
- McKellar P.
- Palmer M. C.
- Richardson T.
- Roggemans P.
- Rowe J.
- Scott J. M.
- Šegon D.
- Sergei I.
- Stano R.
- Stayte J.
- Stevenson T.
- Verbelen F.
- Vida D.
- Wang T.
- Weterings J.
- Wyn-Harris S.

ISSN 3041 - 4261